DESIGN AND AUTOMATIC CALIBRATION OF ANALOG FILTERS FOR VLSI APPLICATIONS

A Dissertation

by

FATIMA T. S. TH. ALMUTAIRI

Submitted to the Office of Graduate and Professional Studies of
Texas A&M University
in partial fulfillment of the requirements for the degree of

DOCTOR OF PHILOSOPHY

Chair of Committee,	Aydin Karsilayan
Committee Members,	Edgar Sanchez-Sinencio
	H. Rusty Harris
	Vivek Sarin
Head of Department,	Miroslav M. Begovic

December 2019

Major Subject: Electrical Engineering

ABSTRACT

A bandstop filter is required in broad-band receivers to attenuate the interference signal from the wanted signal. Due to the voltage, temperature, and process variation, automatic tuning circuitry is required to maintain filter characteristics and improve the filter performance. This research proposes a new design method for a second-order tunable bandstop filter and a new technique to tune the center frequency, the bandwidth, and the attenuation of the bandstop filter.

The first part of the work presents a tunable bandstop filter based on source follower. The filter is designed using a source follower architecture with partial positive feedback and feed-forward paths using a 0.18μm CMOS technology. The filter consumes about 1.4 mW from a 1.8V power supply, and it is designed to have 1.5 GHz center frequency with 360 MHz bandwidth and 80 dB attenuation. The filter achieves 10 dBm IIP3 for two tones at 1.2GHz and 1.203 GHz.

The second part of the work discusses a new automatic tuning scheme for the bandstop filter. The method is tuning the filter parameters such as center frequency, bandwidth, and attenuation by using phase comparison. The phase difference between the input and the output of the bandstop filter is detected by D flip flops. The tuning circuit consists of D flip-flops, counters, switches, digital to analogue converter, and passive components. The tuning method was verified by simulation and experimental results. The simulation results show the frequency tuning error of 0.13% and the bandwidth tuning error of 0.88% at 1.5 GHz with bandwidth of 478MHz. Experiment results were obtained

using discrete components, showing the frequency tuning error of 0.22% and the bandwidth tuning error of 0.66% at 1KHz with bandwidth of 200Hz.

DEDICATION

To my beloved parents

Talaq and Moodi

And my sisters

Reem, Asma and Mona

ACKNOWLEDGEMENTS

I would like to thank many people who have supported me during my PhD studies. First, I would like to express many thanks to my advisor Dr. Aydin Karsilayan for his guidance throughout my research. I am also grateful for Dr. Edgar Sanchez-Sinencio for his guidance and encouragement during the courses at the Texas A&M University. I would also like to thank Dr. H. Rusty Harris who made my first semester at the Texas A&M University a welcoming environment for me. I would like further to thank Dr. Edgar Sanchez-Sinencio, Dr. H. Rusty Harris and Dr. Vivek Sarin for serving on my committee. I would also like to thank Dr. Jose Silva-Martinez for his valuable suggestions and discussions.

I am thankful to the AMSC group, Ella Gallagher, Dr. Judy Amanor-Boadu, Joseph Samy Riad, Sergio Soto Aguilar, and Adriana C Sanabria-Borbon.

I am extremely thankful towards my parents for what they did for me and for their support in all my decisions. I would also like to thank my sisters, Reem and Asma, for their support and advice on how to deal with any problem that I have faced in my life. A special thanks to my youngest sister, Mona. When I need her, she has always been there, and I can count on her.

I would like to also thank Dr. Mohammad Abdul-Azeez Bou-Shahri who is a professor in Civil Engineering Department at Kuwait University. He is the one who convinced me to purse the PhD degree and supported my decision in going to USA.

CONTRIBUTORS AND FUNDING SOURCES

Contributors

This work was supported by a dissertation committee consisting of Professors Aydin Karsilayan, Edgar SánchezSinencio, and H. Rusty Harris of the Department of Electrical and Computer Engineering and Vivek Sarin of the Department of computer science and Engineering.

Funding Sources

Graduate study was supported by a fellowship from Kuwait University Foundation.

NOMENCLATURE

RF	Radio Frequency
SNR	Signal-to-Noise Ratio
LNA	Low Noise Amplifier
Opamps	operational amplifiers
GBP	Gain Bandwidth Product
MOSFET	Metal Oxide Semiconductor Field Effect Transistor
Q	Quality factor
ω_o	Center frequency
α	Attenuation
PVT	Process, Voltage, and Temperature
PLL	Phase Locked Loop
VCF	Voltage-Controlled Filter
VCO	Voltage-Controlled Oscillator
LPF	Low Pass Filter
MLL	Magnitude Locked Loop
LMS	Least Mean Square
CMOS	Complementary Metal-Oxide-Semiconductor
DFF	D flip flop
DVB	Digital Video Broadcasting
EEG	Electroencephalograph

GPS	Global Positioning System
RF	Radio Frequency Module
BW	Band Width
ω_L	Lower cutoff frequency
ω_U	Upper cutoff frequency
Q_{BS}	Quality factor of Bandatop Filter
R	Resistance
C	Capacitance
gm	Transconductance
T	absolute temperature
K	Boltzmann constant
CMFB	Common mode feedback
V_{TH}	Threshold voltage
THD	Total Harmonic Distortion
IIP3	Input Intercept Point

TABLE OF CONTENTS

Page

ABSTRACT ii

DEDICATION iv

ACKNOWLEDGEMENTS v

CONTRIBUTORS AND FUNDING SOURCES vi

NOMENCLATURE vii

TABLE OF CONTENTS ix

LIST OF FIGURES xi

LIST OF TABLES xv

1. INTRODUCTION 1

1.1. Organization 5

2. EXISTING BANDSTOP FILTERS AND TUNING TECHNIQUES 6

2.1. Bandstop Filter Topologies Reported in the Literature 8
2.1.1. Active-RC Filters 8
2.1.2. MOSFET-C Filters 10
2.1.3. G_m-C Filters 11
2.1.4. Active-LC Filters 13
2.2. Automatic Tuning Schemes Reported in The Literature 14
2.3. Frequency Tuning Schemes 16
2.3.1. Phase Locked Loop Using Voltage Controlled Oscillator 16
2.3.2. Frequency Tuning Based on Peak Detection 17
2.4. Quality Factor Tuning Schemes 18
2.4.1. Magnitude Locked Loop (MLL) 18
2.4.2. Enhanced Adaptive Q-Tuning Scheme 19
2.4.3. Digital-Tuning Method Based on Phase Comparison 20
2.5. Attenuation Tuning Schemes 21
2.5.1. Attenuation Tuning Based on Magnitude 21
2.5.2. Self-Tuning by Phase Feedback from Output 22

2.5.3. Self-Tuning by Phase Feedback from Intermediate Node 23

3. PROPOSED BANDSTOP FILTER BASED ON SOURCE FOLLOWER 24

3.1. Principle of Operation 24
3.2. Circuit Description 25
3.3. General Design Considerations 29
3.4. Stability 31
3.5. Noise and Linearity 34
3.6. Input and Output Impedance 40
3.7. Simulation Results 40

4. THE PROPOSED TUNING SCHEME 47

4.1. Principle of the Proposed Tuning Technique 47
4.2. Tuning Scheme 50
4.2.1. Multi-phase Generator 52
4.2.2. Ramp Frequency Control Voltage 55
4.2.3. Frequency Tuning Circuit 57
4.2.4. Attenuation Tuning Circuit 58
4.2.5. Bandwidth Tuning Schemes 59
4.2.6. Limitations of the Tuning Method 62

5. SIMULATION AND EXPERIMENTAL RESULTS 68

5.1. Simulation Results 68
5.2. Prototype Design 73
5.2.1. Filter 74
5.2.2. Tuning Circuit 76
5.2.3. Experimental Results 79

6. CONCLUSIONS 83

6.1. Future work 84

REFERENCES 85

LIST OF FIGURES

Page

Figure 1.1 A typical broad-band RF receiver with baseband blocker rejection, reprinted with permission from [4]. 1

Figure 1.2 A typical broad-band RF receiver with blocker rejection at RF. 4

Figure 2.1 Magnitude response of a second-order bandstop filter. 7

Figure 2.2 Block diagram of a second-order bandstop filter. 8

Figure 2.3 Active-RC bandstop filter, reprinted with permission from [29]. 9

Figure 2.4 Power consumption versus center frequency among the published active RC filters 10

Figure 2.5 MOSFET-C bandstop filter. 11

Figure 2.6 G_m-C bandstop filter, reprinted with permission from [4]. 12

Figure 2.7 Active-LC filter, reprinted with permission from [36]. 14

Figure 2.8 Block diagram of the master-slave tuning scheme. 15

Figure 2.9 Block diagram of a direct tuning scheme. 16

Figure 2.10 Block diagram of the phase locked loop tuning scheme using voltage-controlled oscillator, reprinted with permission from [22]. 17

Figure 2.11 Frequency tuning based on peak detection, reprinted with permission from [51]. 18

Figure 2.12 Block diagram of the magnitude locked loop scheme, reprinted with permission from [46]. 19

Figure 2.13 Block diagram of the enhanced adaptive Q-tuning scheme, reprinted with permission from [22]. 20

Figure 2.14 Block diagram of digital-tuning method based on a phase comparison, reprinted with permission from [19]. 21

Figure 2.15 Block diagram of the attenuation tuning by the phase feedback from output, reprinted with permission from [47] 22

Figure 2.16 Block diagram of the attenuation tuning by the phase feedback from intermediate node, reprinted with permission from [47]. 23

Figure 3.1 Block diagram of the proposed design. 24

Figure 3.2 Proposed bandstop filter, reprinted with permission from [52]. 26

Figure 3.3 Small signal equivalent circuit of the bandstop filter, reprinted with permission from [52]. 26

Figure 3.4 Frequency response of the proposed filter. 30

Figure 3.5 Block diagram of the proposed filter. 31

Figure 3.6 Frequency response of loop transfer functions. 33

Figure 3.7 Output referred noise of the second-order bandstop filter, reprinted with permission from [52]. 35

Figure 3.8 Continuous-time CMFB circuit, reprinted with permission from [26]. 36

Figure 3.9 Magnitude and phase response of the CMFB loop. 37

Figure 3.10 Step response of the CMFB loop. 38

Figure 3.11 Frequency response of the tunable bandstop filter using I_{c1} to tune ω_o, reprinted with permission from [52]. 42

Figure 3.12 Frequency response of the tunable bandstop filter using C_1 to tune ω_o, reprinted with permission from [52]. 43

Figure 3.13 Frequency response of the tunable bandstop filter using I_b to tune BW, reprinted with permission from [52]. 43

Figure 3.14 Frequency response of the tunable bandstop filter using I_d to tune α, reprinted with permission from [52]. 44

Figure 3.15 Frequency response of the second-order bandstop filter. 44

Figure 3.16 IIP3 versus input frequency for two-tone tests ($f_1 = f_{in} - 1MHz$ and $f_2 = f_{in} + 1MHz$), reprinted with permission from [52]. 45

Figure 3.17 1 dB compression point input signal at 1.2 GHz. 45

Figure 3.18 Output signal spectrum with 632.5 mVPP at a 1.2GHz input signal. 46

Figure 4.1 The magnitude and the phase of the bandstop filter at fixed ω_r.....48

Figure 4.2 Attenuation versus $\theta_{max.}$ 49

Figure 4.3 The bandwidth error versus attenuation.....50

Figure 4.4 Overall tuning scheme. 51

Figure 4.5 Clock signals.....52

Figure 4.6 The schematics of the multi-phase generator.....53

Figure 4.7 Multi phases generator waveform.....54

Figure 4.8 The adaptive ramp frequency control voltage. 55

Figure 4.9 Time-domain response of V_f during the tuning processes. 56

Figure 4.10 Frequency tuning scheme. 57

Figure 4.11 Attenuation tuning scheme. 58

Figure 4.12 Phase response of the bandstop filter.....59

Figure 4.13 Bandwidth tuning scheme.....61

Figure 4.14 The controller of the bandwidth tuning scheme. 62

Figure 4.15 Bandwidth tuning error due to the excess phase shift. 64

Figure 4.16 Frequency tuning error due to the resolution of DAC. 66

Figure 4.17 Bandwidth tuning error due to the resolution of DAC. 67

Figure 5.1 Bandstop filter based on source follower 69

Figure 5.2 The squaring current circuit. 70

Figure 5.3 Transient response of the squaring current circuit. 70

Figure 5.4 Transient response of the frequency control voltage. 71

Figure 5.5 Transient response of the attenuation control voltage. 71

Figure 5.6 Transient response of the bandwidth control voltage. 72

Figure 5.7 Frequency response of the bandstop filter. 72

Figure 5.8 Experimental setup. 73

Figure 5.9 Second-order Gm-C bandstop filter. 74

Figure 5.10 Simulink diagram of the frequency ramp control. 77

Figure 5.11 The waveform of the phase generator. 78

Figure 5.12 Experimental transient response of the frequency control voltage. 80

Figure 5.13 Experimental transient response of the attenuation control voltage. 80

Figure 5.14 Experimental transient response the bandwidth control voltage. 81

Figure 5.15 Experimental frequency response of the bandstop filter. 81

LIST OF TABLES

Page

Table 3.1 Filter specifications 29

Table 3.2 Filter parameters..... 29

Table 3.3 Filter Design Parameters, reprinted with permission from [52]..... 41

Table 3.4 Performance of the second-order bandstop filter, reprinted with permission from [52]. 46

Table 4.1 The truth table of the DFF 57

Table 4.2 Attenuation tuning process 59

Table 4.3 Truth table for the coarse-tuning 60

Table 4.4 Truth table for the fine-tuning 60

Table 5.1 Component values used for Gm-C tunable filter 75

Table 5.2 Bandwidth tuning range at f_o =1KHz 82

1. INTRODUCTION

Bandstop filters are usually used in broad-band radio frequency (RF) receivers to reject interferences and blockers, which affect the performance of receivers by reducing the signal-to-noise ratio (SNR) [1]. Blockers may be unintentional, such as communication signals from Bluetooth and Wi-Fi, or intentional as in the case of jamming or spoofing [2]-[3]. A typical broad-band RF receiver with baseband blocker rejection is shown in Figure 1.1, where the bandstop filters are placed after the down-conversion mixer [3]-[5]. This topology requires the low-noise amplifier (LNA) and the mixer to be very linear and have high dynamic range to avoid saturation due to blockers [6]-[7].

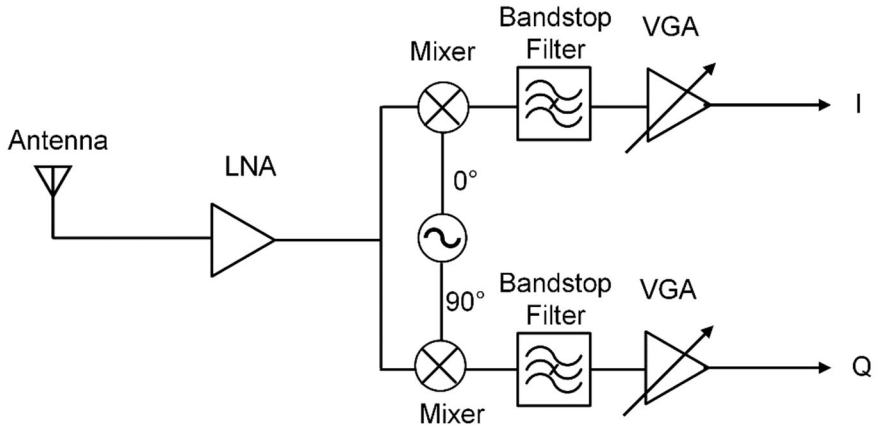

Figure 1.1 A typical broad-band RF receiver with baseband blocker rejection, reprinted with permission from [4].

Several bandstop filter implementations including active-RC, MOSFET-C, Gm-C, and active-LC topologies can be found in the literature [8]-[11]. Active-RC implementation may be preferred for applications requiring high linearity, due to its closed-loop feedback architecture. However, a significant limitation for this implementation is that it requires operational amplifiers (opamps) with high gain-bandwidth (GBW) product, typically ten times higher than the center frequency, resulting in high power dissipation for high frequency applications [12]. Furthermore, a tunable active-RC filter can only be implemented using capacitor or resistor arrays occupying a large area, since active-RC filter characteristics are determined by resistors and capacitors [13]. Alternatively, MOSFET-C filter topology can provide more efficient tunability using MOSFETs in triode region as variable resistors in an active-RC implementation [14]. Although the area can be reduced, linearity will also be reduced due to resistor nonlinearities. In addition, high-GBW opamps are still required, making MOSFET-C realization unsuitable for high-frequency applications.

Gm-C filter topology is an efficient choice for high frequency applications due to moderate levels of power dissipation. Gm-C filter parameters depend on transconductance (Gm) values that can be controlled through bias currents, therefore tunable filters can be realized. However, since the transconductors are used in open loop, linearity of Gm-C filters is limited [12]. Active-LC filters are also suitable for high frequency applications providing high linearity with low power dissipation, however they consume a large area due to inductors [11]. Although tunable active-LC filters can be implemented using a

combination of varactors, capacitor arrays, and active components [15], adding tunability further increases area requirements of active-LC filters.

Frequency characteristics of bandstop filters, such as center frequency (ω_o), quality factor (Q), and attenuation (α), are generally based on the values of active and passive components, which are sensitive to process, voltage, and temperature (PVT) variations. Thus, automatic tuning circuitry is required to obtain the required response and maintain these characteristics [16]-[19]. Filter tuning methods reported in the literature usually target center frequency and quality factor as the parameters to calibrate, however simultaneous control of attenuation at the notch frequency is also critical for bandstop filters. In addition to individual control of each parameter, the tuning system must ensure the stability of the filter when multiples of control loops exist [19].

Several methods for tuning center frequency have been reported in the literature [20]-[21]. The phase-locked loop (PLL) method, where a voltage-controlled oscillator or filter is used as a replica to lock the center frequency to a reference, is the most commonly used technique for tuning the pole frequency. Quality factor tuning methods generally rely on a direct relationship between the filter's gain and quality factor, where a magnitude-locked loop [22] is used to set the gain to a desired reference. These methods are not applicable to all filter types, such as bandstop, and combining frequency and quality factor tuning typically requires two tuning loops converge simultaneously. The problem becomes even more challenging when a third control loop is added for tuning the attenuation, which is required for bandstop filters. In [19], center frequency and quality factor of second-order filters are tuned using phase comparison at two reference

frequencies, where only one loop is enabled at a given time by digital control to prevent instability. However, this technique requires monotonic phase response of the filter, making it unusable for bandstop filters. Besides, multiple references require a frequency synthesizer for the tuning circuit, significantly increasing the overhead.

In this work, a tunable bandstop filter with an automatic tuning circuit is designed, which can be used to reject interferences in broadband receivers at RF (before down-conversion) to avoid mixer saturation as illustrated in Figure 1.2 [23]-[25]. The bandstop filter could be further moved towards the antenna and placed before the LNA, but this adds further constraints to the filter specifications in terms of input matching and noise figure. The optimum location of the filter proposed in this work is between the LNA and the mixer, due to filter's capacitive input impedance and noise contribution.

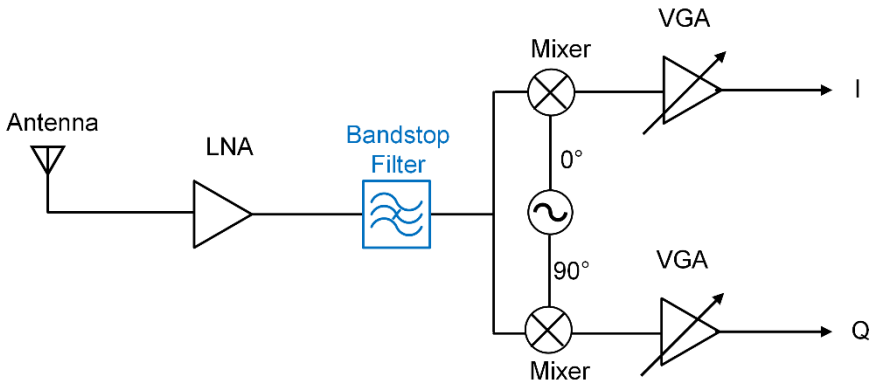

Figure 1.2 A typical broad-band RF receiver with blocker rejection at RF.

The proposed filter structure is based on the source follower topology [26], providing low power dissipation and high linearity. This topology is also suitable for high

frequency applications due to the simplicity of the architecture, where tuning of the filter is achieved through DC bias currents. A new automatic tuning scheme based on phase comparison is also introduced to calibrate the proposed bandstop filter, where center frequency, quality factor and attenuation of the filter are digitally controlled to ensure stability by enabling one loop at a given time.

1.1. Organization

This dissertation consists of six chapters. The first chapter presents the introduction and the motivation for this research. The second chapter provides an overview of second-order bandstop filter implementations, and briefly discusses the advantages and disadvantages of each implementation, along with tuning methods currently used to control the center frequency, quality factor, and attenuation in these topologies. Design methodology of the proposed second-order bandstop filter, along with design considerations such as stability, noise, and linearity, is explained in chapter three. In chapter four, the proposed tuning method to calibrate the center frequency, bandwidth, and attenuation of the bandstop filter is presented. Chapter five shows the simulation and experimental results of the proposed filter and the tuning method. Chapter six summarizes the major contributions of this research and offers suggestions for future work.

2. EXISTING BANDSTOP FILTERS AND TUNING TECHNIQUES

A second-order (biquadratic) bandstop filter can be identified with three critical parameters: Center frequency (ω_o), quality factor (Q), and attenuation at ω_o ($1/\alpha$) [27]-[28]. Based on these parameters, the transfer function of a bandstop filter can be written as:

$$\frac{V_{out}(s)}{V_{in}(s)} = \frac{s^2 + \alpha\, {\omega_o}/{Q}\, s + \omega_o^2}{s^2 + {\omega_o}/{Q}\, s + \omega_o^2} \tag{1}$$

The magnitude response of Eq. (1) is plotted in Figure 2.1, where the 3-dB frequencies ω_U and ω_L are given by

$$\omega_U = \left(1 + \frac{1}{2}\sqrt{\frac{1-2\alpha^2}{Q^2}}\right)\omega_o \tag{2}$$

$$\omega_L = \left(1 - \frac{1}{2}\sqrt{\frac{1-2\alpha^2}{Q^2}}\right)\omega_o \tag{3}$$

where

$$\omega_o = \sqrt{\omega_L \omega_U} \tag{4}$$

Bandwidth (BW) of the bandstop filter is defined by the difference of 3-dB frequencies (ω_U-ω_L), which can be expressed as:

$$BW = \omega_U - \omega_L = \frac{\omega_o}{Q}\sqrt{1-2\alpha^2} \tag{5}$$

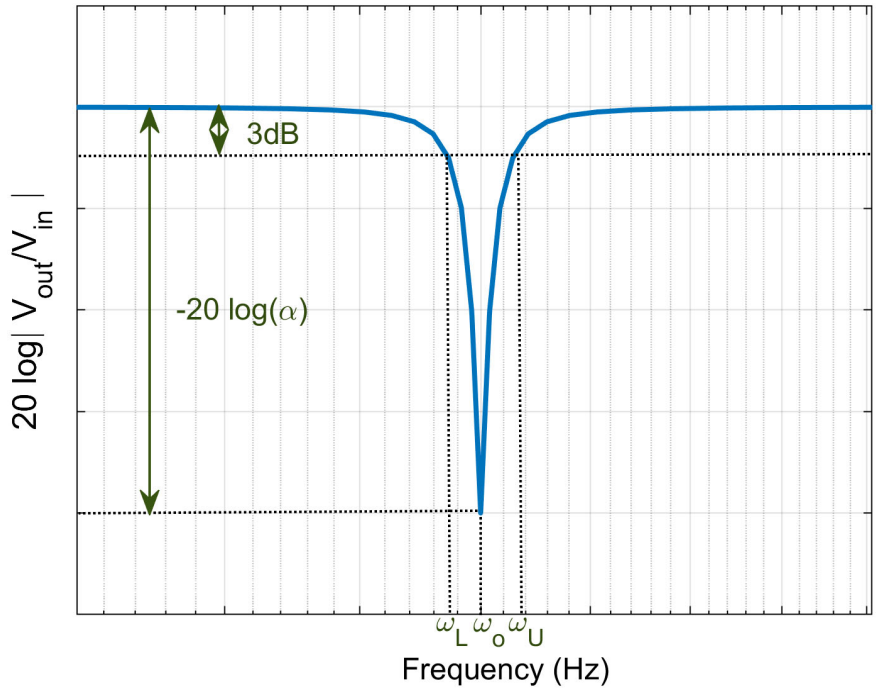

Figure 2.1 Magnitude response of a second-order bandstop filter.

Figure 2.2 shows a block diagram to implement a second-order bandstop filter, consisting of two negative-feedback loops and one feedforward path. The negative feedback loops Loop1 and Loop2 mainly determine the quality factor and the center frequency of the filter, respectively, whereas the feedforward path and the adder are used to convert the bandpass response (V_{BP}) to bandstop (V_{out}).

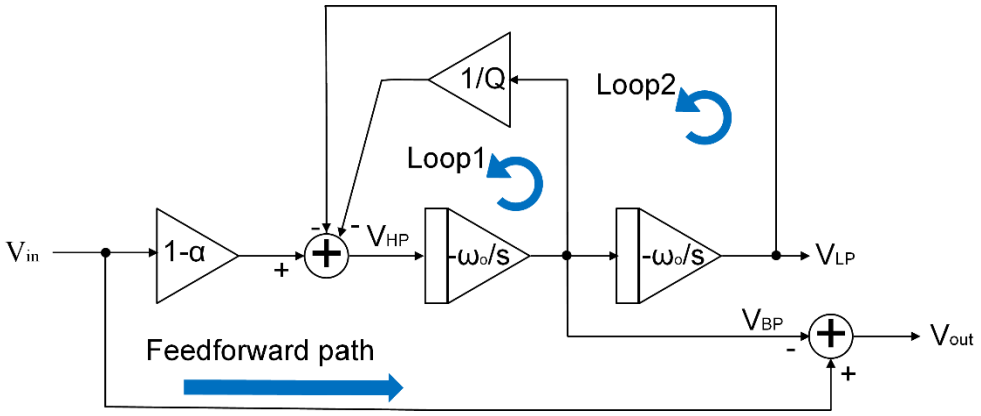

Figure 2.2 Block diagram of a second-order bandstop filter.

2.1. Bandstop Filter Topologies Reported in the Literature

2.1.1. Active-RC Filters

Figure 2.3 shows an active-RC bandstop filter based on Tow-Thomas Biquad [29], which has the following transfer function

$$\frac{V_{out}}{V_{in}} = -\frac{s^2 + \omega_o^2}{s^2 + \frac{\omega_o}{Q}s + \omega_o^2} \tag{6}$$

The expressions of ω_o and Q are obtained as:

$$\omega_o = \frac{1}{RC} \tag{7}$$

$$Q = \frac{R_Q}{R} \tag{8}$$

In [29], a bandstop filter was designed using the Tow-Thomas topology to have 60 Hz center frequency with a quality factor of 2. Although the design specification for α was zero, corresponding to infinite attenuation at the center frequency, 40 dB attenuation was

measured due to nonidealities of opamps, resulting in α=0.01. The total harmonic distortion for a 100mV input was reported as -70 dB, where the power dissipation of the filter was 150 nW.

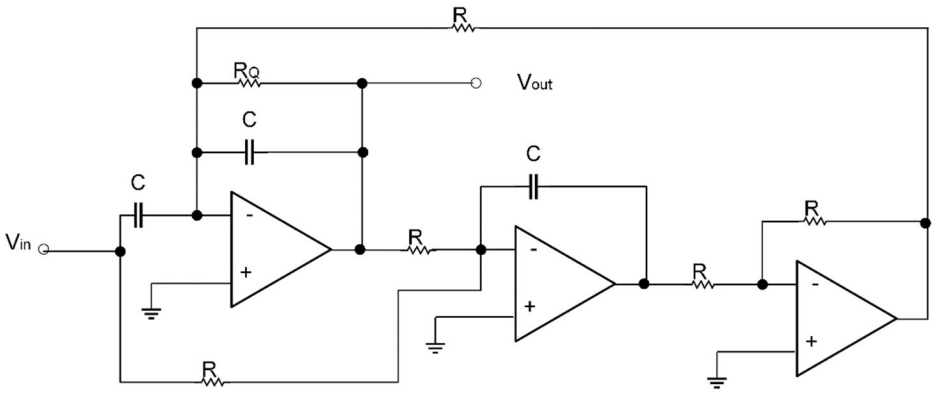

Figure 2.3 Active-RC bandstop filter, reprinted with permission from [29].

The Tow-Thomas biquad topology in Figure 2.3 can be modified to realize lowpass filters, simply by rearranging the passive components and feedforward paths, therefore similar power dissipation levels can be expected when lowpass or other types of filters are designed based on the same topology. Figure 2.4 shows the power consumption of several lowpass active-RC filters [30]-[33] based on Tow-Thomas biquad versus their pole frequencies, where a linear relationship between power dissipation and operating frequency can be observed. Consequently, second-order active-RC topology at GHz frequencies will be expected to provide power dissipation levels exceeding hundred milliwatts.

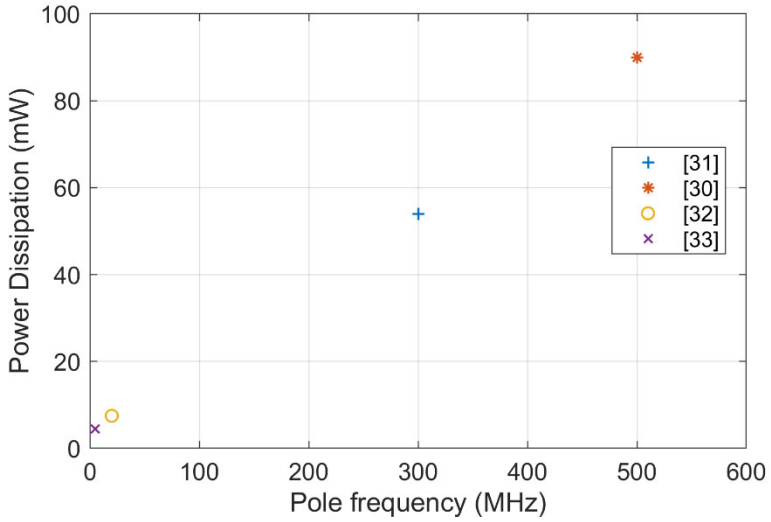

Figure 2.4 Power consumption versus center frequency among the published active RC filters

2.1.2. MOSFET-C Filters

Figure 2.5 shows the MOSFET-C bandstop filter that is implemented based on the Tow-Thomas active-RC bandstop filter by using a MOSFET as a variable resistance [34]. This filter has the same transfer function of the active-RC filter given in Eq. (6), where the resistance R in Eqs. (7) and (8) can be substituted with:

$$R = \frac{1}{\mu\, C_{ox} \frac{W}{L} (V_{Gs} - V_T)} \tag{9}$$

$$V_{Gs} = V_{bi} - V_s \text{ , i=1..6} \tag{10}$$

where μ is the mobility, C_{ox} is the oxide capacitance per unit area, and V_T is the threshold voltage.

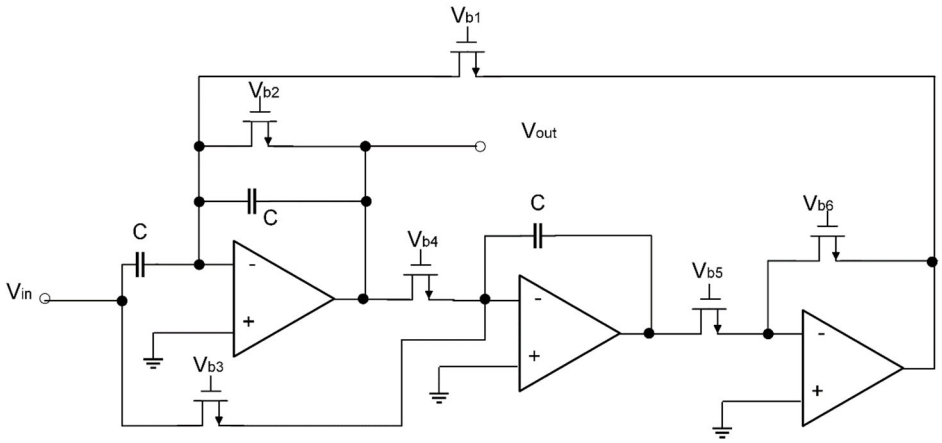

Figure 2.5 MOSFET-C bandstop filter.

Characteristics of MOSFET-C and active-RC filters are similar in terms of power dissipation and frequency of operation, whereas MOSFET-C filters provide continuous tuning capability, but lower linearity. In [33] and [35], active-RC and MOSFET-C lowpass filters are presented, respectively, based on the Tow-Thomas biquad in Fig. 2.5. Although the two filters report similar orders of bandwidth and power dissipation, the input third-order intercept point (IIP3) of the MOSFET-C filter was reported as 11 dBm, whereas the active-RC filter achieved 20 dBm.

2.1.3. G_m-C Filters

Figure 2.6 shows a typical second-order G_m-C bandstop filter. Assuming ideal transconductors, the transfer function of this filter can be written as:

$$\frac{V_{out}}{V_{in}} = \frac{g_{m5}}{g_{m6}} \frac{s^2 + \omega_o^2}{s^2 + \frac{\omega_o}{Q} s + \omega_o^2} \tag{11}$$

Assuming $g_{m1} = g_{m2}$, the expressions of ω_o and Q are obtained as:

$$\omega_o = \frac{1}{C}\sqrt{g_{m3}g_{m4}} \tag{12}$$

$$Q = \frac{1}{g_{m2}}\sqrt{g_{m3}g_{m4}} \tag{13}$$

A second-order tunable bandstop filter based on Fig. 2.6 was designed in [4], where power dissipation was reported as 12.5 mW when the center frequency was set to 278 MHz with a quality factor of 10, achieving 49 dB attenuation at the center frequency. In contrast, the active-RC bandpass filter in [31] consumed 56 mW to have 300 MHz center frequency and a quality factor of 5. In general, when compared with active-RC topology, lower levels of power dissipation can be achieved using Gm-C filter topology in sub-GHz frequencies.

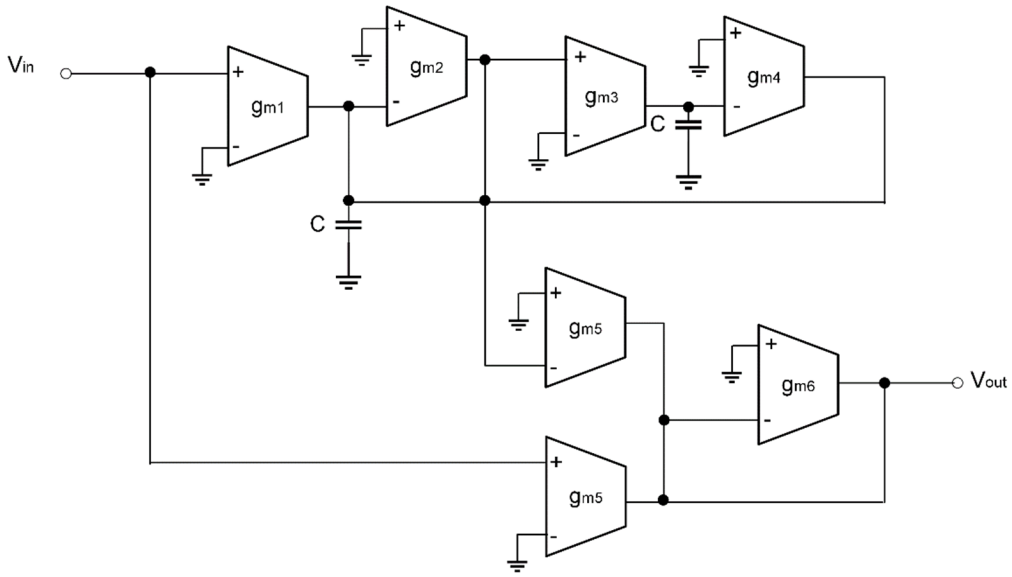

Figure 2.6 G_m-C bandstop filter, reprinted with permission from [4].

2.1.4. Active-LC Filters

A second-order active-LC bandstop filter is shown in Figure 2.7. The transfer function of this bandstop filter can be written as:

$$\frac{V_{out}}{V_{in}} = g_{m2}R_L \frac{s^2 + \alpha\frac{\omega_o}{Q}s + \omega_o^2}{s^2 + \frac{\omega_o}{Q}s + \omega_o^2} \tag{14}$$

The expressions of ω_o, Q and α are obtained as:

$$\omega_o = \sqrt{\frac{1}{LC}} \tag{15}$$

$$Q = \frac{1}{r_s}\sqrt{\frac{L}{C}} \tag{16}$$

$$\alpha = 1 - \frac{g_{m3}g_{m2}L}{g_{m1}r_sC} \tag{17}$$

where r_s is internal series resistance of the inductor.

In [11], the active-LC bandstop filter in Fig. 2.7 was designed to have 1.15 GHz center frequency with a quality factor of 46 and attenuation of 60 dB, where the power dissipation of the filter was 10 mW. The input third-order intercept point (IIP3) and 1dB compression point of the filter were 12dBm and -2dBm, respectively.

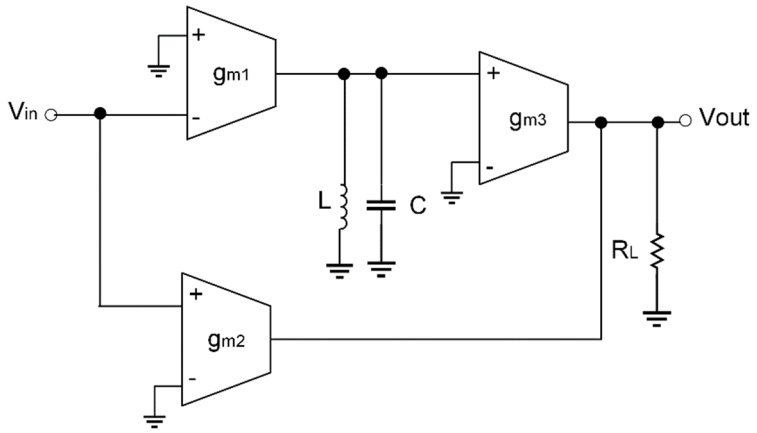

Figure 2.7 Active-LC filter, reprinted with permission from [36].

2.2. Automatic Tuning Schemes Reported in The Literature

Due to process, voltage, and temperature (PVT) variations, active continuous-time filters require an automatic tuning circuit to maintain filter parameters, such as center frequency, quality factor, and attenuation. Sections 2.3, 2.4, 2.5, and 2.6 summarize the tuning methods for filter parameters that have been reported in [19], [22], [37]-[46].

Filters with practical tuning systems cannot process the actual input and tuning reference signals simultaneously. To resolve this problem, direct or indirect techniques are used to apply tuning schemes to filters, where the most common indirect technique is the master-slave method. This technique requires two filters (master and slave) that have the same circuit implementation. The tuning circuit is connected to the master filter, whereas the slave filter is used to filter the input signal while sharing the filter control signals from the master filter. A block diagram of the master-slave scheme is shown in Figure 2.8. This method occupies a large area due to the extra filter, and its efficiency

relies on the accuracy of matching between the master and slave filter parameters, which can vary due to the fabrication tolerances [47]-[48].

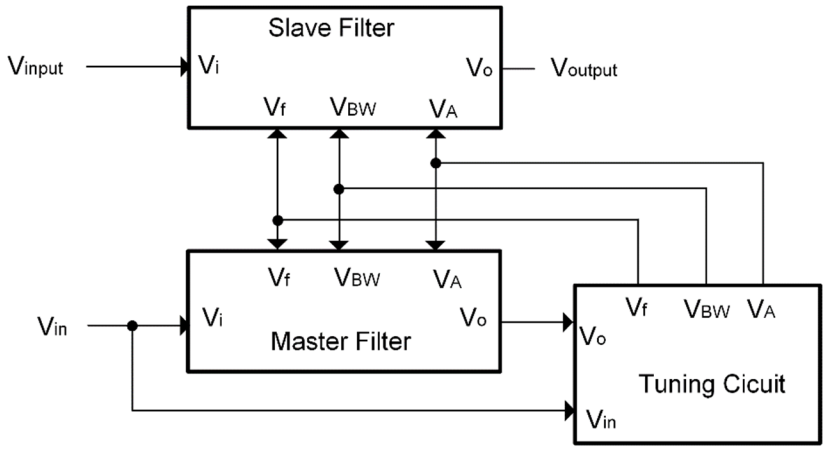

Figure 2.8 Block diagram of the master-slave tuning scheme.

Direct tuning is another technique for applying the tuning scheme as shown in Figure 2.9 [49]-[50]. The tuning process is applied directly to the filter for a certain period until the filter parameters achieve the desired values, and then disabled while holding the filter control signals. This scheme requires switches placed at the input and the output of the filter, which is used at a lower frequency to determine the tuning and filtering periods.

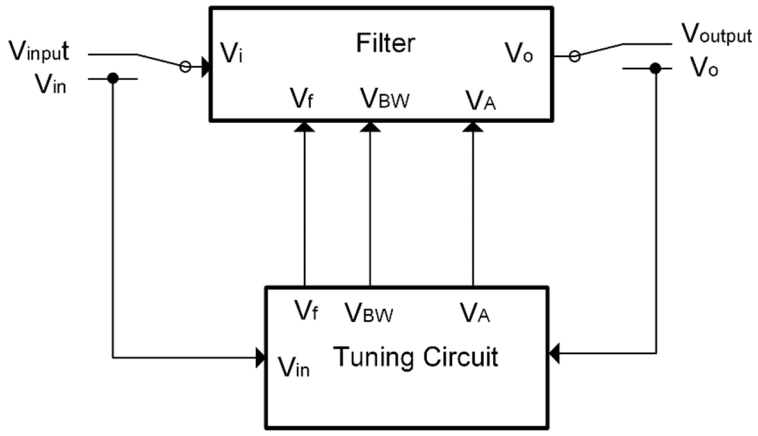

Figure 2.9 Block diagram of a direct tuning scheme.

2.3. Frequency Tuning Schemes

The literature covers many frequency tuning schemes [22], [37]-[43], such as phase locked loop (PLL) using voltage-controlled oscillator (VCO) [22] and frequency tuning based on peak detection [43]. Most of the frequency tuning schemes are applied using the master-slave method rather than the direct tuning method. The PLL using VCO technique has been reported to offer a tuning error of less than 1% [22].

2.3.1. Phase Locked Loop Using Voltage Controlled Oscillator

Figure 2.10 shows the PLL tuning scheme using a voltage-controlled oscillator. When the filter's output is connected to its input in a positive feedback configuration, a voltage-controlled oscillator (VCO) is obtained, which oscillates at the filter's center frequency. By detecting the phase/frequency difference between the reference and oscillation frequencies, the center frequency of the filter can be tuned to the desired value [22], [43]. The accuracy of this method is limited by the mismatch between the filter in

VCO and the slave filter. In [22], the tuning error was around 1% to have a 100 MHz center frequency with a quality factor of 20.

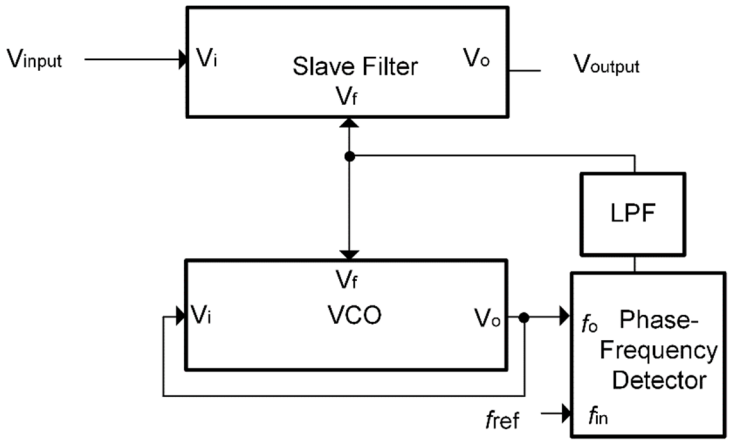

Figure 2.10 Block diagram of the phase locked loop tuning scheme using voltage-controlled oscillator, reprinted with permission from [22].

2.3.2. Frequency Tuning Based on Peak Detection

Center frequency of a second-order bandpass filter can be tuned by detecting the frequency control voltage corresponding to the peak output magnitude when a reference input at f_{ref} is applied at the desired center frequency. As illustrated in Figure 2.11, the frequency control voltage (V_f) of the master filter is swept within its valid range using V_{ramp}, where the tuning circuit detects the value of V_{ramp} at the peak output and applies it to the slave filter as V_f, tuning its center frequency to the desired value (f_{ref}). Using this method, the tuning error is reported to be less than 0.3% at a center frequency of 105 MHz with a quality factor of 32 [44].

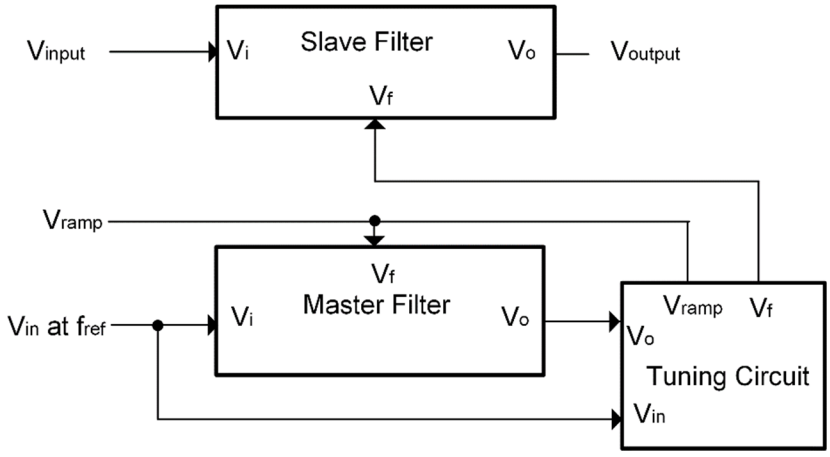

Figure 2.11 Frequency tuning based on peak detection, reprinted with permission from [51].

2.4. Quality Factor Tuning Schemes

Quality factors (Q) of filters operating at high frequencies are sensitive to filter parasitics, especially at high Q values exceeding 10. Thus, a Q-tuning scheme is necessary for such filters to adjust the quality factor. In the literature, several Q-tuning techniques have been reported [19], [22], [46].

2.4.1. Magnitude Locked Loop (MLL)

Some types of filters can be designed to exhibit a direct relationship between the quality factor and the gain at a certain frequency. The MLL method uses this information to tune the quality factor of the filter as shown in Figure 2.12 [46], where a sinusoidal signal at the desired center frequency is applied to the input of the filter. The tuning loop converges when the input and the output of the master filter have the same amplitude, setting the filter's gain and quality factor to Q_d. Some implementations, such as an active-

LC filter cannot apply this method because there is no direct relationship between the filter's gain and quality factor.

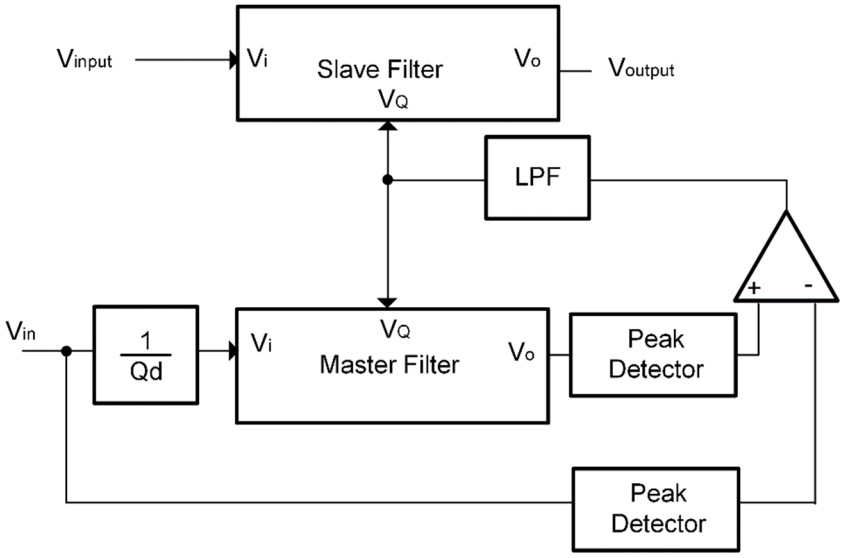

Figure 2.12 Block diagram of the magnitude locked loop scheme, reprinted with permission from [46].

2.4.2. Enhanced Adaptive Q-Tuning Scheme

Figure 2.13 shows the implementation of the enhanced adaptive Q-tuning scheme, where MLL-based Q tuning with least-mean-square (LMS) algorithm was combined with PLL-based frequency tuning scheme [22]. By simultaneously using the VCO phase for frequency detection and VCO amplitude for quality factor detection, not only a second master filter is avoided, but also Q tuning accuracy was isolated from frequency tuning errors. In addition, modification of the LMS algorithm allowed lower tuning errors due to offsets, and the harmonics of the reference signal did not affect the tuning accuracy. This

scheme has been reported to have a tuning error of less than 1% for both center frequency and quality factor at 100 MHz with a quality factor of 20 [22].

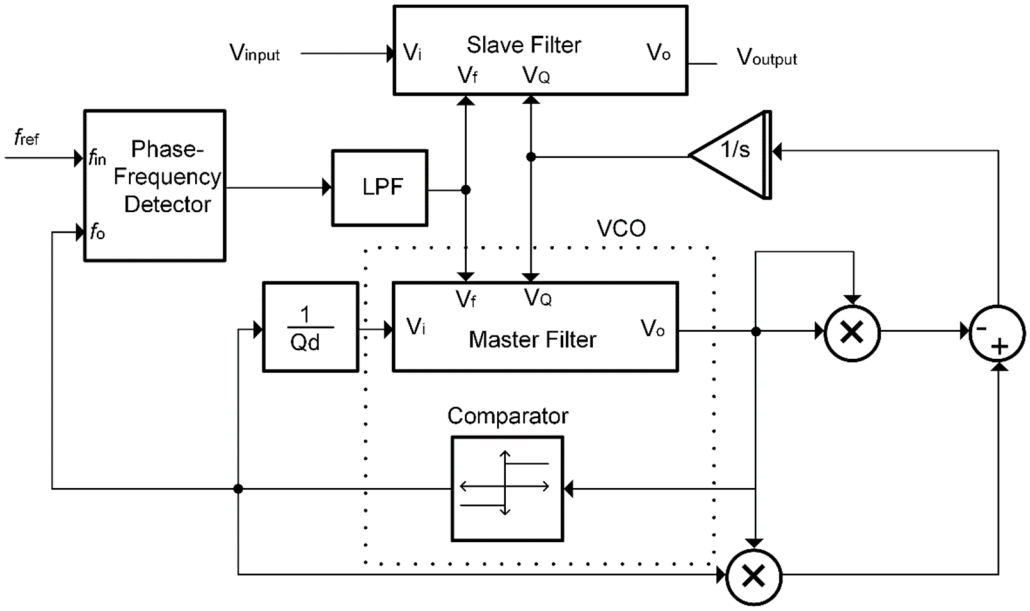

Figure 2.13 Block diagram of the enhanced adaptive Q-tuning scheme, reprinted with permission from [22].

2.4.3. Digital-Tuning Method Based on Phase Comparison

The digital tuning scheme, shown in Figure. 2.14, is based on a phase comparison to detect and tune the center frequency and quality factor [19]. The tuning scheme relies on locking the output phase of a second-order filter to known references at its 3-dB frequencies. Using binary phase comparison and digital control of tuning loops, this method allows simultaneous convergence of frequency and quality factor control loops, and was verified with 1% tuning accuracy at 5.5 MHz for Q of 20 [19].

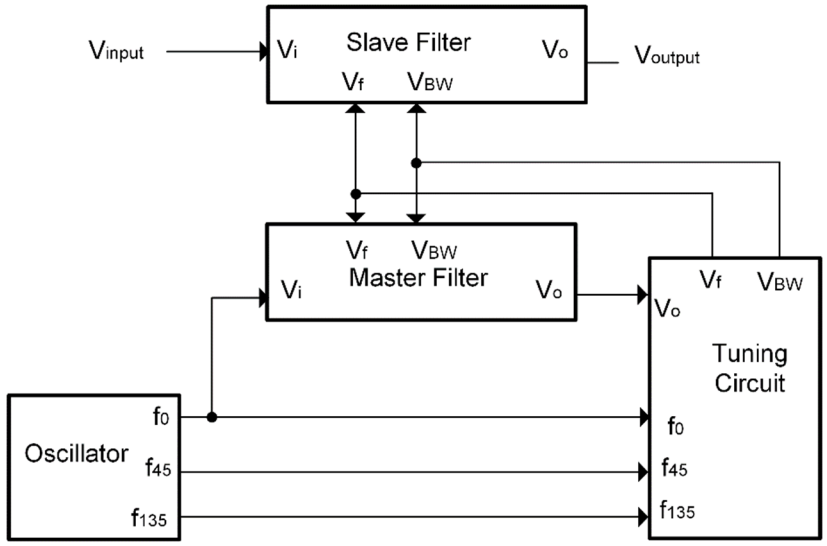

Figure 2.14 Block diagram of digital-tuning method based on a phase comparison, reprinted with permission from [19].

2.5. Attenuation Tuning Schemes

The function of the bandstop filter is to attenuate unwanted signals at the center frequency; thus, the amount of attenuation must be significant in order to make sure that the unwanted signals are rejected. Most researchers have focused on tuning the quality factor and center frequency because these parameters are necessary to characterize lowpass, highpass, and bandpass filters. Unfortunately, there are few methods for tuning attenuation, possibly because this parameter applies only to bandstop filters [47].

2.5.1. Attenuation Tuning Based on Magnitude

To detect the attenuation of a bandstop filter, first an input signal at the center frequency should be applied. The attenuation control voltage is then adjusted until the magnitude at the output of the filter is minimized [47]. Note that if the input signal is a non-ideal sinusoidal signal, it may cause an error in the attenuation loop depending on the

magnitude detection method. In addition, any frequency tuning error will significantly affect attenuation tuning.

2.5.2. Self-Tuning by Phase Feedback from Output

Block diagram of the self-tuning method by phase feedback from the filter output is shown in Figure 2.15. This tuning method is based on comparing the output of the bandstop filter with a reference signal that has a 90° phase shift [47]. When the phase of the output signal achieves 90°, it means that the bandstop filter has a large attenuation. To reach the 90° phase shift, the reference frequency should be set to:

$$\omega_{ref} = \omega_o \left(\frac{-\sqrt{\alpha}}{2Q} + \sqrt{1 + \frac{\alpha}{4Q^2}} \right) \tag{18}$$

Since the bandstop filter output amplitude is very small at the center frequency, phase detection usually causes large tuning errors using this method.

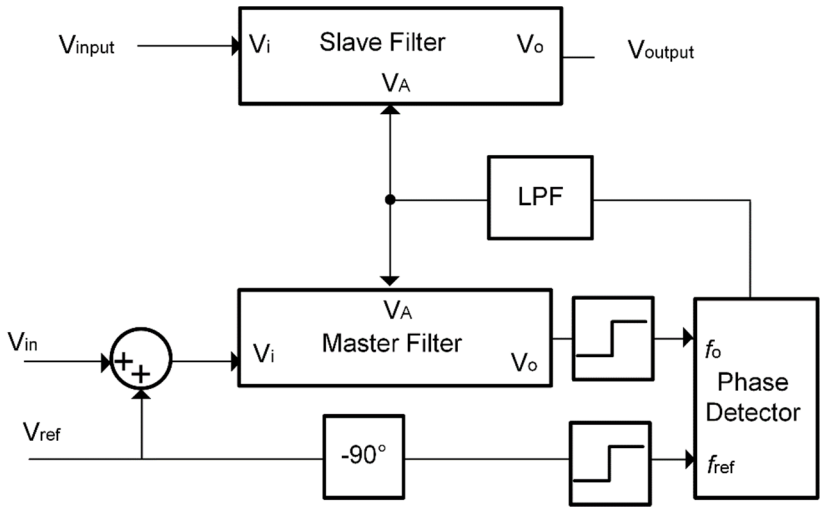

Figure 2.15 Block diagram of the attenuation tuning by the phase feedback from output, reprinted with permission from [47].

2.5.3. Self-Tuning by Phase Feedback from Intermediate Node

Figure 2.16 shows the block diagram of self-tuning method by phase feedback from an intermediate node providing the bandpass response, so that the phase at the intermediate node will be equal to 90° when the reference frequency is equal to the center frequency. Although the output amplitude is sufficiently large for phase detection, a significant drawback of this technique is that the filter design must have both bandpass and bandstop outputs [47].

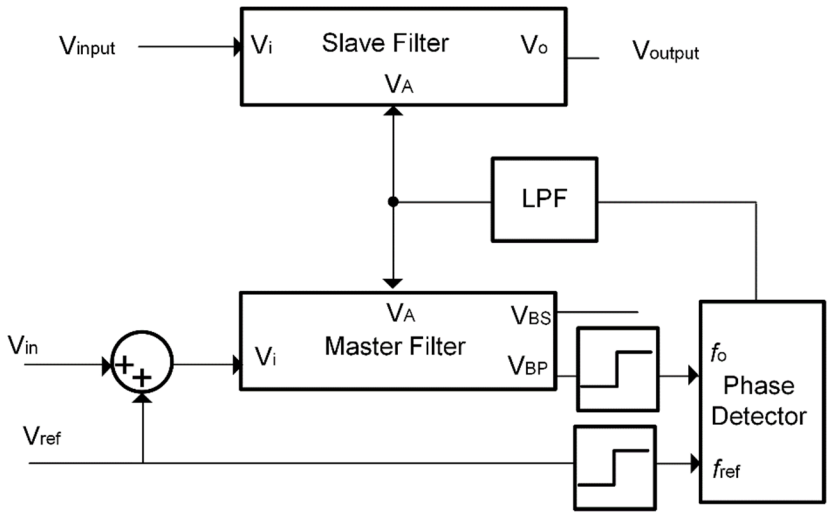

Figure 2.16 Block diagram of the attenuation tuning by the phase feedback from intermediate node, reprinted with permission from [47].

3. PROPOSED BANDSTOP [1]FILTER BASED ON SOURCE FOLLOWER*

This chapter presents the proposed second-order bandstop filter. This filter was designed for high frequency applications that require high linearity, low power and a small area. Principle of operation, circuit description, transfer function, design procedure, sensitivity, stability and linearity analysis, and simulation results are all presented herein.

3.1. Principle of Operation

Figure 3.1 shows the block diagram of the proposed design, where one negative feedback loop is formed with two forward paths to generate complex zeros for the bandstop filter.

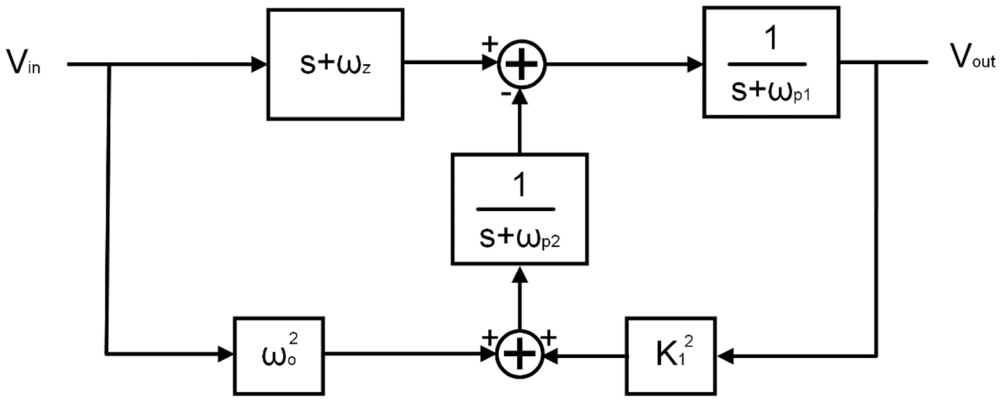

Figure 3.1 Block diagram of the proposed design.

---

* Parts of this chapter are reprinted with permission from "Fully-differential second-order tunable bandstop filter based on source follower," by Fatima Almutairi and Aydin Karsilayan, Electronics Letters, 55 (3), 122–124, 2019 and with permission from "A Tunable Bandstop Filter Based on Source Follower," by Fatima Almutairi and Aydin Karsilayan, 2019 IEEE 62nd International Midwest Symposium on Circuits and Systems (MWSCAS).

The transfer function from V_{in} to V_{out} can be written as:

$$\frac{V_{out}}{V_{in}} = \frac{s^2 + (\omega_z + \omega_{p2})s + \omega_z\omega_{p2} + \omega_o^2}{s^2 + (\omega_{p1} + \omega_{p2})s + \omega_{p1}\omega_{p2} + K_1^2} \quad (19)$$

The attenuation of the bandstop filter can be calculated as:

$$\alpha = \frac{\omega_z + \omega_{p2}}{\omega_{p1} + \omega_{p2}} \quad (20)$$

To increase the attenuation of the bandstop filter, the circuit that determines ω_{p2} must be implemented using a partial positive feedback to cancel ω_z.

3.2. Circuit Description

The proposed fully-differential second-order bandstop filter based on a source follower is shown in Figure 3.2. This filter is composed of a super-source follower with feed-forward paths and a partial positive feedback [26], [52]. The super-source follower is composed of transistors M_a and M_c, as well as current sources I_a, I_{c1}, and I_{c2}, where I_{c2} is added to control the transconductance of M_c. The feed-forward path provided by C_c generates the zero for the bandstop filter. The positive feedback is implemented by the cross-coupled M_b transistors, which are used to enhance the quality factor.

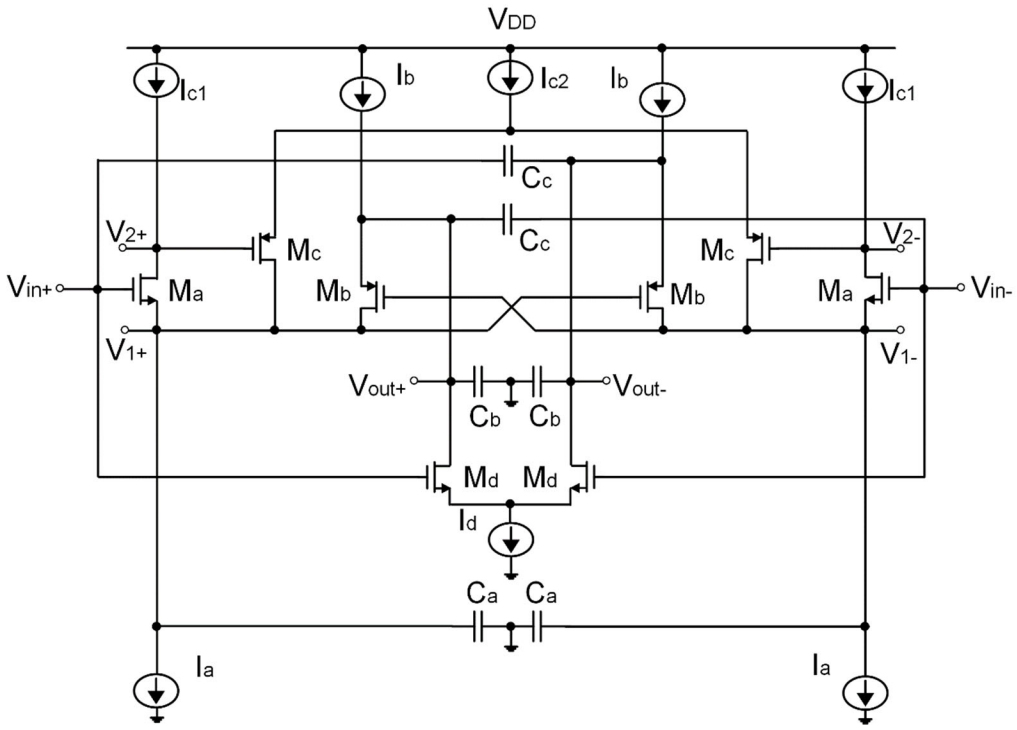

Figure 3.2 Proposed bandstop filter, reprinted with permission from [52].

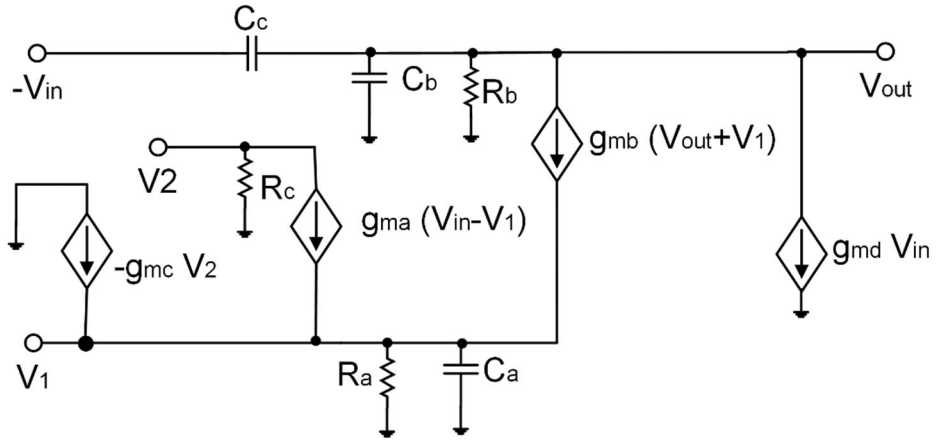

Figure 3.3 Small signal equivalent circuit of the bandstop filter, reprinted with permission from [52].

Figure 3.3 shows the small-signal equivalent circuit of the proposed bandstop filter. Nodal equations at V_1, V_2, and V_{out} can be written as:

$$V_1 = \frac{V_2}{g_{ma}R_c} + V_{in} \tag{21}$$

$$V_2 = \frac{g_{ma}V_{in} + g_{mb}V_{out} - \left(-g_{mb} + g_{ma} + sC_a + {}^1/_{R_a}\right)V_1}{g_{mc}} \tag{22}$$

$$V_{out} = \frac{(sC_c + g_{md})V_{in} - g_{mb}V_1}{s(C_b + C_c) + \left(g_{mb} + {}^1/_{R_b}\right)} \tag{23}$$

where R_a, R_c, and R_b are equivalent resistances at nodes V_1, V_2, and V_{out}, respectively. The transconductances of M_a, M_b, M_c, and M_d are given as g_{ma}, g_{mb}, g_{mc}, and g_{md}, respectively, where $g_{mb} >> 1/R_b$ and $g_{ma} >> 1/R_a$.

From Eqs. (21), (22), and (23), transfer functions from V_{in} to V_1, V_2 and V_{out} can be obtained by:

$$\frac{V_1}{V_{in}} = -\frac{s\left(\frac{g'_{ma}}{C_a} - \frac{C_c}{C'_c C_a}g_{mb}\right) + \frac{g_{mb}(g'_{ma} - g_{md})}{C'_c C_a}}{s^2 + BWs + \omega_o^2} \tag{24}$$

$$\frac{V_2}{V_{in}} = -R_c g_{ma}\frac{s^2 + \left(\frac{g_{mb}(C_c - C'_c + C_a)}{C'_c C_a}\right)s + \frac{g_{md}g_{mb}}{C'_c C_a}}{s^2 + BWs + \omega_o^2} \tag{25}$$

$$\frac{V_{out}}{V_{in}} = -K_1\frac{s^2 + \alpha BWs + \omega_o^2}{s^2 + BWs + \omega_o^2} \tag{26}$$

where:

$$K_1 = \frac{C_c}{C'_c} \tag{27}$$

$$\omega_o = \sqrt{\frac{g'_{ma} g_{mb}}{C_a C'_c}} \tag{28}$$

$$BW = \frac{g_{mb} C_a + C'_c (g'_{ma} - g_{mb})}{C_a C'_c} \tag{29}$$

$$\alpha = \frac{g_{md} C_a + C_c (g'_{ma} - g_{mb})}{g_{mb} C_a + C'_c (g'_{ma} - g_{mb})} \tag{30}$$

$$g'_{ma} = g_{ma}(1 + R_c g_{mc}) \tag{31}$$

$$C'_c = C_c + C_b \tag{32}$$

The center frequency of the bandstop filter given in Eq. (28) can be tuned by C_a or g_{ma}. The variable C_a can then be implemented using a switched capacitor bank or a varactor [53], whereas g_{ma} is controlled by the biasing current (I_{c1}) [54], and g_{ma} is expressed as:

$$g_{ma} = \sqrt{2 I_{c1} \mu_n C_{ox} \left(\frac{W_a}{L_a}\right)} \tag{33}$$

Attenuation, bandwidth (BW) of the bandstop filter can be tuned using g_{md} and g_{mb} through current sources I_d and I_b, respectively, as follows:

$$g_{md} = \sqrt{I_d \mu_n C_{ox} \left(\frac{W_d}{L_d}\right)} \tag{34}$$

$$g_{mb} = \sqrt{2(I_b - I_d) \mu_p C_{ox} \left(\frac{W_b}{L_b}\right)} \tag{35}$$

3.3. General Design Considerations

The bandstop filter was designed for wideband receivers and intended to attenuate signal with a frequency equal to 2 GHz. Table 3.1 shows the specifications of the proposed filter.

Table 3.1 Filter specifications

Specification	Value
Bandwidth	380MHz
Attenuation	>40 dB
Center Frequency	2 GHz
K_1	1

The filter parameters can be calculated using Eqs. (27-30) and Table 3.1. Table 3.2 shows the values of the filter's parameters. The frequency response of the bandstop filter at nodes V_1, V_2, and V_{out} is shown in Figure 3.4.

Table 3.2 Filter parameters.

Parameter	Value
g_{ma}	1 mS
g_{mb}	2.4 mS

Table 3.2 Continued.

Parameter	Value
g_{mc}	400 µS
g_{md}	1.76 mS
R_a	10 kΩ
R_b	1 kΩ
R_c	350 Ω
C_a	100 fF
C_b	20 fF
C_c	140 fF

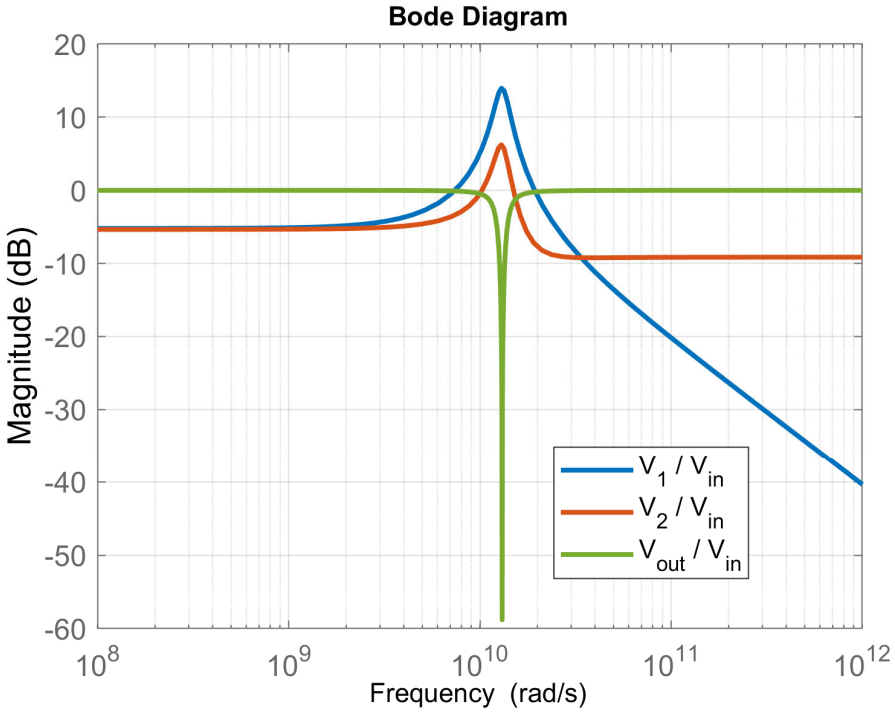

Figure 3.4 Frequency response of the proposed filter.

3.4. Stability

One of the most important constraints for a bandstop filter is its stability, which can either be investigated by determining the phase margin of the open loop or by locating the poles of the transfer function of the bandstop filter.

The block diagram in Figure 3.5 represents the proposed bandstop filter illustrated in Figure 3.2. As shown in Figure 3.5, the system was given two feedback loops: the first is a unity negative feedback loop, and the second is a negative feedback loop with gain.

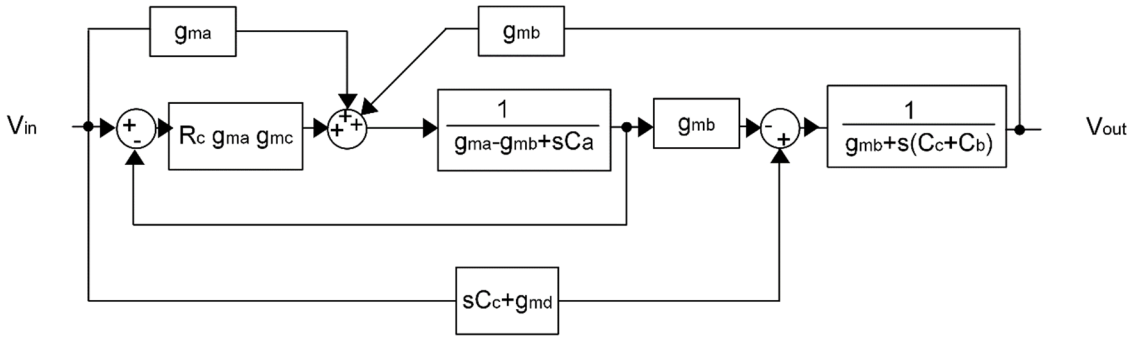

Figure 3.5 Block diagram of the proposed filter.

The loop gain transfer function was determined by using the block diagram reduction and setting the input voltage source to zero. The proposed filter consists of two loops as portrayed in Figure 3.5. The first loop can be determined when the loop breaks after (R_C g_{ma} g_{mc}). The loop gain transfer function is written as:

$$G_{Loop_1}(s) = \frac{-R_c g_{ma} g_{mc}(g_{mb} + sC'_c)}{(a_1 s^2 + a_2 s + a_3)} \qquad (36)$$

where:

$$a_1 = C_a C'_c \tag{37}$$

$$a_2 = C_a g_{mb} + C'_c(g_{ma} - g_{mb}) \tag{38}$$

$$a_3 = g_{ma} g_{mb} \tag{39}$$

Assuming $|\omega_{p2}| >> |\omega_{p1}|$, the poles and zero of the loop gain transfer function can be expressed as:

$$\omega_{p1} \approx \frac{g_{ma} g_{mb}}{g_{mb} C_a + C'_c(g_{ma} - g_{mb})} \tag{40}$$

$$\omega_{p2} \approx \frac{g_{mb}}{C'_c} + \frac{(g_{ma} - g_{mb})}{C_a} \tag{41}$$

$$\omega_{z1} \approx \frac{g_{mb}}{C'_c} \tag{42}$$

The second loop can be determined when the loop breaks before g_{mb}. The loop gain transfer function is written as:

$$G_{Loop_2}(s) = \frac{{g_{mb}}^2}{\big(g_{mb} + s(C_b + C_c)\big)(g'_{ma} - g_{mb} + sC_a)} \tag{43}$$

The frequency response of the loops gain transfer function are shown in Figure 3.6. The phase margin can be calculated by determining the phase difference between the phase of the loop gain at the gain crossover frequency and 180°. The DC gain of the first loop is 2.9 dB with a phase margin equal to 60° and the DC gain of the first loop is 5.6 dB with a phase margin equal to 5°, as shown in Figure 3.6.

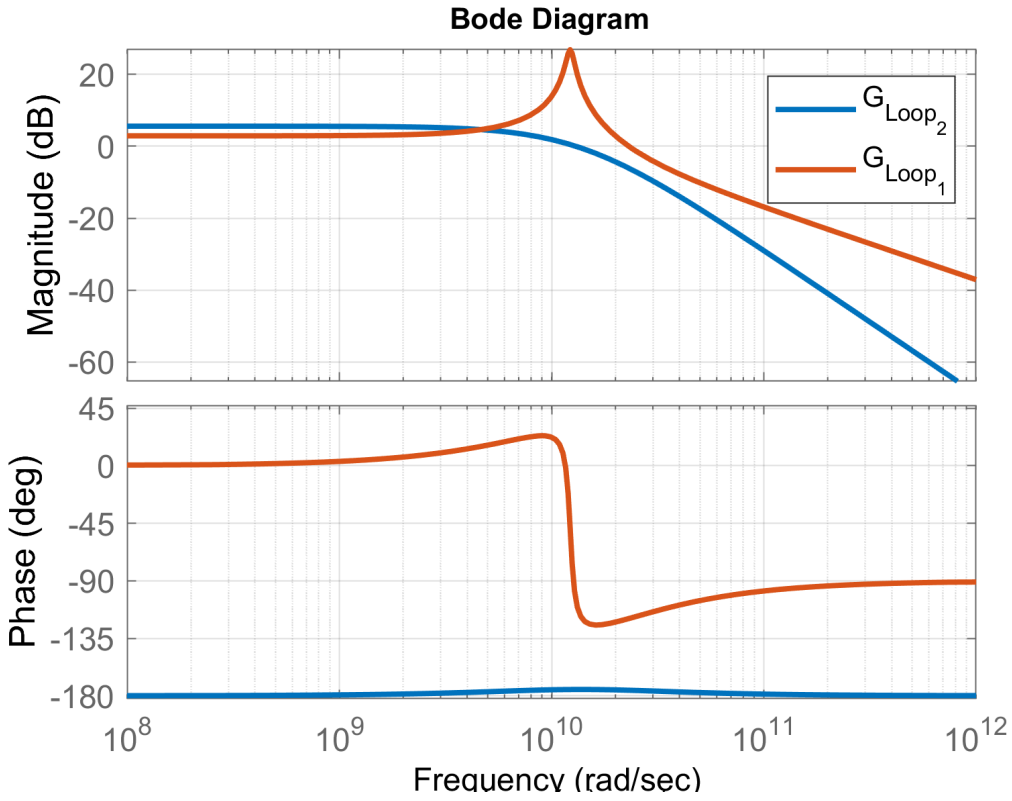

Figure 3.6 Frequency response of loop transfer functions.

Routh-Hurwitz criterion is used to determine the stability of the transfer function, indicated by the pole locations in the complex s-plane. The characteristic polynomial of Eq. (26) is:

$$s^2 + BWs + \omega_o^2 \tag{44}$$

where:

$$BW = \frac{g_{mb}C_a + C'_c(g'_{ma} - g_{mb})}{C_a C'_c} \tag{45}$$

$$\omega_o^2 = \frac{g'_{ma}g_{mb}}{C_a C'_c} \tag{46}$$

To ensure the stability of the filter, the poles of the system should be on the left half of the s-plane, which requires the following condition to satisfied:

$$g_{mb} < \frac{C'_c g'_{ma}}{(C'_c - C_a)} \tag{47}$$

3.5. Noise and Linearity

Noise of the filter can be calculated based on input-referred noise voltage sources of transistors. In general applications, both thermal and flicker noise components need to be included of the transistors [55]. The flicker and thermal noise densities were modeled as voltage sources, which are written as:

$$V_f^2 = \frac{K_f \, g_{mi}}{C_{ox}^2 W_i L_i f} \tag{48}$$

$$V_{th}^2 = \frac{8K_i \, T}{3g_{mi}} \tag{49}$$

where T is the absolute temperature, K is the Boltzmann constant, and g_m is the transconductance of the transistor.

Flicker noise sources will be ignored for the proposed filter due to high frequency of operation. The equivalent input referred noise voltage in Figure. 3.2 can be written as:

$$\overline{V_{n,in}^2} = \frac{16KT}{3}\left(\frac{g_{m,Ib}}{g_{md}^2} + \frac{1}{g_{md}} + \frac{1}{g_{ma}} + \frac{g_{mc}}{R_c^2 g_{mc}^2 g_{ma}^2} + \frac{g_{m-Ic1}}{g_{ma}^2} + \frac{g_{mb}}{g_{mc}^2} + \frac{g_{m-Ia}}{R_c^2 g_{mc}^2 g_{ma}^2}\right) \tag{50}$$

The integrated input referred noise up to the notch frequency (ω_o) can be expressed as:

$$V_{noise,in}^2 = \overline{V_{n,in}^2}\sqrt{\frac{g_{mb}(1+R_c g_{mc})g_{ma}}{C_a(C_c+C_b)}} \tag{51}$$

Figure 3.7 shows amplitude spectral densities of individual noise sources reflected at the output as functions of frequency. The dominant noise at low frequencies is the thermal noise of M_b, whereas noise contributions of I_a, I_b, M_a, and M_b dominant around the center frequency.

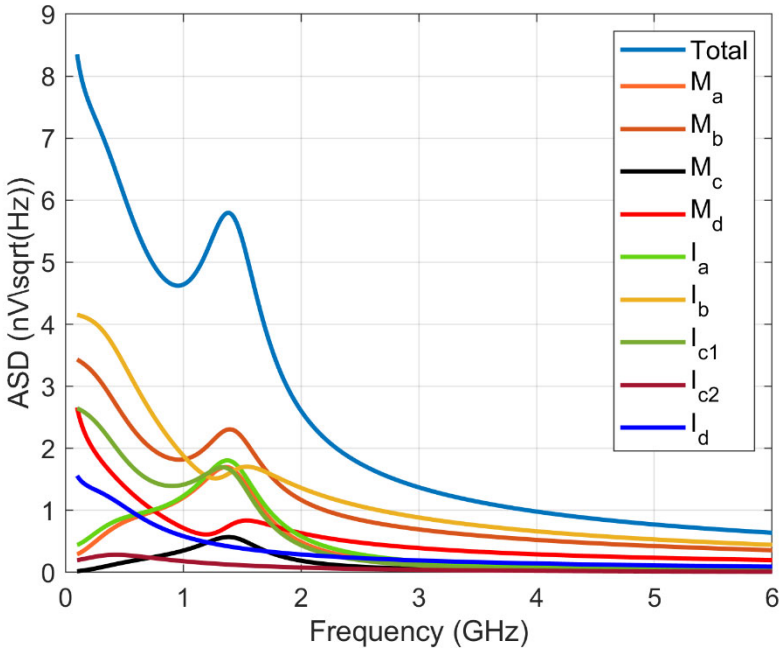

Figure 3.7 Output referred noise of the second-order bandstop filter, reprinted with permission from [52].

A common mode feedback (CMFB) circuit was used to adjust one of the biasing currents, maintaining and stabilizing the output voltage at the preset DC level. As shown in Figure 3.8, the CMFB circuit consists of the common mode detector and a differential

amplifier [56]. The common mode detector is used to sense the output common mode voltage. A differential amplifier is an error amplifier in which the output voltage of the error amplifier is used to modify I_a and sets the output voltage to V_{CM}. The R_{CM} and C_{CM} are used to improve the phase margin of the CMFB loop.

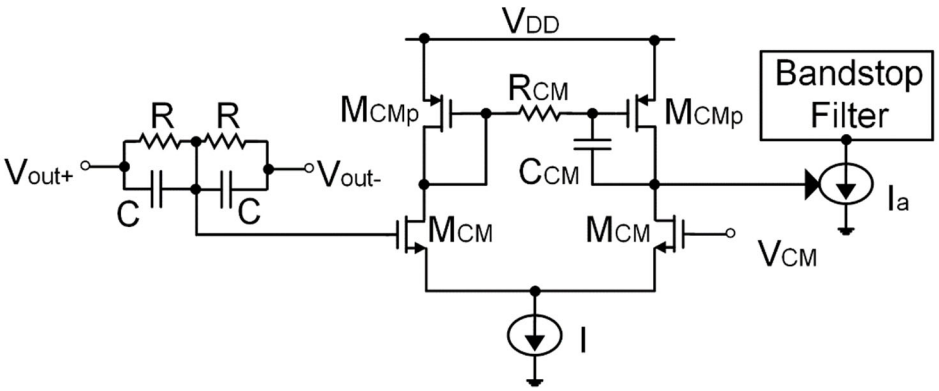

Figure 3.8 Continuous-time CMFB circuit, reprinted with permission from [26].

The common mode feedback loop transfer function $G_{CM}(s)$ is written as:

$$G_{CM}(s) = \frac{K_{CM}\left(\frac{s}{\omega_z}+1\right)}{\left(\frac{s^2}{\omega_o^2}+\frac{s}{Q\omega_o}+1\right)\left(\frac{s}{\omega_{p1}}+1\right)\left(\frac{s}{\omega_{p2}}+1\right)} \tag{52}$$

where:

$$\omega_z = \frac{1}{2\left(R_{CM}+\frac{1}{g_{mCMp}}\right)C_{CM}} \tag{53}$$

$$\omega_{p1} = \frac{\left(g_{oCMp}+g_{oCM}\right)}{C_{CM}R_{CM}g_{mCMp}} \tag{54}$$

$$\omega_{p2} = \frac{g_{oCMp}}{C_o} \tag{55}$$

$$K_{CM} = \frac{g_{mIa}g_{mCM}}{(g_{oCMp} + g_{oCM})g_{ma}\left(1 + \frac{g_{mc}}{g_{oIc1} + g_{oa}}\right)} \tag{56}$$

where g_{mCM} and g_{mCMp} are transconductances of M_{CM} and M_{CMp}, respectively, and g_{oCM} and g_{oCMp} are output conductances of M_{CM} and M_{CMp}, $C_o=2C_{gs,a}+C_{db,CM}+C_{db,CMp}$. The frequency response of the CMFB and step response of the closed loop system are shown in Figures 3.9 and 3.10, respectively.

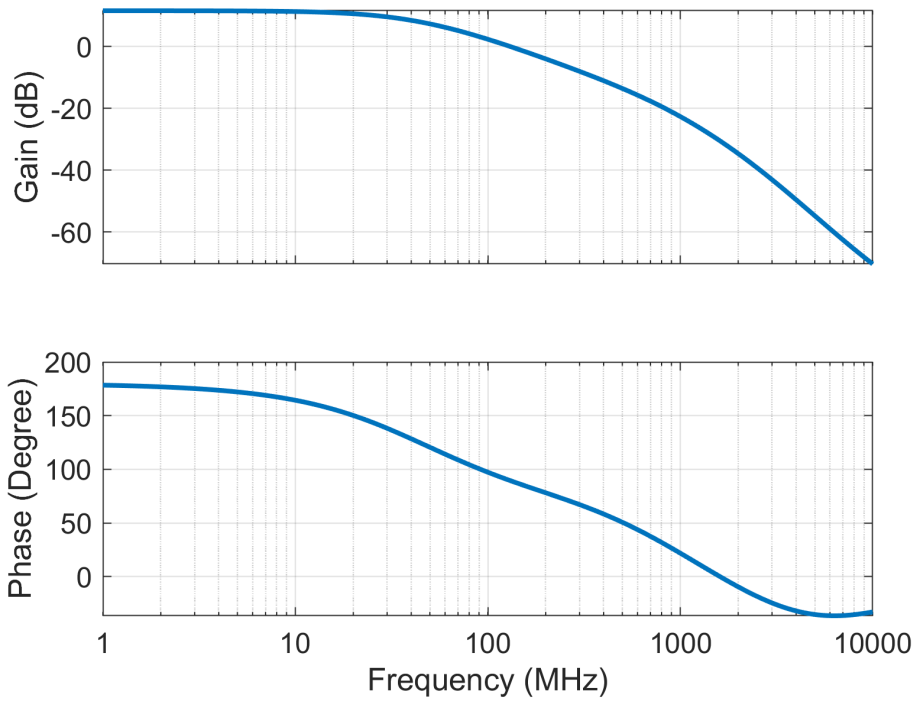

Figure 3.9 Magnitude and phase response of the CMFB loop.

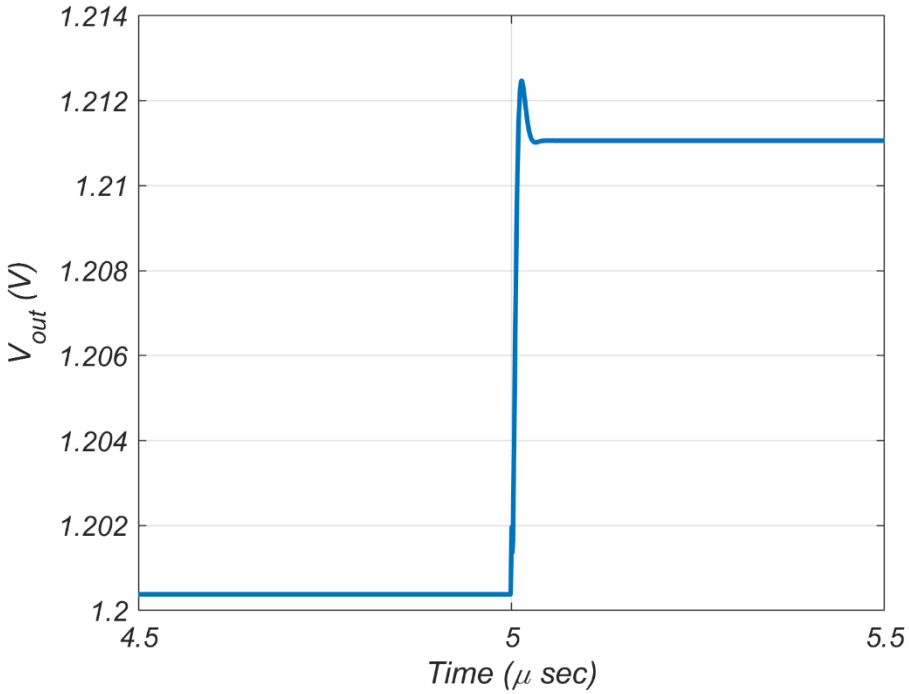

Figure 3.10 Step response of the CMFB loop.

The linearity of the filter could be maximized by setting the common mode level to achieve the maximum output swing. The common mode voltage level (V_{CM}) and maximum output swing are written as:

$$V_{CM} = V_{DD} - V_{OVb} - V_{THn} \tag{57}$$

$$V_{o,0-P} = V_{THn} \tag{58}$$

The non-linearity of the MOS transistor came from the square law of the MOSFET model used to convert voltage to current. The drain currents of M_a, M_b and M_d can be expressed as:

$$I_{Drain,a} = K_a(V_{in} + V_{CM} - V_{THn} - V_1)^2 \tag{59}$$

$$I_{Drain,b} = K_b\left(V_{out} + V_{CM} - \left|V_{THp}\right| + V_1\right)^2 \tag{60}$$

$$I_{Drain,d} = K_d(V_{in} + V_{CM} - V_{THn} - V_{OVd})^2 \tag{61}$$

The currents I_a-$I_{c2}/2$ and I_b are written as:

$$I_a - I_{c2}/2 = I_{Drain,a} + I_{Drain,b} \tag{62}$$

$$I_b = I_{Drain,d} + I_{Drain,b} \tag{63}$$

where V_{OVd} is the minimum voltage required to maintain the MOS in the saturation region, $K_i = \left(\frac{W_i}{L_i}\right)\mu_{n,p}C_{ox}$ and $i = a, b, c\ and\ d$.

From Eqs. (62) and (63), Eq. (64) shows the expression of V_{out}.

$$V_{out} = \frac{-K_d V_{in}\sqrt{\frac{I_d}{K_d} - \left(\frac{V_{in}}{2}\right)^2}}{K_b\left(2V_{CM} - V_{THn} - |V_{THp}| + \frac{K_d}{K_a}\sqrt{\frac{I_d}{K_d} - \left(\frac{V_{in}}{2}\right)^2}\right)} \tag{64}$$

Using the Taylor series expansion of Eq. (64), V_{out} can be expressed as:

$$v_{out} = a_0 + a_1 V_{in} + a_2 V_{in}^2 + a_3 V_{in}^3 \tag{65}$$

where,

$$a_1 = \frac{-K_d\sqrt{\frac{I_d}{K_d}}}{K_b\left(2V_{CM} - V_{THn} - |V_{THp}| + \frac{K_d}{K_a}\sqrt{\frac{I_d}{K_d}}\right)} \tag{66}$$

$$a_2 = 0 \tag{67}$$

$$a_3 = \frac{3K_d\left(K_d\sqrt{\frac{I_d}{K_d}} - K_a\left(2V_{CM} - V_{THn} - V_{THp} + \frac{K_d}{K_a}\sqrt{\frac{I_d}{K_d}}\right)\right)}{4K_bK_a\sqrt{\frac{I_d}{K_d}}\left(2V_{CM} - V_{THn} - |V_{THp}| + \frac{K_d}{K_a}\sqrt{\frac{I_d}{K_d}}\right)^2} \tag{68}$$

From Eqs. (65), the input intercept point (IIP3) can be written as:

$$IIP3 = \sqrt{\frac{3}{4}\frac{|a_1|}{|a_3|}} \tag{69}$$

According to Eqs. (66), (68) and (69), a better linearity could be achieved by using a larger V_{CM}. However, in order to keep all the transistors working in saturation, the boundaries of V_{CM} are written as:

$$V_{OV_{Ia}} + V_{OV_b} + \left|V_{THp}\right| - V_{THn} \leq V_{CM} \leq V_{DD} + V_{OV_{Ib}} \tag{70}$$

Furthermore, linearity could be improved by increasing I_d, causing an increase in the power consumption. The power consumption is expressed as:

$$P_{consumption} = V_{DD}(I_d + 2I_a) \tag{71}$$

3.6. Input and Output Impedance

The output impedance for the proposed filter is written as:

$$Z_{out} = \frac{\frac{s}{C_b} + \frac{g'_{ma} - g_{mb}}{C_a C_b}}{s^2 + s\left(\frac{g'_{ma} - g_{mb}}{C_a} + \frac{g_{mb}}{C_b}\right) + \frac{g'_{ma} g_{mb}}{C_a C_b}} \tag{72}$$

which can be approximated to $1/g_{mb}$ at low frequencies.

The input impedance for the proposed filter can be written as:

$$Z_{in} \approx \frac{s^2 + BWs + \omega_o^2}{sC_c\left((1 - K_1)s^2 + (1 - K_1\alpha)BWs + (1 - K_1)\omega_o^2\right)} \tag{73}$$

3.7. Simulation Results

The performance of the proposed second-order bandstop filter was determined using a 180 nm CMOS technology. The supply voltage was 1.8 V, with the transistor ratios

given in Table 3.3. The center frequency of the bandstop filter was tuned between 1 GHz and 1.7 GHz, using different values for the capacitor (C_1) or biasing current (I_{c1}), as shown in Figures 3.11 and 3.12, respectively. Notably, the bandwidth and attenuation in the bandstop filter changed because they depend on the value of C_1 and g_{m1}. Figure 3.13 also shows the bandwidth of the proposed filter as varied by the current source (I_b) where the bandwidth was varied between 250 MHz to 475 MHz. The center frequency and attenuation in the bandstop filter also varied depending on the value of g_{m2}. The biasing current (I_d) was used to tune the attenuation of the bandstop filter, as shown in Figure 3.14.

The frequency responses of all the nodes at the bandstop filter are shown in Figure 3.15. Figure 3.16 shows the IIP3 for two tones spaced by 2 MHz. The linearity of the filter was reduced at 1.5 GHz, due to the peaking at node V_2 (as shown in Figure 3.15), which limited the output swing. Also, the input referred noise spectral density attained was 5.8 nV\√Hz. Figure 3.17 shows the 1 dB compression point at a 1.2 GHz input signal (14 dBm). The total harmonic distortion was measured, achieving 40 dB with a 0.6325 output signal at a 1.2 GHz input frequency, as shown in Figure 3.18. The filter performance is summarized in Table 3.4.

Table 3.3 Filter Design Parameters, reprinted with permission from [52]

M_a	3.5µ/0.2µ
M_b	15.25µ/0.36µ
Mc	15µ/0.36µ
Md	0.8µ/0.18µ

Table 3.3 Continued

I_a (A)	455µ
I_b (A)	211µ
I_{c1} (A)	140µ
I_{c2} (A)	104µ
I_d (A)	152µ
C_1 (F)	100f
C_2 (F)	50f
C_3 (F)	200f

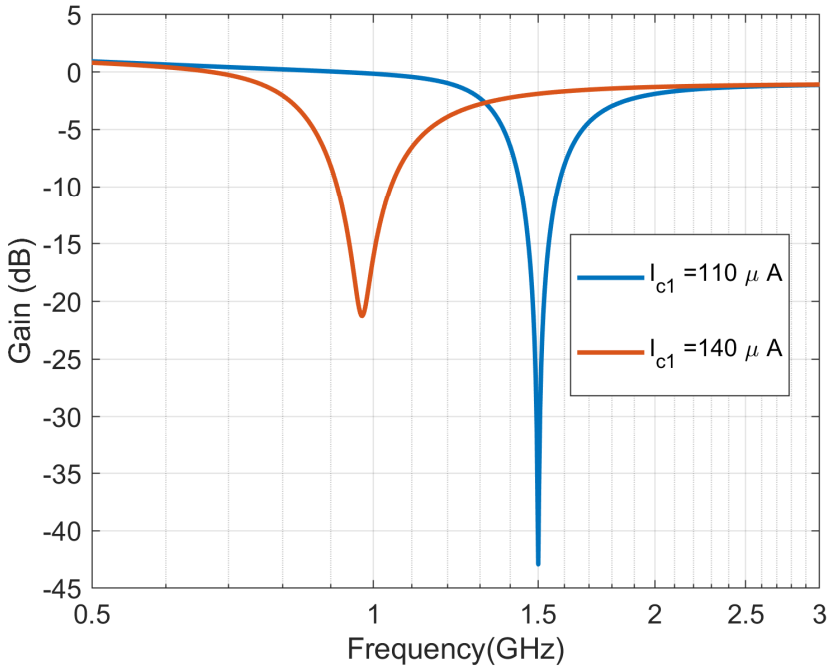

Figure 3.11 Frequency response of the tunable bandstop filter using I_{c1} to tune ω_o, reprinted with permission from [52].

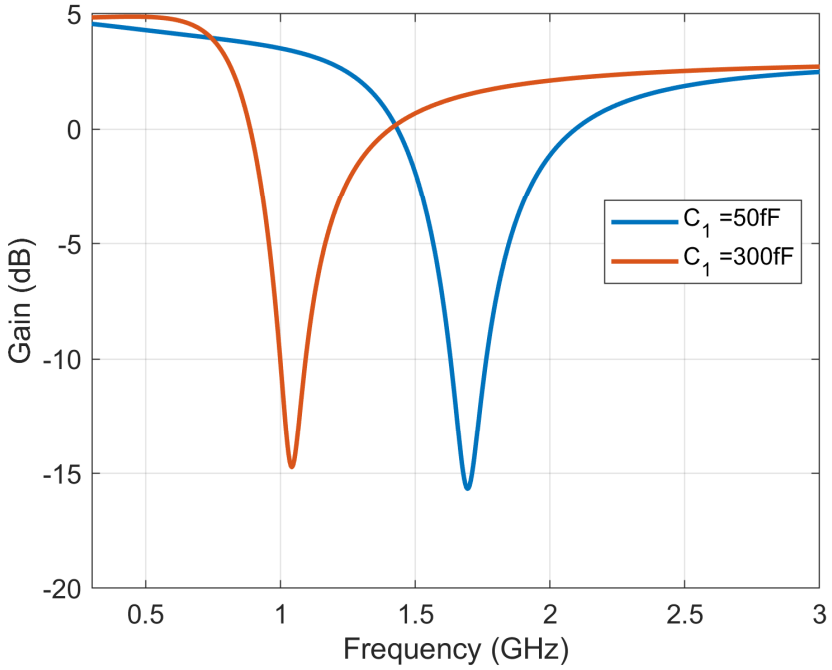

Figure 3.12 Frequency response of the tunable bandstop filter using C_1 to tune ω_o, reprinted with permission from [52].

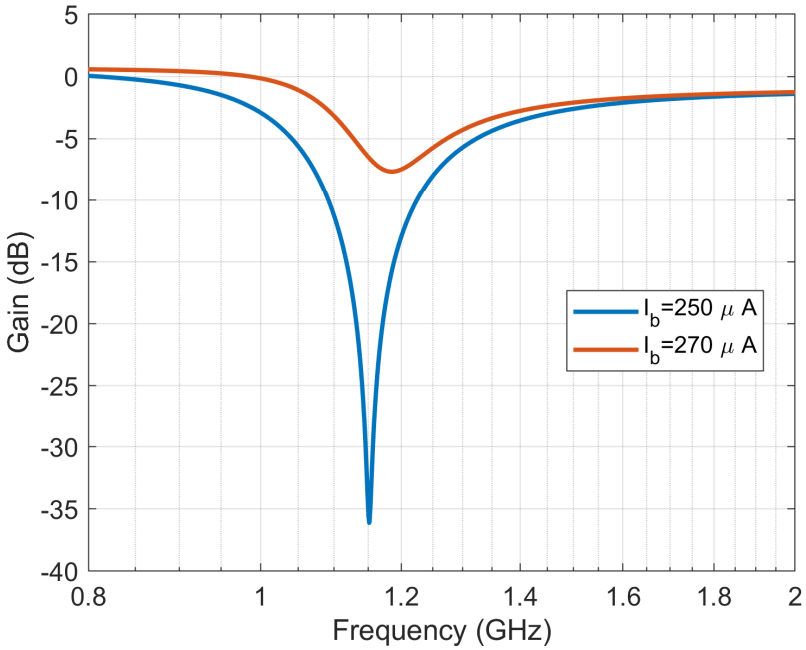

Figure 3.13 Frequency response of the tunable bandstop filter using I_b to tune BW, reprinted with permission from [52].

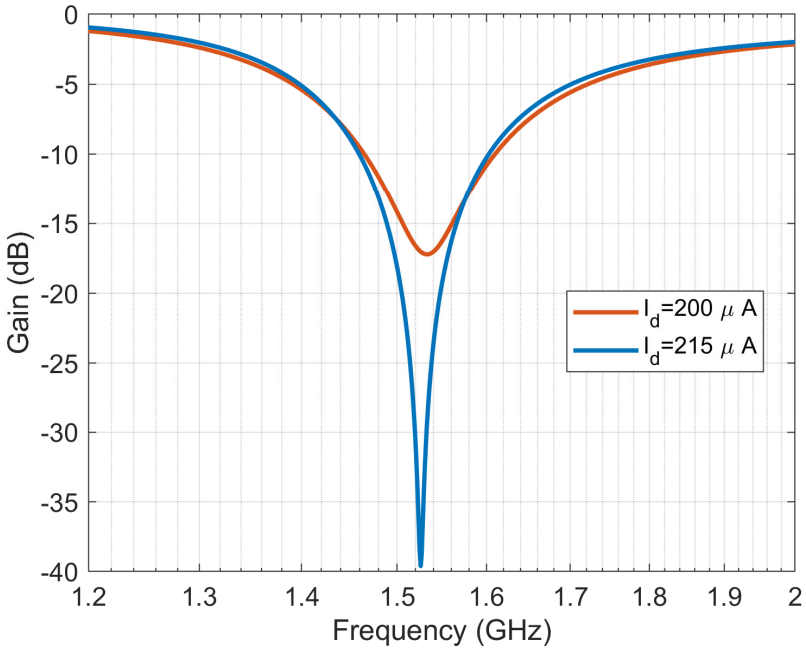

Figure 3.14 Frequency response of the tunable bandstop filter using I_d to tune α, reprinted with permission from [52].

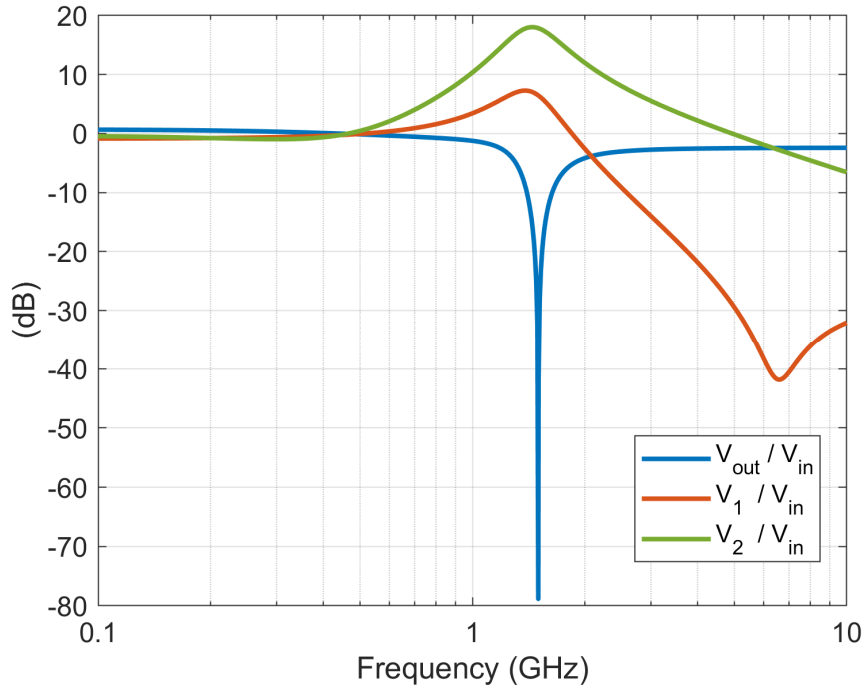

Figure 3.15 Frequency response of the second-order bandstop filter.

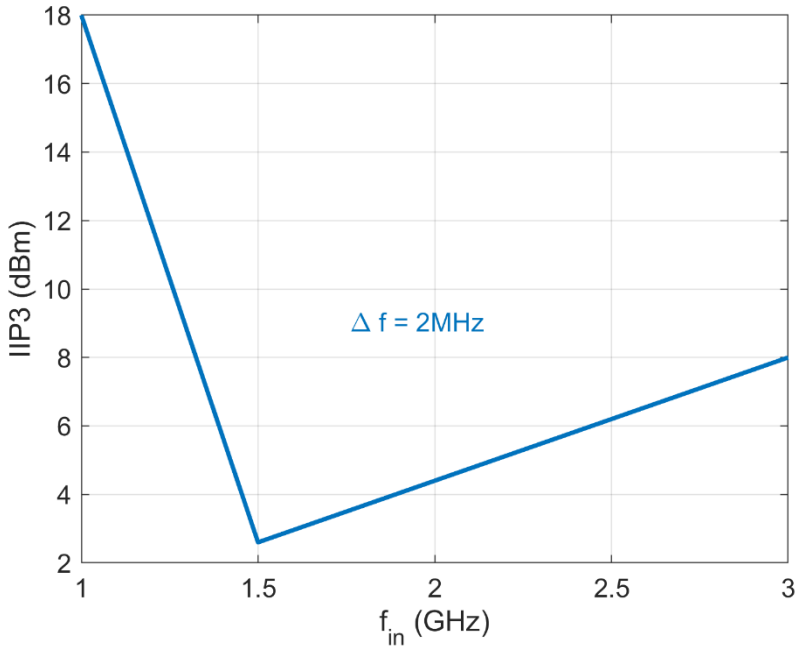

Figure 3.16 IIP3 versus input frequency for two-tone tests ($f_1 = f_{in} - 1MHz$ and $f_2 = f_{in} + 1MHz$), reprinted with permission from [52].

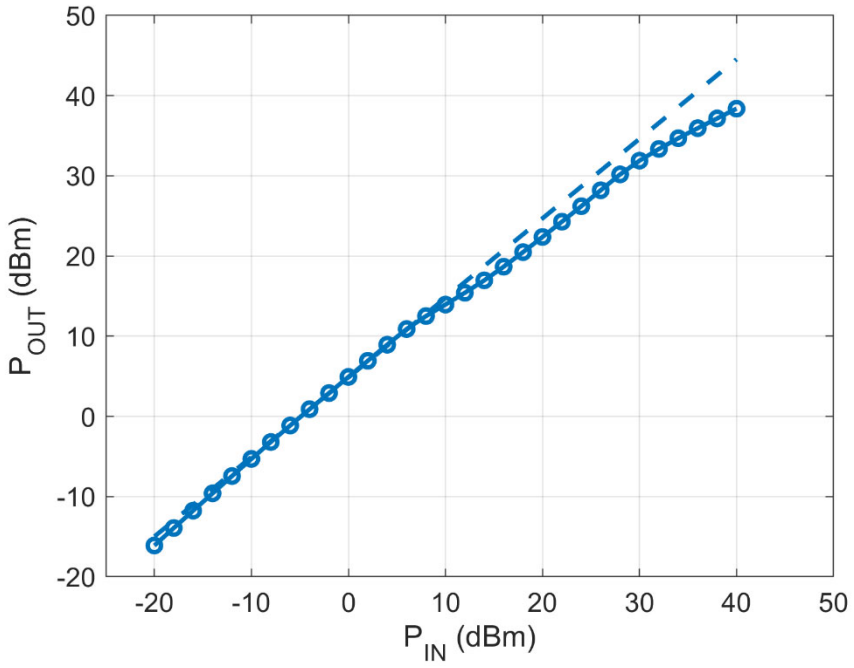

Figure 3.17 1 dB compression point input signal at 1.2 GHz.

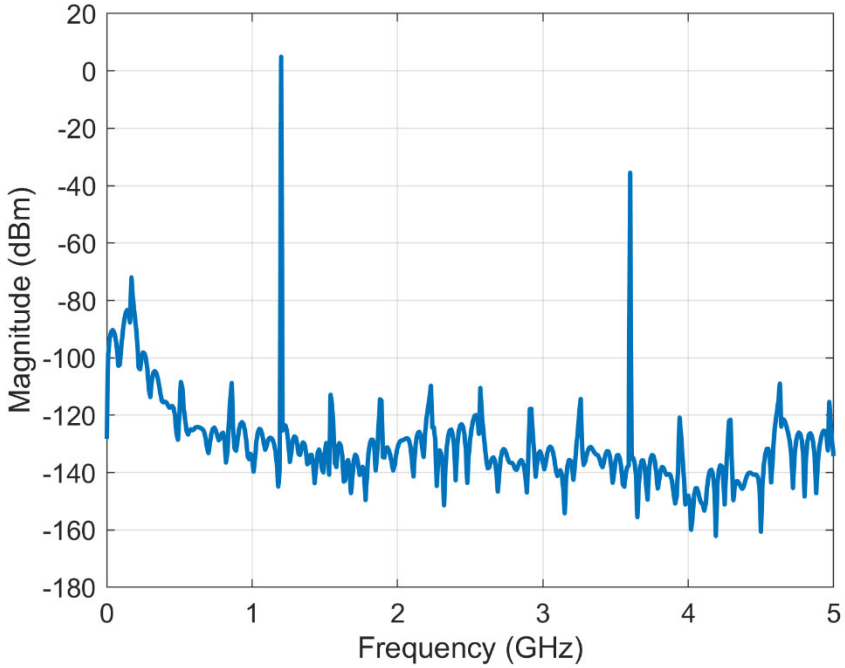

Figure 3.18 Output signal spectrum with 632.5 mVPP at a 1.2GHz input signal.

Table 3.4 Performance of the second-order bandstop filter, reprinted with permission from [52].

CMOS technology (nm)	180
Order	2
Supply Voltage (V)	1.8
Power Consumption (mw)	1.4
Out-band IIP3 (dBm)	2.6
Total input referred noise (nV/$\sqrt{Hz}$)	5.8
$V_{in_{max}}$ at (THD=-40dB) (mV)	238

4. THE PROPOSED TUNING SCHEME

This chapter presents the proposed tuning technique used to tune the frequency characteristics in the bandstop filter. Principle operation, implementation and limitation are all presented below.

4.1. Principle of the Proposed Tuning Technique

The transfer function of the bandstop filter can be written as:

$$\frac{V_{out}}{V_{in}} = -K\frac{s^2 + \alpha\ BW\ s + \omega_o^2}{s^2 + BWs + \omega_o^2} \tag{74}$$

The magnitude and phase response of the transfer function in Eq. (74) at reference frequency (ω_r) can be written as:

$$|H(j\omega_r)| = \frac{\sqrt{(\omega_o^2 - \omega_r^2)^2 + (\alpha\ BW\ \omega_r)^2}}{\sqrt{(\omega_o^2 - \omega_r^2)^2 + (\ BW\ \omega_r)^2}} \tag{75}$$

$$\angle H(j\omega_r) = tan^{-1}\left(\frac{\alpha\ BW\ \omega_r}{\omega_o^2 - \omega_r^2}\right) - tan^{-1}\left(\frac{\alpha\ BW\ \omega_r}{\omega_o^2 - \omega_r^2}\right) \tag{76}$$

The filter parameters such as ω_o, BW, and α can be detected by sweeping the center frequency control voltage (V_f) within a certain interval of time (T) and by observing the phase difference between the input and the output. Figure 4.1 shows the magnitude and the phase of the bandstop filter when a sinusoidal input frequency at ω_r is applied and V_f is swept.

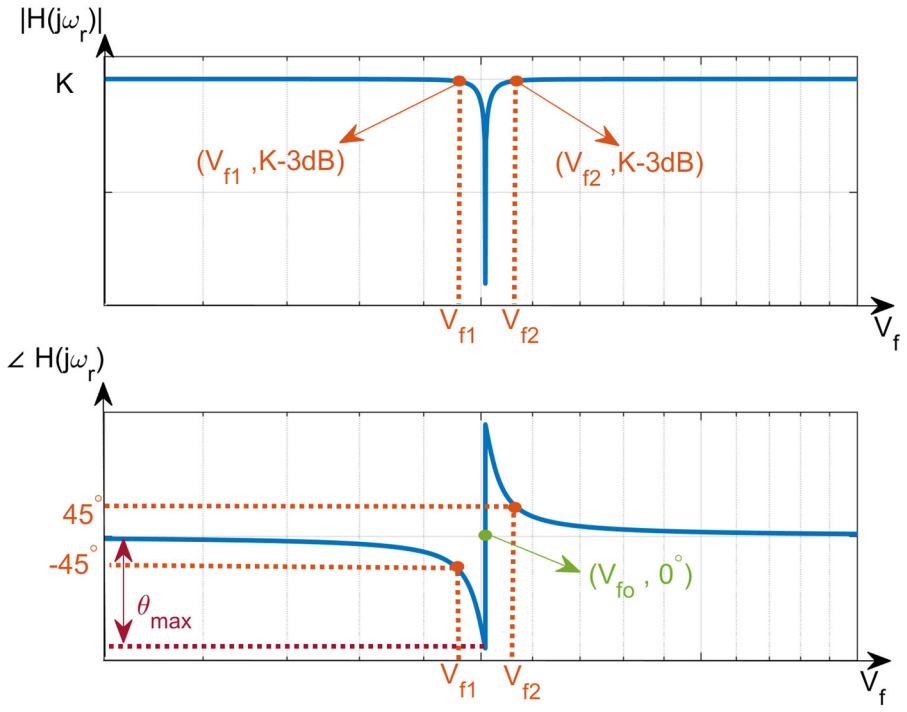

Figure 4.1 The magnitude and the phase of the bandstop filter at fixed ω_r.

The principle of frequency tuning is based on detecting V_f corresponding to $\angle H(j\omega_r) = 0$, while V_f is swept and a sinusoidal signal at ω_r is applied at the input. When the detected control voltage V_{fo} is applied to the filter, its ω_o will be equal to ω_r.

The attenuation tuning method is based on comparing the phase difference between the input and the output of the bandstop filter with the desired maximum phase shift (θ_{max}). The absolute value of maximum phase shift θ_{max} can be calculated by taking the derivative of the phase in Eq. (76) with respect to ω_o and setting the derivative to zero, which can be written as:

$$\theta_{max} \approx tan^{-1}\left(\frac{-\alpha+1}{2\sqrt{\alpha}}\right) \tag{77}$$

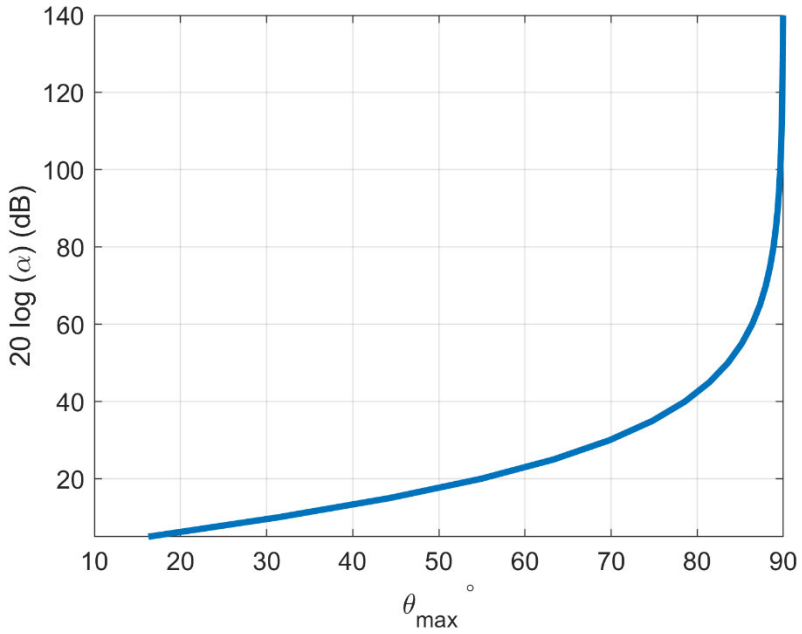

Figure 4.2 Attenuation versus θ_{max}.

Figure 4.2 shows attenuation at ω_o (which is 1/α) in dB as a function of θ_{max}. Note that greater than 60 dB attenuation can be obtained when θ_{max}=90°.

After attenuation at ω_o is tuned, the filter bandwidth can be controlled by detecting V_f corresponding to $\angle H(j\omega_r) = 45°$ and $\angle H(j\omega_r) = -45°$ as shown in Figure 4.1. The relationship between ω_o and V_f is assumed to be linear. Therefore, by subtracting the detecting voltages V_{f1} and V_{f2} and dividing it by (V_{fo}/ω_r), the BW can be detected. The attenuation should be more or equal to 40 dB to have a bandwidth tuning error less than 1% as shown in Figure 4.3.

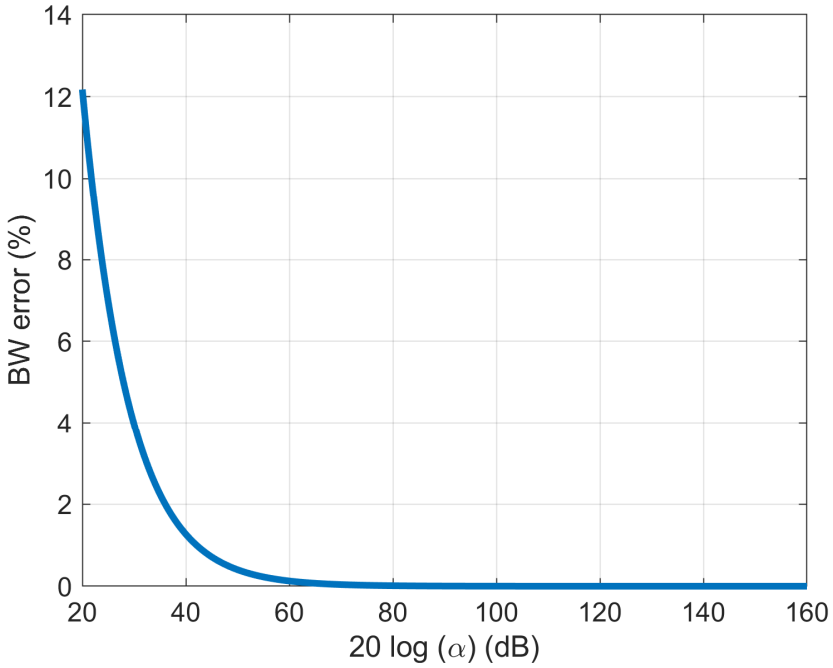

Figure 4.3 The bandwidth error versus attenuation.

4.2. Tuning Scheme

Figure 4.4 shows the block diagram of the proposed tuning scheme, where the master-slave method is used. In this scheme, the bandstop filter is fed by an input signal that has a frequency equal to the desired center frequency. During the tuning process, the control voltage of the center frequency is swept by applying V_{ramp} signal shown in Figure 4.5. Thus, filter parameters ω_o, α, and BW are detected from the transient response by determining the phase difference between the input and the output of the filter. The tuning cycles are determined by the clock signal (CLK_T), which is generated by the frequency divider from the reference clock (CLK_{ref}). Figure 4.5 shows the clock signals that are used in the tuning circuit.

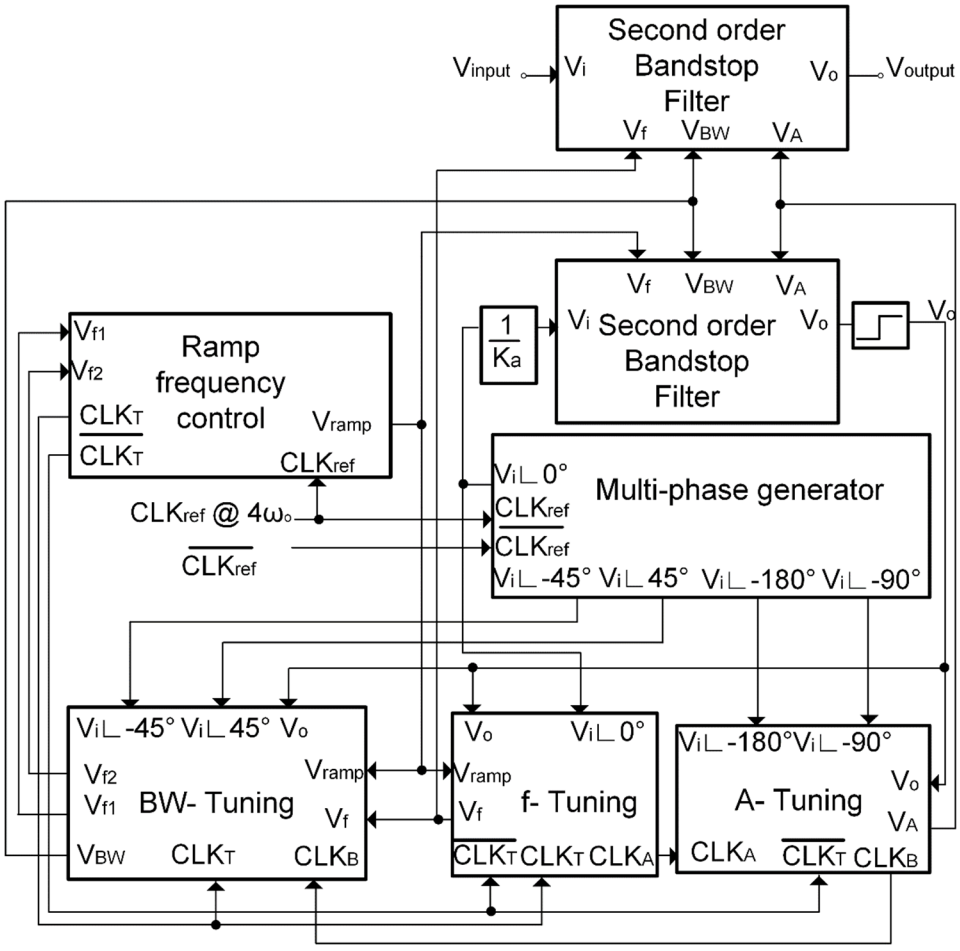

Figure 4.4 Overall tuning scheme.

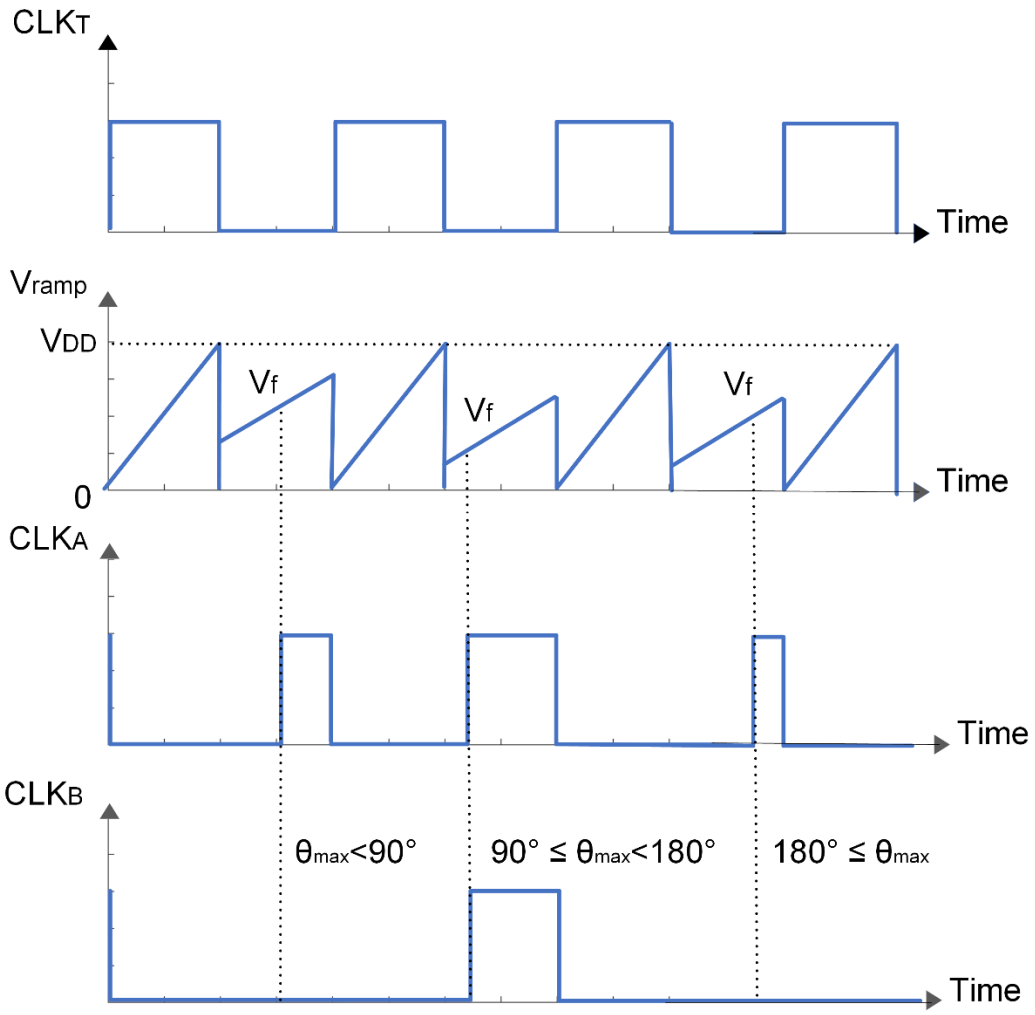

Figure 4.5 Clock signals.

4.2.1. Multi-phase Generator

The schematic of the multi-phase generator is shown in Figure 4.6. The circuit is fed by the clock signals *CLK* and $\overline{CLK}$, and consists of N identical positive edge-triggered D flip flops to implement a frequency divider. Thus, the frequency of the output signals can be expressed as:

$$\omega_o = \frac{\omega_{CLK}}{2N} \tag{78}$$

The phase shift between consecutive output signals can be written as:

$$Phase\ shift = \frac{360}{2N} \tag{79}$$

where N is the number of D flip-flops.

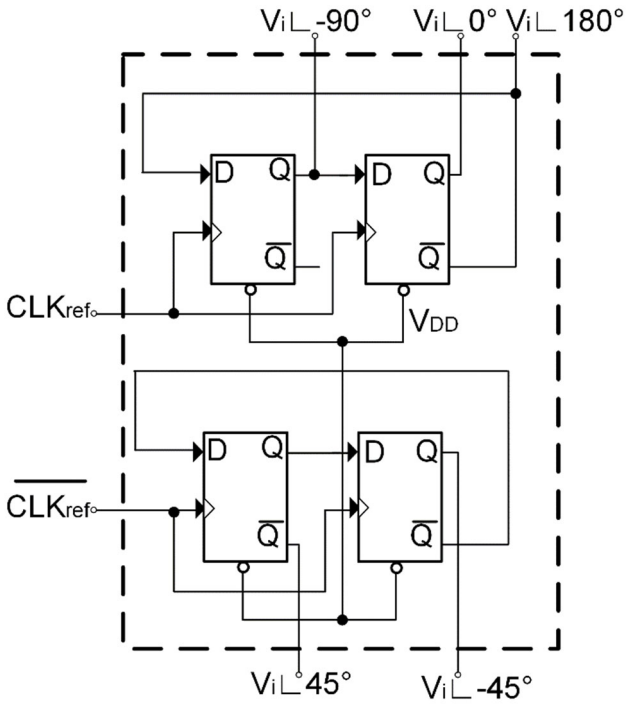

Figure 4.6 The schematics of the multi-phase generator.

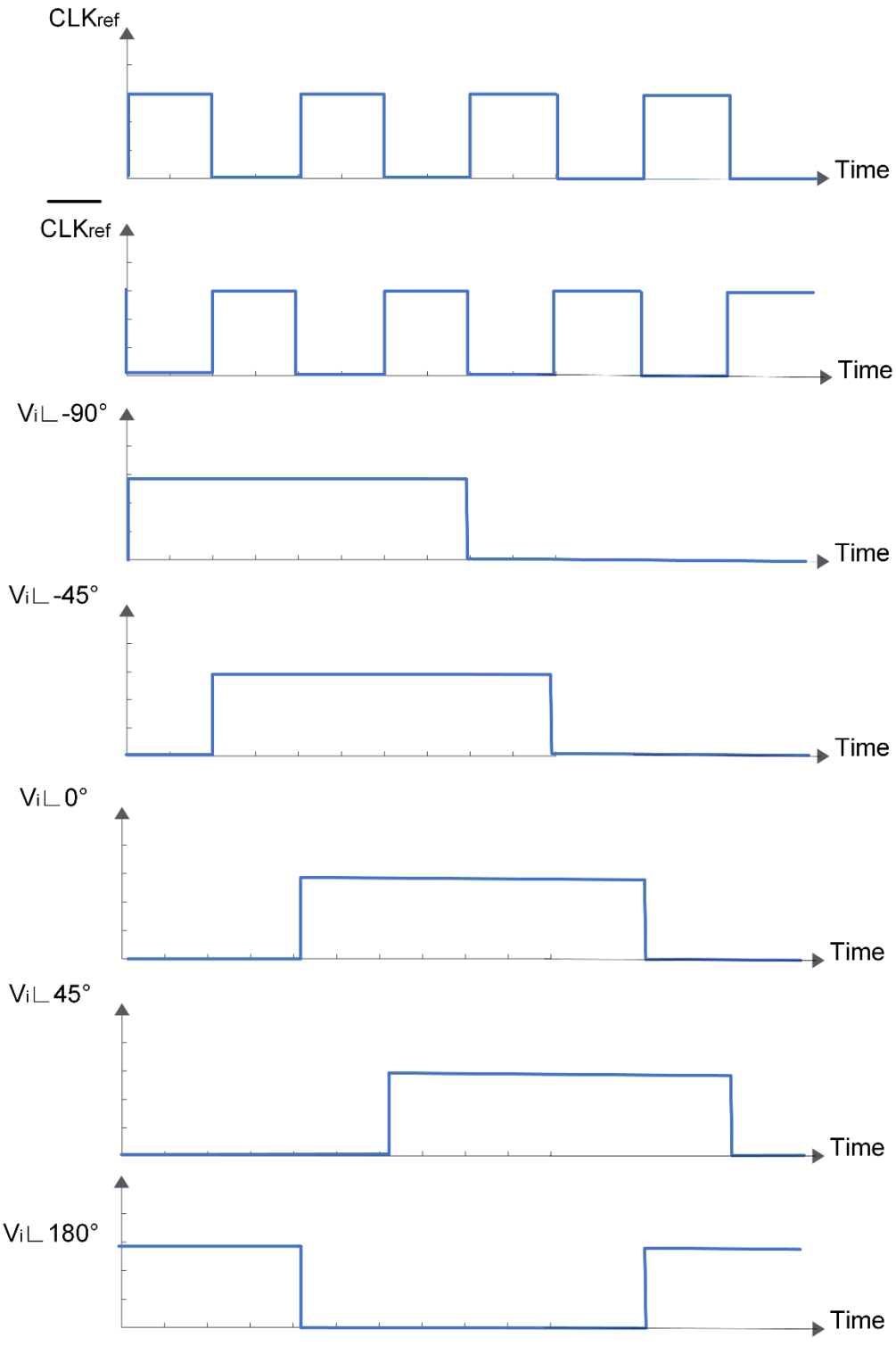

Figure 4.7 Multi phases generator waveform.

The tuning method was designed to have input phases of the signals to be -45°, 45°, 90° and 180°. Thus, N should be equal to 2. As shown in Figure 4.7, $V_i\angle -90°$ flips up when the *CLK* has the first rising edge. In the second rising edge, $V_i\angle -45°$ flips up. $V_i\angle 0°$ follows $V_i\angle -45°$ at the third rising edge. $V_i\angle 45°$ flips up in the fourth rising edge. $V_i\angle -90°$ flips down at the fifth rising edge because the D has low voltage. $V_i\angle -45°$, $V_i\angle 0°$ and $V_i\angle 45°$, respectively flip down at the sixth, seventh and eighth rising edges. This process will generate four square signals with delays equal to the period of CLK as shown in Figure 4.7.

4.2.2. Ramp Frequency Control Voltage

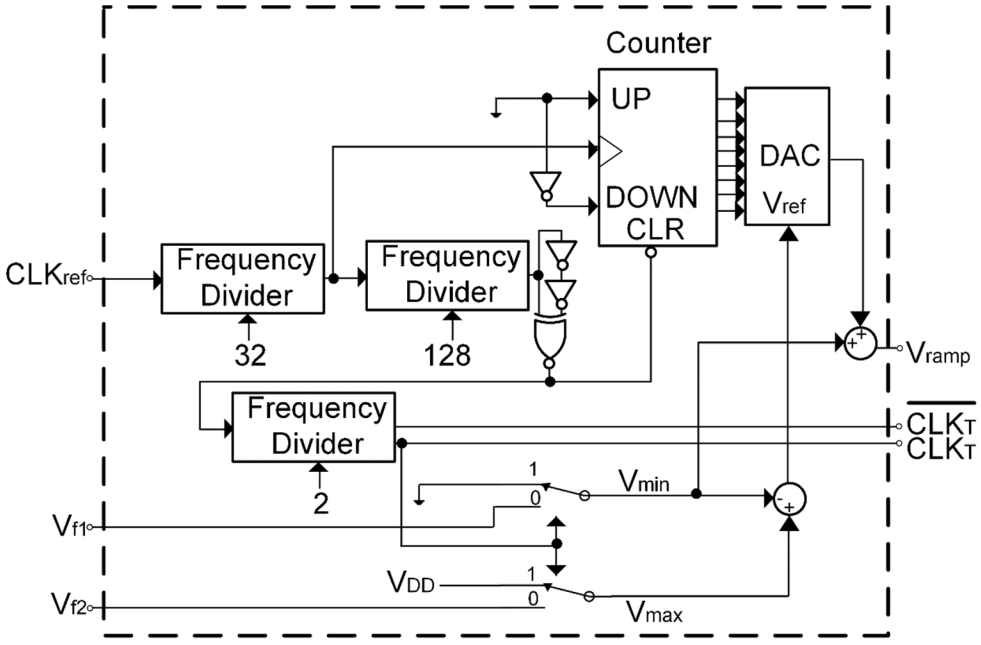

Figure 4.8 The adaptive ramp frequency control voltage.

Figure 4.8 shows the ramp generator circuit, whereas its output V_{ramp} is shown in Figure 4.8. The circuit also generates the clock signal (CLK_T) that controls the duration of the tuning process. CLK_T can be written as:

$$\omega_{CLK_T} = \frac{\omega_{CLK_{ref}}}{2N_1N_2} \tag{80}$$

The down counter is used to generate the step voltage for the V_{ramp} that can be used to detect voltages in the tuning scheme. The duration of the step level can be determined by the first frequency divider. The limit of the V_{ramp} is set by the V_{min} and V_{max}, whereas they update their values from the bandwidth tuning scheme. Figure 4.9 illustrates the transient response of the V_{ramp}.

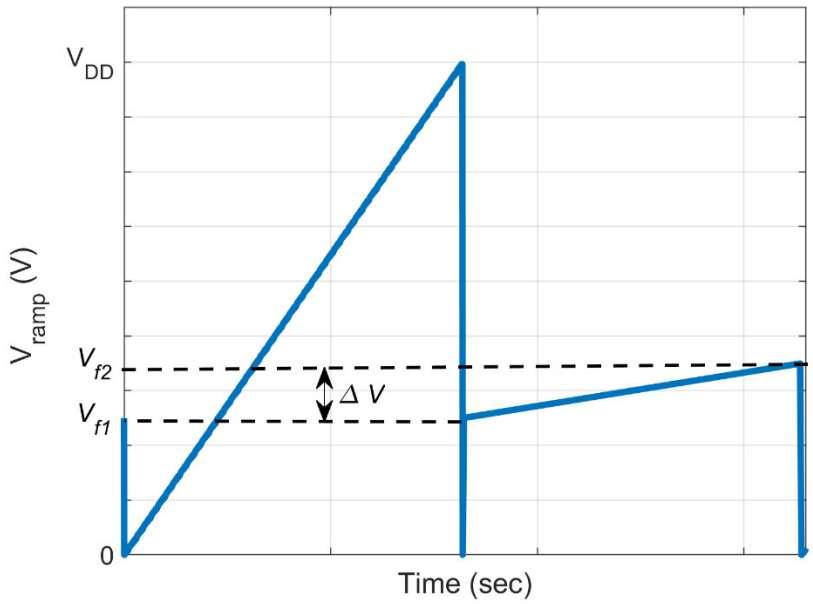

Figure 4.9 Time-domain response of V_f during the tuning processes.

4.2.3. Frequency Tuning Circuit

Figure 4.10 shows the frequency tuning circuit, where the D flip flop (DFF) is used as a binary phase detector. Initially V_o lags V_i setting $\bar{Q}$ to high. When V_o leads V_i, $\bar{Q}$ will be switched from high to low, causing the sample and hold circuit to hold the value of V_{ramp} as V_f , corresponding to $\omega_o = \omega_r$. The frequency tuning circuit will generate the clock signal (CLK_A) as shown in Figure 4.5, which is used to turn on the attenuation tuning loop. Table 4.1 is summarized the cases of the DFF.

Table 4.1 The truth table of the DFF

CLK	D	Q
↑	1	1
↑	0	0

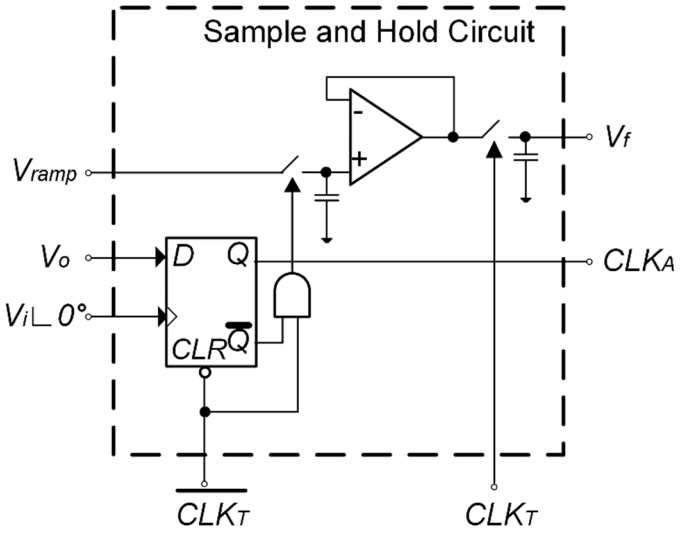

Figure 4.10 Frequency tuning scheme.

4.2.4. Attenuation Tuning Circuit

Figure 4.11 shows the attenuation tuning circuit. Initially, Q_1 and Q_2 are set to low. If θ_{max} exceeds 90°, Q_1 will be switched from low to high. If θ_{max} further exceeds 180°, Q_2 is switched from low to high as well, which also indicates that α is negative as shown in Figure 4.12. The DFF1 in Figure 4.11 is used as phase detector, whereas the DFF2 is used as a latch. Table 4.2 shows tuning process for the attenuation control voltage (V_A). If ($90° \leq \theta_{max} < 180°$), there will be no action for V_A and the bandwidth tuning loop will turn on by the clock signal (CLK_B) as shown in Figure 4.5. To decrease the overhead, analog converter (DAC) in Figure 4.11 can be avoided by using digitally controllable, which can be designed to control α directly by the counter output.

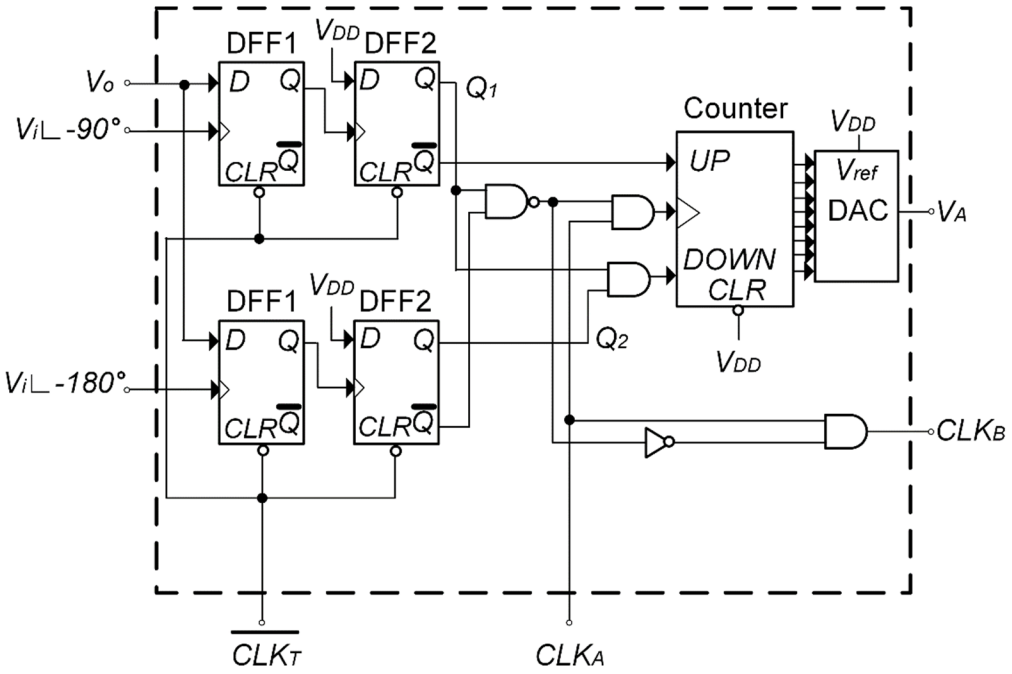

Figure 4.11 Attenuation tuning scheme.

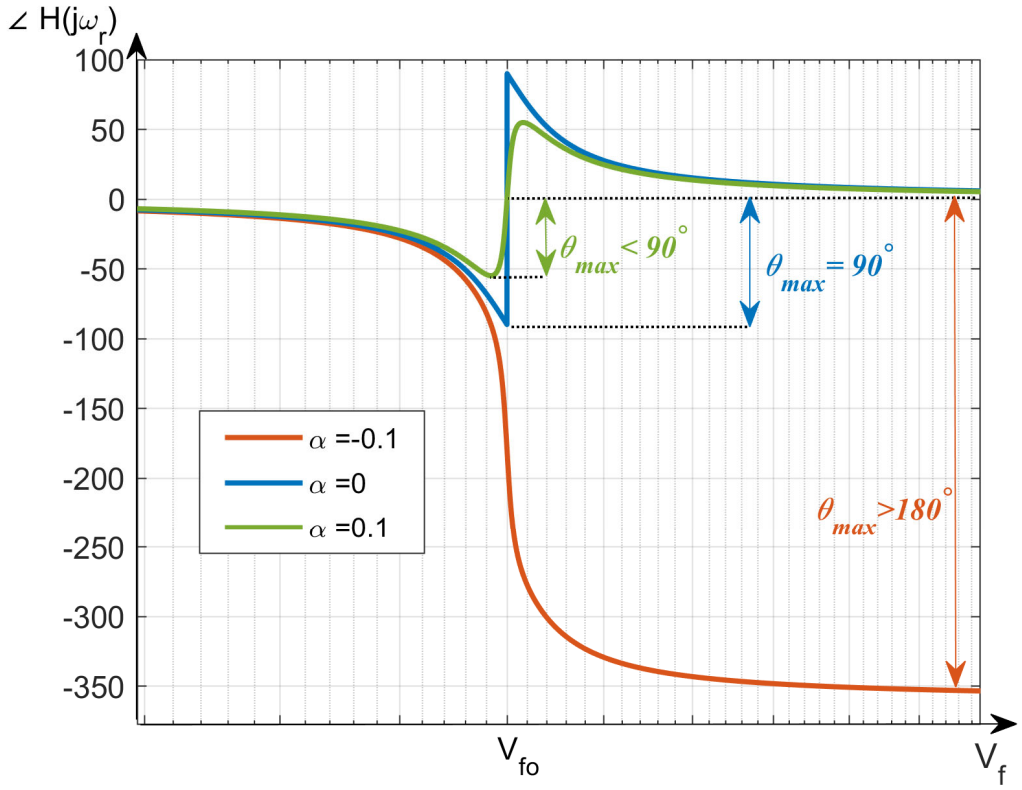

Figure 4.12 Phase response of the bandstop filter.

Table 4.2 Attenuation tuning process

Condition	UP	DOWN	Action
$\theta_{max} < 90°$	1	0	$V_A \uparrow$
$90° \leq \theta_{max} < 180°$	0	0	No Action
$180° \leq \theta_{max}$	0	1	$V_A \downarrow$

4.2.5. Bandwidth Tuning Schemes

The proposed bandwidth tuning circuit is shown in Figure 4.13. Initially, $\overline{Q_{22}}$ is set to high and Q_{11} is set to low. If $\angle H(j\omega_r) < -45°$, $\overline{Q_{22}}$ will switch from high to low and the

sample and hold circuit will hold the value of V_{ramp} as V_{f1}. If $\angle H(j\omega_r) > 45°$, the Q_{11} will switch from low to high. The sample circuit will hold the value of V_{ramp} as V_{f2} when Q_{11} switches from high to low at $\angle H(j\omega_r) < 45°$. ΔV and V_r can be written as:

$$\Delta V = V_{f2} - V_{f1} \tag{81}$$

$$V_r = V_f \frac{BW_{desired}}{\omega_r} = \frac{V_f}{Q_d} \tag{82}$$

Table 4.3 and Table 4.4 illustrate the coarse and fine tuning process for the BW, respectively. Figure 4.14 provides the controller block shown in Figure 4.13, which is composed of fine and coarse tuning circuit. The coarse control uses a large increment in each step at the bandwidth tuning scheme, whereas the fine control is used to improve the resolution.

Table 4.3 Truth table for the coarse-tuning

Condition	UP	DOWN	Action
$\Delta V < 0.9\ V_r$	1	0	$\uparrow V_{BW}$
$\Delta V > 1.1 V_r$	0	1	$\downarrow V_{BW}$
$0.9V_r < \Delta V < 1.1\ V_r$	0	0	No Action

Table 4.4 Truth table for the fine-tuning

Condition	UP	Action
$\Delta V < V_r$	1	$\uparrow V_{BW}$
$\Delta V > V_r$	0	$\downarrow V_{BW}$

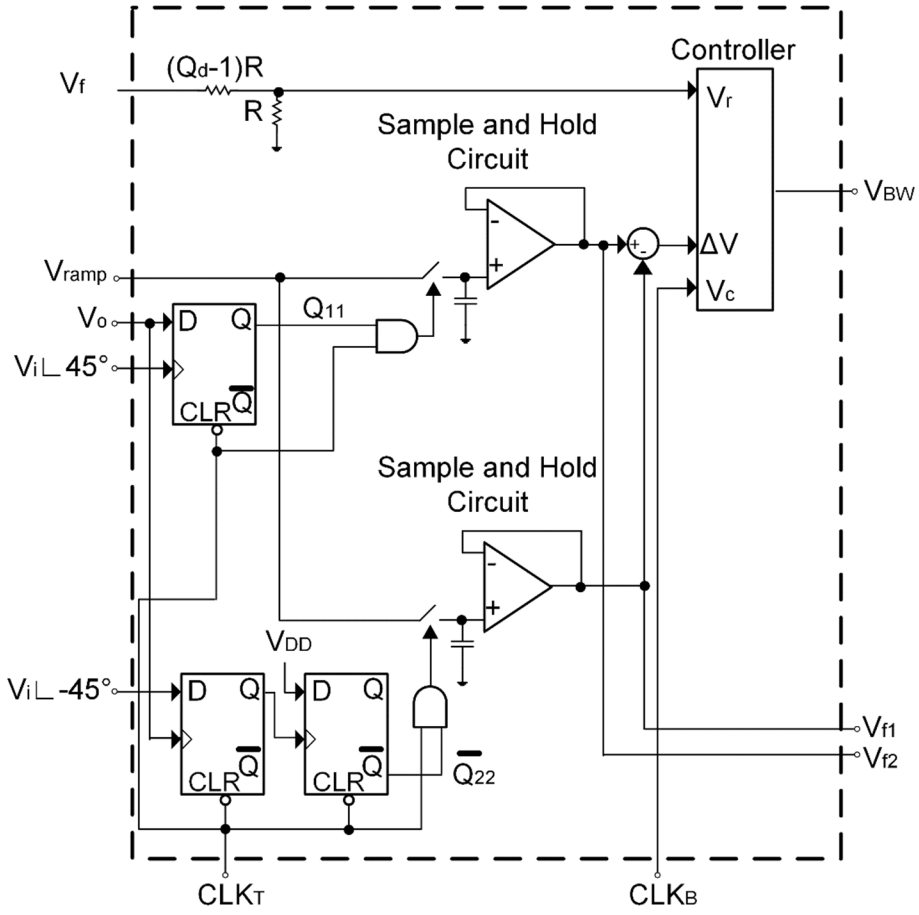

Figure 4.13 Bandwidth tuning scheme.

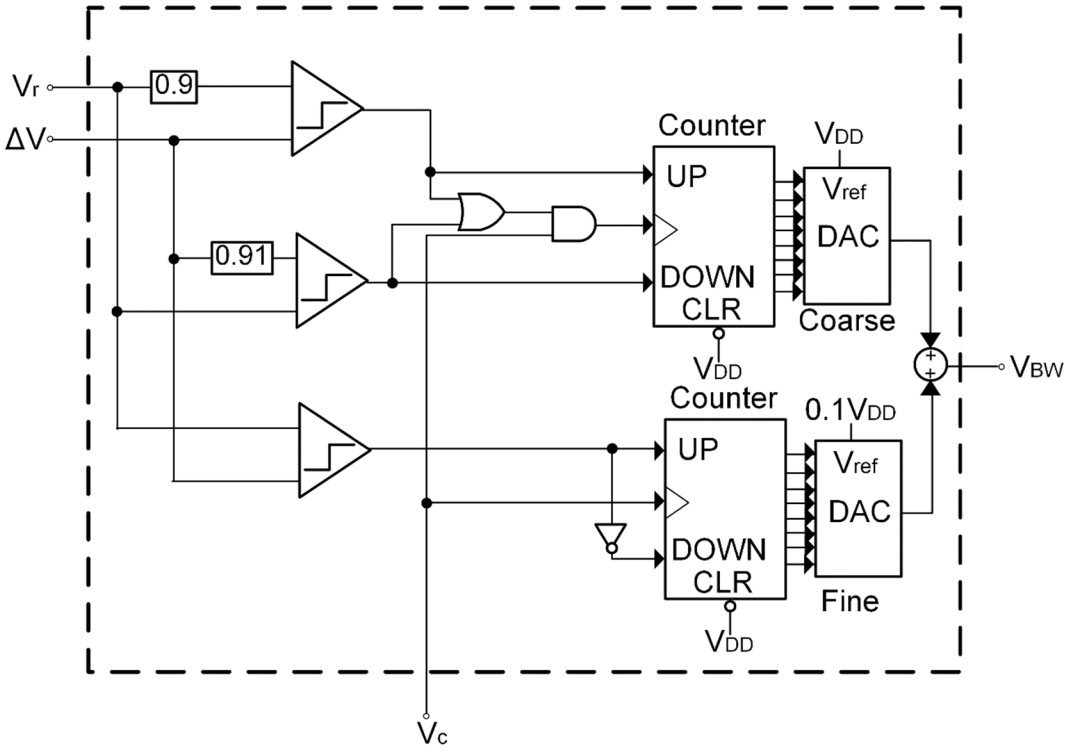

Figure 4.14 The controller of the bandwidth tuning scheme.

4.2.6. Limitations of the Tuning Method

The limitations of the tuning scheme will be discussed in this section. The main effects of the accuracy come from the resolution of the DAC. Furthermore, this technique is introduced to tune filter at high frequency. So, the effect of the high frequency poles should be examined.

4.2.6.1. Effect of Excess Phase Shifts

The bandstop filter can be implemented using Gm-C filter as shown in Figure 2.6. Due to high frequency poles of the transconductance, the phase response of the bandstop filter shows excess phase shift. Assuming that transconductors can be modeled with a pole at $X\omega_o$

$$G_m(s) = \frac{G_m}{1 + \frac{s}{X\omega_O}} \tag{83}$$

Using (82), the transfer function of the bandstop filter can be expressed as,

$$H(s) = \frac{\left(\frac{1}{X\omega_O}\right)^2 s^4 + \left(\frac{2}{X\omega_O}\right) s^3 + \left(1 + \frac{\alpha}{X\omega_O}\right) s^2 + (\alpha BW)s + \omega_o^2}{\left(\frac{1}{X\omega_O}\right)^2 s^4 + \left(\frac{2}{X\omega_O}\right) s^3 + \left(1 + \frac{1}{X\omega_O}\right) s^2 + (BW)s + \omega_o^2} \tag{84}$$

Figure 4.15 shows the BW tuning errors versus X and *Q*, where the center frequency and bandwidth control voltage are assumed to be continuous. When Q < 5 and X < 15, the BW-tuning error is less than 2%.

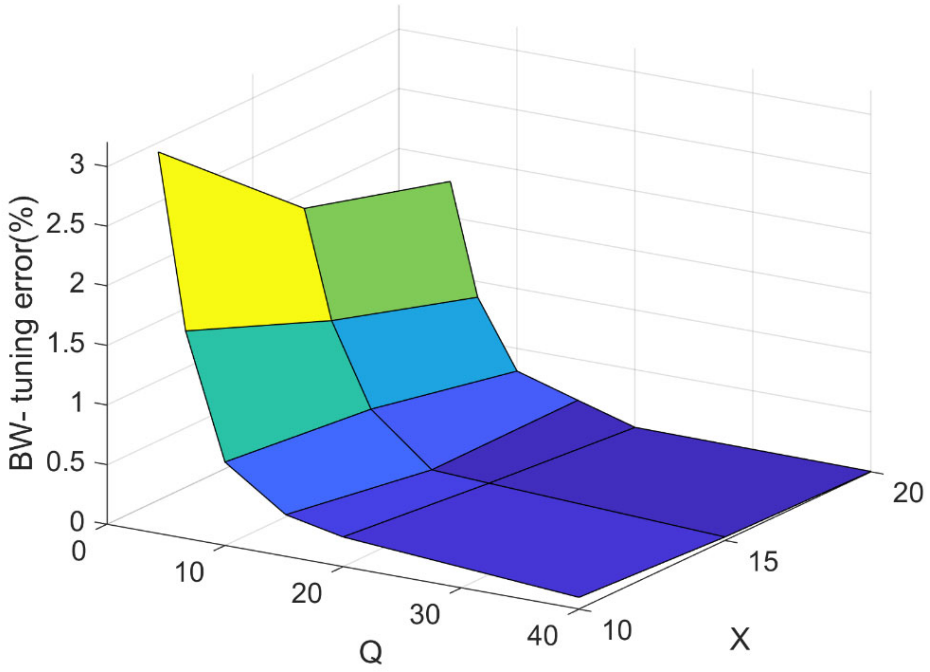

Figure 4.15 Bandwidth tuning error due to the excess phase shift.

4.2.6.2. The resolution of V_{ramp} and DAC

The accuracy of the tuning scheme relies on the resolution of V_{ramp}, which can be estimated by the Least Significant Bit (LSB) of the DAC in Figure 4.8. LSB can be written as,

$$LSB = \frac{V_{ref}}{2^M} \tag{85}$$

In Figure 4.9, V_{ref} is set to V_{DD} when the CLK_T is high. When the CLK_T is low, the voltage range V_{ref} is set to ΔV to decrease LSB and the tuning process will start as shown in Figure 4.5.

Resolution of the DAC (M bits) in Figure 4.8 results in frequency tuning error. The center frequency variation can be written as:

$$\Delta f_o = \frac{f_o}{2^M} \tag{86}$$

From Eq. (86), the frequency tuning error can be expressed as:

$$f - tuning\ Error = \frac{f_o - f_o \pm \Delta f_o}{f_o} \times 100 \tag{87}$$

$$f - tuning\ Error = \frac{1}{2^M} \times 100 \tag{88}$$

To determine the bandwidth tuning error, the bandwidth variation is depending on the quality factor variation because the bandwidth is tuned by the voltage that controls the quality factor as shown in Figure 4.14. Thus, the quality factor variation can be expressed as:

$$\Delta Q = \frac{Q}{2^M} \tag{89}$$

The desired bandwidth can be given by:

$$BW = \frac{\omega_o}{Q} \tag{90}$$

From Eqs. (88) and (89), the bandwidth tuning error can be written as:

$$BW - tuning\ Error = \frac{\Delta BW}{BW} \times 100 \tag{91}$$

$$BW - tuning\ Error = \left(\frac{{\omega_o}/{Q} - {\omega_o}/{(Q + \Delta Q)}}{{\omega_o}/{Q}} \right) \tag{92}$$

$$BW - tuning\ Error = \left(1 - \frac{1}{1 + {1}/{2^M}} \right) \times 100 \tag{93}$$

$$BW - tuning\ Error = \left(\frac{1}{2^M + 1} \right) \times 100 \tag{94}$$

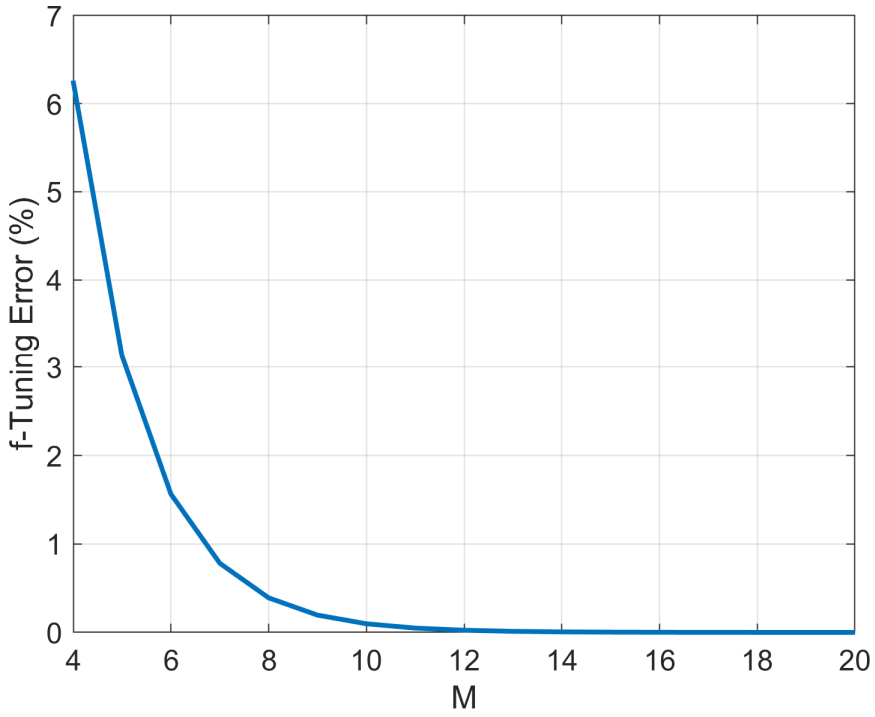

Figure 4.16 Frequency tuning error due to the resolution of DAC.

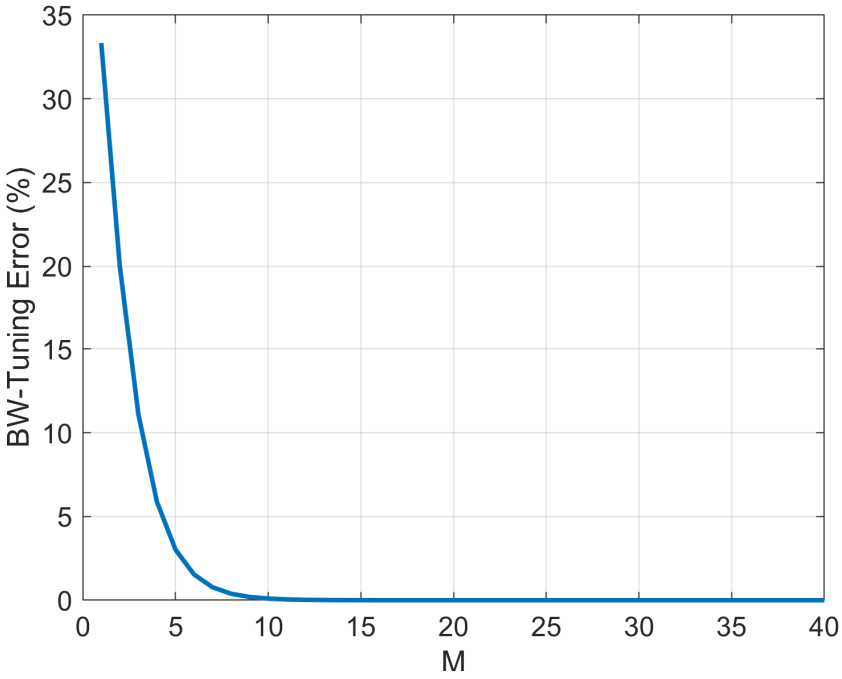

Figure 4.17 Bandwidth tuning error due to the resolution of DAC.

Note that from Figures 4.16 and 4.17, the frequency and bandwidth tuning errors are less than 1% when $M \geq 8$.

5. SIMULATION AND EXPERIMENTAL RESULTS

In this chapter, the simulated results of the proposed bandstop filter in chapter 3 and the proposed tuning scheme in chapter 4 are described. The experimental results of the proposed tuning scheme are also discussed in this chapter.

5.1. Simulation Results

The bandstop filter shown in Figure 5.1 with the proposed tuning scheme shown in Figure 4.4 was simulated using 180nm CMOS technology with a power supply voltage of 1.8 V. The relationship between the V_f and ω_o is linear, and the circuit, as shown in Figure 5.2, is used to generate V_f that controls ω_o. Figure 5.3 illustrates the transient response of squaring the control voltage of current I_{c1}. Figure 5.5 and Figure 5.6 show the control voltage of the attenuation and bandwidth for the bandstop filter. The tuning circuit begins detecting α by comparing θ_{max} with 90° and 180°. When θ_{max} is less than 90°, the V_A will increase as shown in Figure 5.5. At t = 50 µsec with $\theta_{max} \geq 90°$, the BW loop begins detecting and tuning the BW, as shown in Figure 5.6. From t = 50 µsec to 100 µsec, α and BW tuning loops are switched (ON and OFF) depending on the conditions shown in Tables 4.2, 4.3, and 4.4, respectively. Note when t > 100 µsec, the coarse control of the bandwidth turns off because the bandwidth tuning error is now less than 10%. Figure 5.4 shows the control voltage of the center frequency, where ω_o is depending on V_f and V_{BW}. During the bandwidth tuning loop, V_f is changing to achieve $\omega_o = \omega_r$. The tuning loops converge in 150 µsec to achieve ω_o at 1.5 GHz with BW = 478 MHz. The frequency

response of the bandstop filter before and after tuning is shown in Figure 5.7. The frequency tuning error is 0.13%, and bandwidth tuning error is 0.88%.

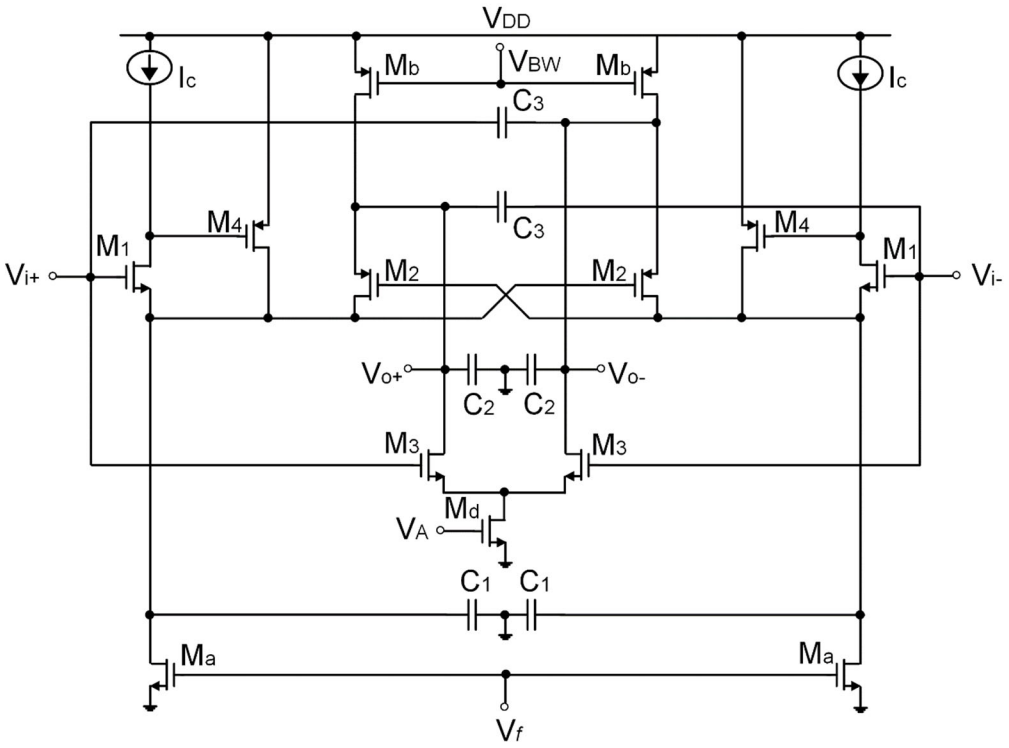

Figure 5.1 Bandstop filter based on source follower

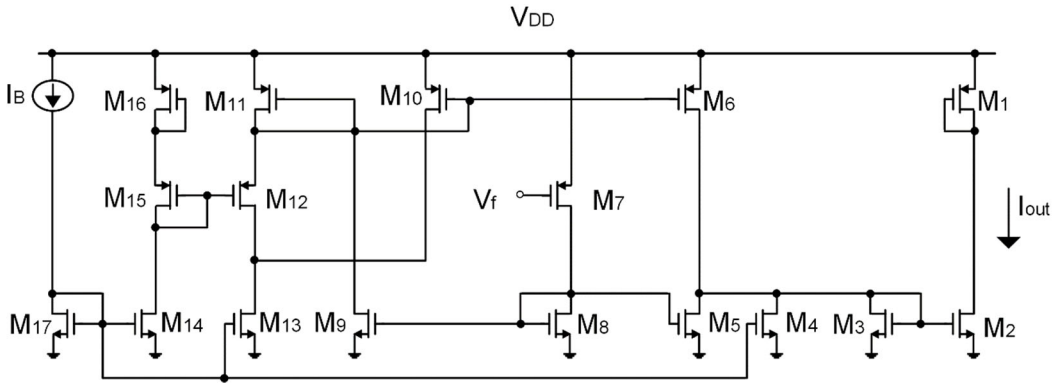

Figure 5.2 The squaring current circuit.

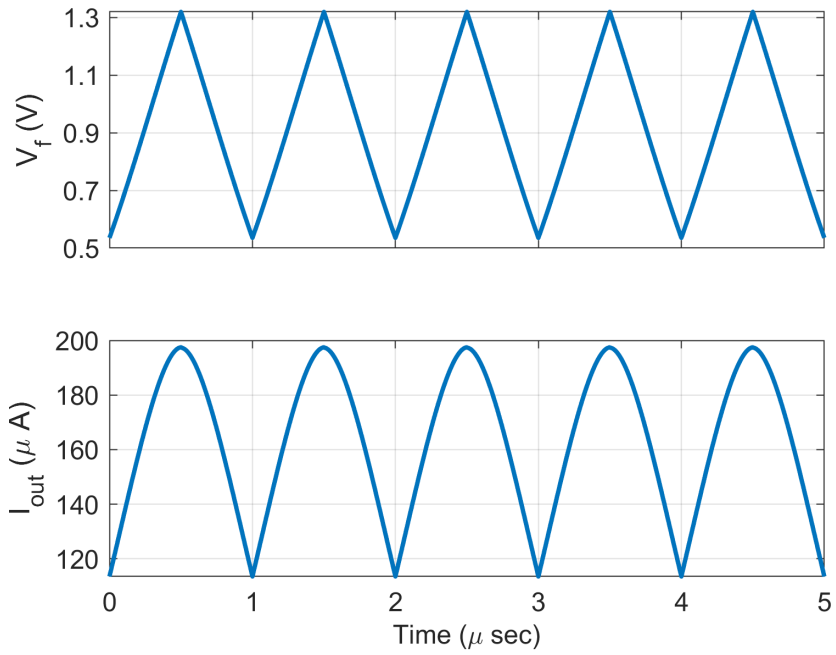

Figure 5.3 Transient response of the squaring current circuit.

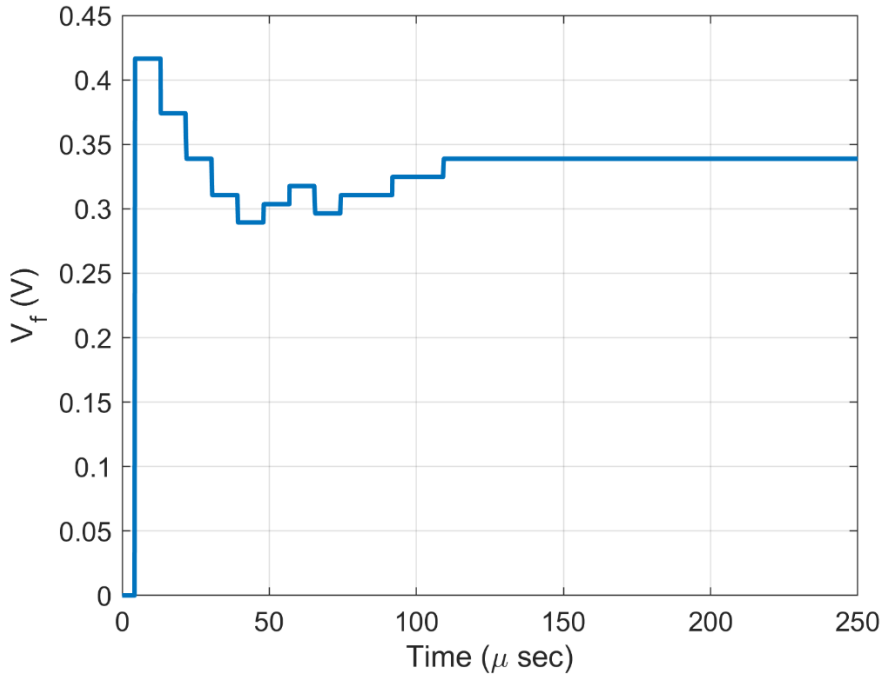

Figure 5.4 Transient response of the frequency control voltage.

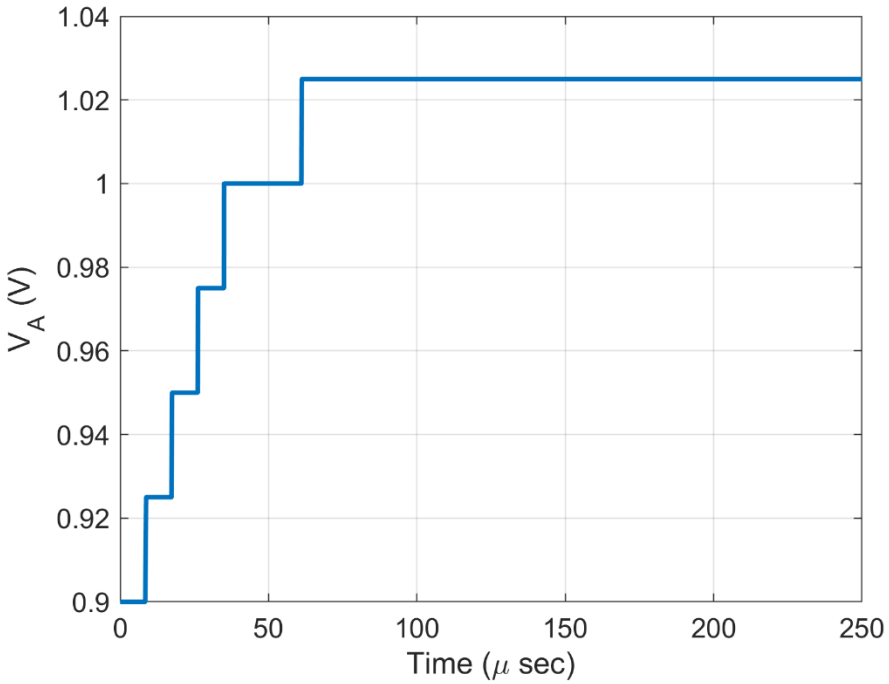

Figure 5.5 Transient response of the attenuation control voltage.

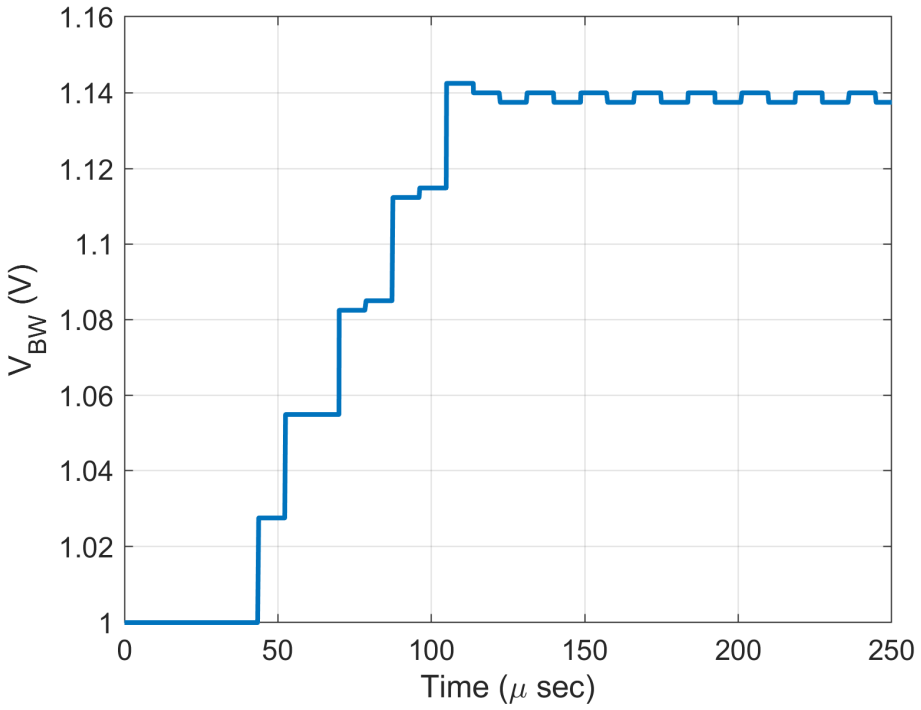

Figure 5.6 Transient response of the bandwidth control voltage.

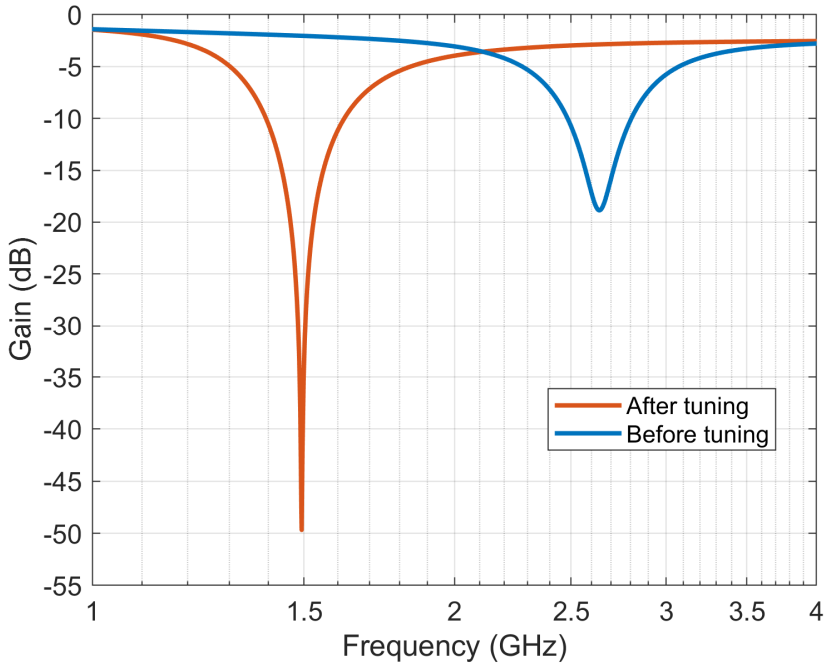

Figure 5.7 Frequency response of the bandstop filter.

5.2. Prototype Design

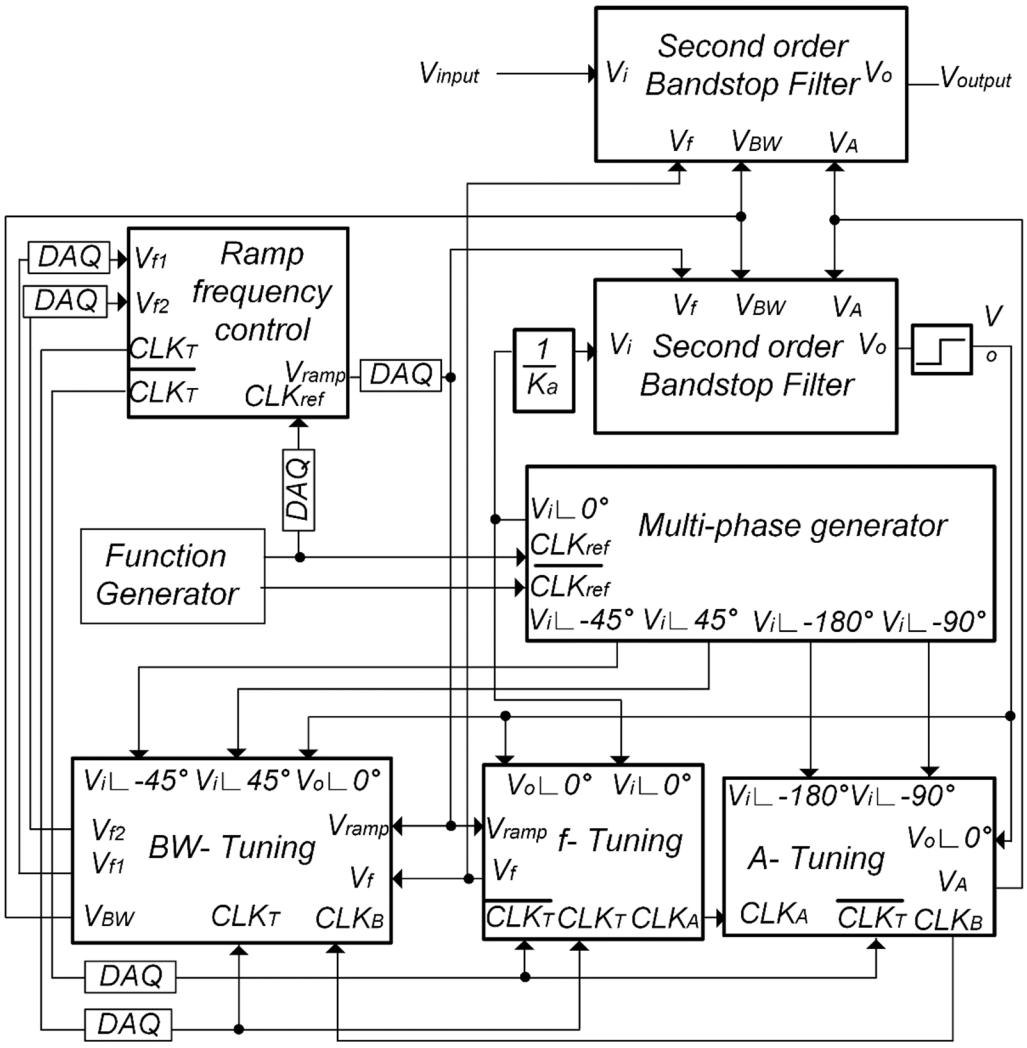

Figure 5.8 Experimental setup.

A 1 kHz center frequency second-order bandstop filter with the proposed tuning scheme was experimentally verified. The experimental setup is shown in Figure 5.8.

5.2.1. Filter

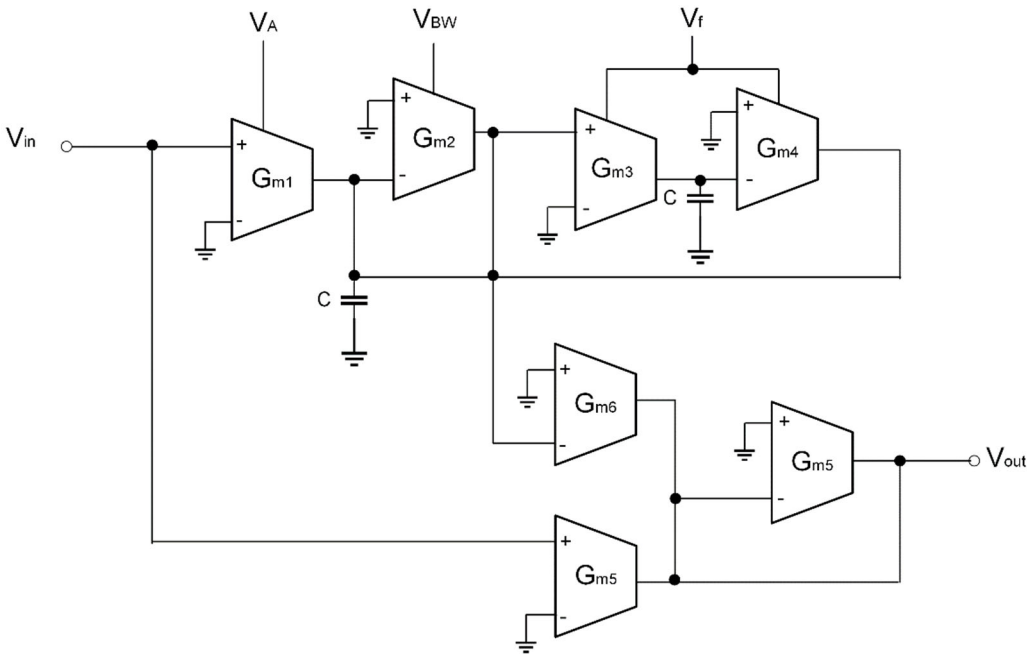

Figure 5.9 Second-order Gm-C bandstop filter.

Figure 5.9 shows the Gm-C bandstop filter, which demonstrates the performance of the proposed tuning scheme. The Gm-C filter was implemented using 13600CP transconductors, discrete resistors and capacitors. Table 5.1 shows the value of the discrete capacitor and resistor used to implement the Gm-C filter.

Table 5.1 Component values used for Gm-C tunable filter

C	15nF
R1	1.5MΩ
R2	2.12MΩ
R3,4	420KΩ
R5	32KΩ
R6	39KΩ

The transfer function of the bandstop filter can be written as:

$$\frac{V_{out}}{V_{in}} = -K\frac{s^2 + \alpha\frac{\omega_o}{Q}s + \omega_o^2}{s^2 + \frac{\omega_o}{Q}s + \omega_o^2} \tag{95}$$

The expressions ω_o, Q, BW, α, and gain (K) are obtained as:

$$K = \frac{G_{m5}}{G_{m6}} \tag{96}$$

$$\omega_o = \frac{G_{m3}}{C} = \frac{K_3 V_f}{C} \tag{97}$$

$$Q = \frac{G_{m3}}{G_{m2}} = \frac{K_3 V_f}{K_2 V_{BW}} \tag{98}$$

$$BW = \frac{G_{m2}}{C} = \frac{K_2 V_{BW}}{C} \tag{99}$$

$$\alpha = \frac{G_{m2} - G_{m1}}{G_{m2}} = \frac{K_2 V_{BW} - K_1 V_A}{K_2 V_{BW}} \tag{100}$$

where $G_{m3}=G_{m4}$.

5.2.2. Tuning Circuit

The tuning scheme was implemented using commercial chips with NI myDAQ interfacing with Simulink. The NI myDAQ hardware was provided by the data acquisition toolbox in Simulink. This toolbox has an analog input and output blocks, which are used to read and send data. The frequency ramp control circuit was designed using the block diagram in Simulink as shown in Figure 5.10. The block diagram has three inputs and three outputs. The frequency ramp control circuit generates V_{ramp}, CLK_T, and $\overline{CLK}_T$, where V_{f1}, $V_{f2,}$ and CLK_{ref} are read by the circuit. The frequency ramp control circuit consists on UP counter, DAC, and frequency dividers. The frequency divider is implemented using DFF. XNOR gate and delay are used to change the pulse width of the square wave. The switches are used to change the V_{ramp} limits.

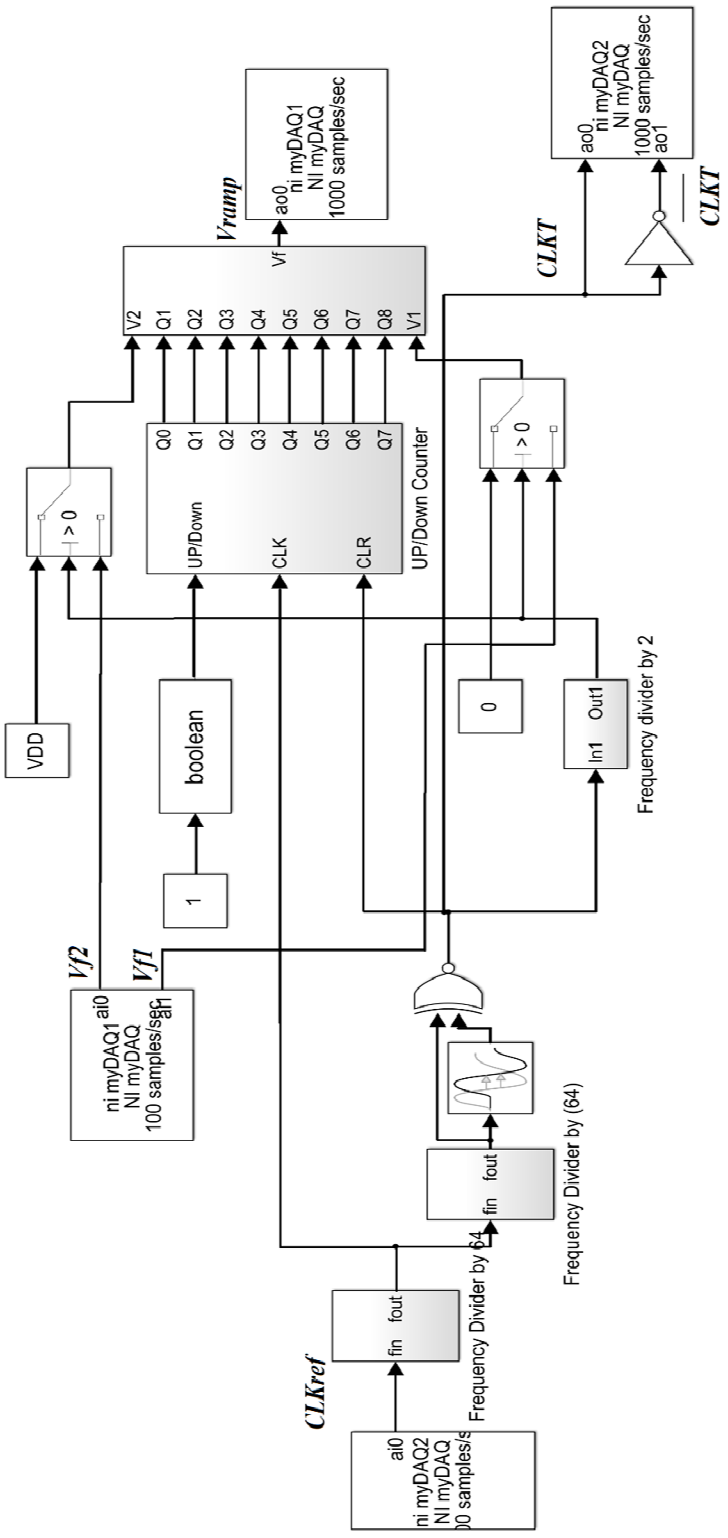

Figure 5.10 Simulink diagram of the frequency ramp control.

The multi-phase generator was built in breadboard using DFF (NTE74HC175). Figure 5.11 shows the transient response of the phase generator's waveform. LM324N is an operational amplifier used to convert the output signal to square wave. The converter is necessary to apply the tuning method. Furthermore, the proposed method is based on detecting the phase shift between the input and the output of the filter. Thus, the two signals will always share the same waveform type.

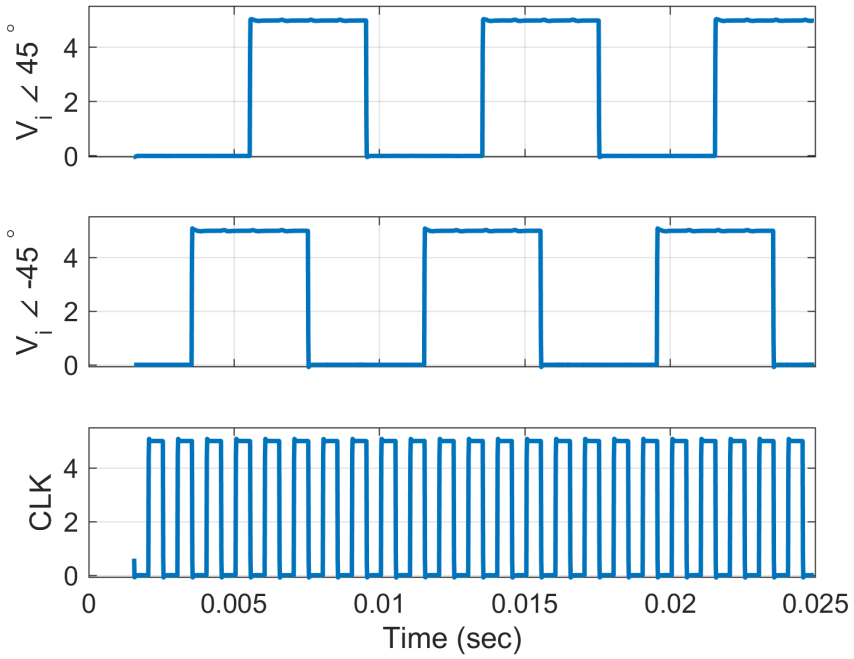

Figure 5.11 The waveform of the phase generator.

The frequency tuning circuit was designed using DFF (NTE74HC175) and a sample and hold circuit (LF398). The value of the capacitor used to hold the detecting

voltage is equal to (470μF). In the attenuation circuit, the proposed circuit was built using DFF (NTE74HC175), an UP\Down counter (74f269), a DAC (NTE808), and logic gates, such as the Inverter gate, AND gate, and gate NAND gate. The bandwidth tuning scheme consists of DFF (NTE74HC175), sample and hold (LF398), an attenuator, comparator, counter, DAC, and gates.

5.2.3. Experimental Results

Figure 5.12 shows the control voltage of the center frequency during the tuning process. Note that ω_o of the Gm-C filter is independent of α and BW. V_{ramp} has limits, which are set from the bandwidth tuning circuit. Also, V_{ramp} is increased by step size, which is set by V_{f1} and V_{f2}. Figure 5.13 and Figure 5.14 show the voltage controls of the attenuation and bandwidth, respectively, for the bandstop filter. The bandwidth tuning loop starts when $90° \leq \theta_{max} \leq 180°$. Also, the two loops are switched (ON, OFF) during the tuning process. At t> 30 sec, the fine controller starts to tune the control voltage of the bandwidth. The frequency response of the tuned and untuned bandstop filter is shown in Figure 5.15. The tuning error is thus 0.22% for frequency tuning and 0.66% for bandwidth tuning at 1 kHz with a bandwidth of 200 Hz. Table 5.2 summarizes the results for fixed reference frequency and varying bandwidths. The center frequency sets at 1kHz where the bandwidth varies between 180 Hz to 225 Hz. Notice that the percentage errors for the center frequency and bandwidth are less than 1%.

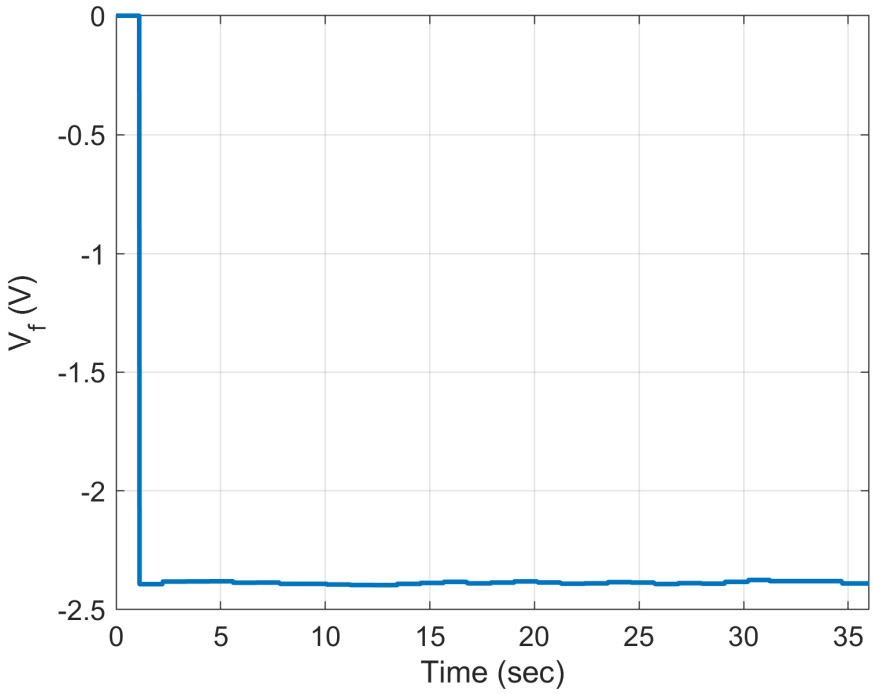

Figure 5.12 Experimental transient response of the frequency control voltage.

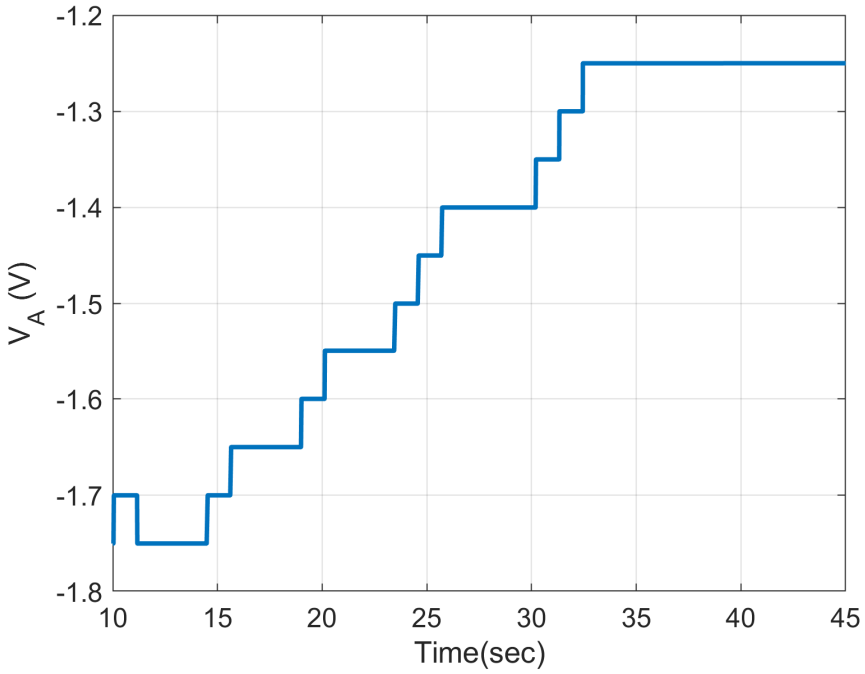

Figure 5.13 Experimental transient response of the attenuation control voltage.

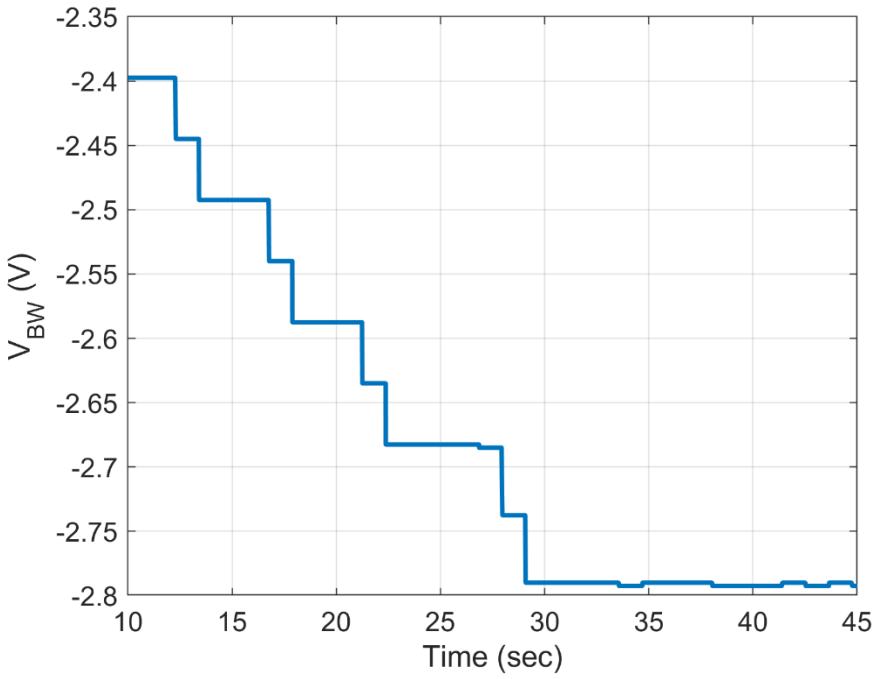

Figure 5.14 Experimental transient response the bandwidth control voltage.

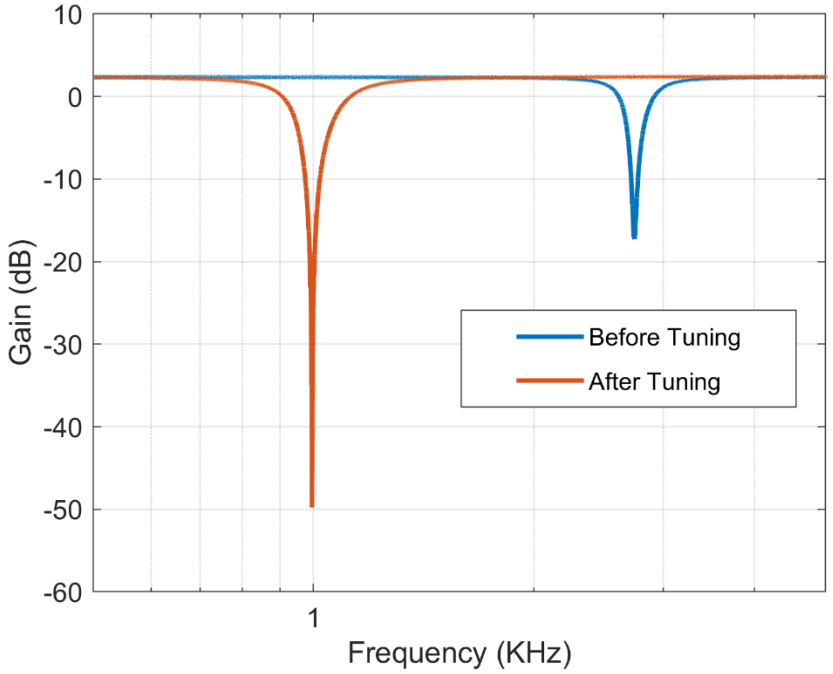

Figure 5.15 Experimental frequency response of the bandstop filter.

Table 5.2 Bandwidth tuning range at f_o =1KHz

f_r *(Hz)*	BW_d *(Hz)*	f_o *(Hz)*	BW_m *(Hz)*	$f_{Tuning\ Error}$ *(%)*	$BW_{Tuning\ Error}$ *(%)*
1000	225	997	225.8	0.3	0.4
1000	220	1005	221.9	0.5	0.86
1000	200	1000	201.5	0	0.75
1000	180	997.8	181.2	0.22	0.66

6. CONCLUSIONS

This chapter provides the conclusion of the study's contribution to the research community, and also provides recommendations and suggestions for future research based on all the findings.

A new second-order bandstop filter was implemented based on a source follower to reject RF frequencies with a low power consumption and a high linearity. The filter is designed to have a center frequency at 1.5 GHz with a bandwidth of around 478 MHz. Based on the simulation results, the proposed filter is more efficient in terms of linearity, noise, and dynamic range at low power consumption. Furthermore, the proposed bandstop filter is designed to be tunable. The parameters of the bandstop filter such as ω_o, BW, and α can be tuned digitally using switchable capacitor banks or switchable current sources.

A new automatic tuning scheme was proposed to tune center frequency, bandwidth, and attenuation of the second-order bandstop filter. The tuning scheme is based on phase comparison using digital control to detect and tune the filter parameters. Due to digital control enabling only one loop at a given time, reliable tuning is achieved.

The proposed filter and the tuning circuit were simulated using a 0.18u CMOS process, where the results show a frequency tuning error of 0.13% and a bandwidth tuning error of 0.88% at 1.5 GHz based on a bandwidth of 478MHz. The experimental results were also used to verify the proposed tuning method. The Gm-C filter topology was used to implement a second-order bandstop filter. The frequency tuning error was around 0.22% and the bandwidth tuning error was around 0.66% at 1KHz with a bandwidth of

200Hz. Thus, the simulation and experimental results show that the frequency and the bandwidth tuning have an error less than 1%.

6.1. Future work

The proposed tuning technique can be further explored to tune the parameters of a high-order bandstop filter. The high-order bandstop filter can be implemented by connecting biquadratic filters in series. Each filter will have its own center frequency, bandwidth, and attenuation. Thus, the high-order bandstop filter can be designed to reject a wider range of frequencies.

REFERENCES

[1] B. Razavi, "RF Microelectronics", 2nd ed, NJ: Prentice Hill, pp. 18-19, 2011.

[2] J. L. Goodman, “A Software Perspective on GNSS Receiver Integration and Operation”, *In: Rycroft M. (eds) Satellite Navigation Systems. Space Studies*, 8, Springer, Dordrecht, pp. 119, 2003.

[3] H. Shih, C. Kuo, W. Chen, T. Yang and K. Juang, "A 250 MHz 14 dB-NF 73 dB-Gain 82 dB-DR Analog Baseband Chain With Digital-Assisted DC-Offset Calibration for Ultra-Wideband," in *IEEE Journal of Solid-State Circuits*, 45(2), pp. 338-350, Feb. 2010.

[4] B. Kelleci, T. W. Fischer, K. Shi, Y. Zhou, A. I. Karsilayan and E. Serpedin, "Narrowband Interference Suppression in Multi-Band OFDM Ultra Wideband Communication Systems: A Mixed-Mode Approach," *2006 IEEE 12th Digital Signal Processing Workshop & 4th IEEE Signal Processing Education Workshop*, Teton National Park, WY, pp. 55-59, 2006.

[5] C. Barth, I. R. Linscott and U. S. Inan, "A Double notch RF filter architecture for SAW-less GPS receivers," *2011 IEEE International Symposium of Circuits and Systems (ISCAS),* Rio de Janeiro, pp. 1804-1807, 2011.

[6] S. Cui, K. C. Teh, K. H. Li, Y. L. Guan and C. L. Law, "BER performance of transmitted-reference UWB systems with notch filter in the presence of inter-pulse interference and partial-band interference," *2007 6th International Conference on Information, Communications & Signal Processing*, Singapore, pp. 1-5, 2007.

[7] D. Psychogiou, R. Gómez-García and D. Peroulis, "RF Wide-Band Bandpass Filter With Dynamic In-Band Multi-Interference Suppression Capability," in *IEEE Transactions on Circuits and Systems II: Express Briefs*, 65(7), pp. 898-902, July 2018.

[8] G. S. Moschytz, "A comparison of continuous-time active RC filters for the analog front end," *Int. J. Circuit Theory Appl*, 35 (5), pp. 575–595, Sep. 2007.

[9] K. N. Salama, H.O. Elwan and A. M. Soliman, "Parasitic-capacitance-insensitive voltage-mode MOSFET-C filters using differential current voltage conveyor, " *Circuits, Systems and Signal Processing*, 20 (1), 11-26, January 2001.

[10] Chun-Ming Chang, "New multifunction OTA-C biquads," in *IEEE Transactions on Circuits and Systems II: Analog and Digital Signal Processing*, 46 (6), pp. 820-824, June 1999.

[11] M. H. Koroglu and P. E. Allen, "LC notch filter for image-reject applications using on-chip inductors," in *Electronics Letters*, 37 (5), pp. 267-268, 1 March 2001.

[12] A. C. Sanabria-Borbon and E. Sanchez-Sinencio, "Efficient use of gain-bandwidth product in active filters: Gm-C and Active-R alternatives," *2017 IEEE 8th Latin American Symposium on Circuits & Systems (LASCAS)*, Bariloche, pp. 1-4, 2017.

[13] H. Amir-Aslanzadeh, E. J. Pankratz and E. Sanchez-Sinencio, "A 1-V +31 dBm IIP3, Reconfigurable, Continuously Tunable, Power-Adjustable Active-RC LPF," in *IEEE Journal of Solid-State Circuits*, 44 (2), pp. 495-508, Feb. 2009.

[14] Z. Czarnul and Y. P. Tsividis, "Implementation of MOSFET-C filters based on active RC prototypes," in *Electronics Letters*, 24 (3), pp. 184-185, 4 Feb. 1988.

[15] L. Mohammadi and K. Koh, "2–4 GHz Q-tunable LC bandpass filter with 172-dBHz peak dynamic range, resilient to +15-dBm out-of-band blocker," *2015 IEEE Custom Integrated Circuits Conference (CICC)*, San Jose, CA, pp. 1-4, 2015.

[16] J. M. Stevenson and E. Sanchez-Sinencio, "An Accurate Quality Factor Tuning Scheme for IF and High Q Continuous-Time Filter," IEEE J. Solid-state Circuits, 33 (12), pp. 1970-1978, Dec. 1998.

[17] H. Liu and A. I. Karsilayan, "Frequency and Q tuning of active-LC filters," *The 2002 45th Midwest Symposium on Circuits and Systems,* Tulsa, OK, USA, pp. II-II, 2002.

[18] F. Bahmani, T. Serrano-Gotarredona and E. Sanchez-Sinencio, "An accurate automatic quality factor tuning scheme for second-order LC filters," IEEE Transactions on Circuits and Systems I: Regular Papers, 54 (4), 745-756, 2007.

[19] T. Sumesaglam and A. I. Karsilayan, "A digital automatic tuning technique for high-order continuous-time filters," in *IEEE Transactions on Circuits and Systems I: Regular Papers*, 51 (10), pp. 1975-1984, Oct. 2004.

[20] J. Khoury, "Design of a 15-MHz CMOS continuous-time filter with on-chip tuning," *IEEE J. Solid-State Circuits*, 26 (12), pp. 1988–1997, Dec. 1991.

[21] T. Viswanathan, S. Murtuza, V. Syed, J. Berry, and M. Staszel, "Switched-capacitor frequency control loop," *IEEE J. Solid-State Circuits*, 17 (4), pp. 775–778, Aug. 1982.

[22] P. Kallam, E. Sanchez-Sinencio and A. I. Karsilayan, "An enhanced adaptive Q-tuning scheme for a 100-MHz fully symmetric OTA-based bandpass filter," in *IEEE Journal of Solid-State Circuits*, 38 (4), pp. 585-593, April 2003.

[23] P. Sepidband and K. Entesari, "A CMOS Wideband Receiver Resilient to Out-of-Band Blockers Using Blocker Detection and Rejection," in *IEEE Transactions on Microwave Theory and Techniques*, 66 (5), pp. 2340-2355, May 2018.

[24] M. H. Koroglu and P. E. Allen, "A 1.9GHz image-reject front-end with automatic tuning in a 0.15 μm CMOS technology," *2003 IEEE International Solid-State Circuits Conference, 2003. Digest of Technical Papers. ISSCC*, San Francisco, CA, USA, 1, pp. 264-492, 2003.

[25] B. Floyd, S. Reynolds, U. Pfeifer, T. Beukema, J. Grzyb and C. Haymes, "A silicon 60GHz receiver and transmitter chipset for broadband communications," *2006 IEEE International Solid-State Circuits Conference - Digest of Technical Papers*, San Francisco, CA, pp. 649-658, 2006.

[26] F. T. Almutairi and A. I. Karsilayan, "Fully-differential second-order tunable bandstop filter based on source follower," *Electronics Letters*, 55 (3), 122–124, 2019.

[27] R. Schaumann, M. S. Ghausi, and K. R. Laker, "Design of Analog Filters: Passive, Active RC and Switched-Capacitor," Englewood Cliffs, NJ: Prentice-Hall, 1990.

[28] R. Schaumann , H. Xiao and M. E. V Valkenburg, "Design of Analog Filters," 2nd Edition, Oxford University Press, Inc., New York, NY, 2009.

[29] H. A. Alzaher, N. Tasadduq and Y. Mahnashi, "A Highly Linear Fully Integrated Powerline Filter for Biopotential Acquisition Systems," in *IEEE Transactions on Biomedical Circuits and Systems*, 7 (5), pp. 703-712, Oct. 2013.

[30] J. Harrison and N. Weste, “A 500 MHz CMOS anti-alias filter using feed-forward op-amps with local common-mode feedback*,” in IEEE ISSCC Dig. Tech. Papers*, pp. 132–133, Feb. 2003.

[31] T. Laxminidhi, V. Prasadu, and S. Pavan, “Widely programmable high frequency active RC filters in CMOS technology,” *IEEE Trans. Circuits Syst. I, Reg. Papers*, 56 (2), pp. 327–336, Feb. 2009.

[32] H. Amir-Aslanzadeh, E. J. Pankratz and E. Sanchez-Sinencio, "A 1-V +31 dBm IIP3, Reconfigurable, Continuously Tunable, Power-Adjustable Active-RC LPF," in *IEEE Journal of Solid-State Circuits*, 44 (2), pp. 495-508, Feb. 2009.

[33] A. Vasilopoulos, G. Vitzilaios, G. Theodoratos, and Y. Papananos, “A low-power wideband reconfigurable integrated active-RC filter with 73 dB SFDR*,” IEEE J. Solid-State Circuits,* 41, pp. 1997–2008, Sep. 2006.

[34] I. S. Han and S. B. Park, "Voltage-controlled linear resistor by two MOS transistors and its application to active RC filter MOS integration," in *Proceedings of the IEEE*, 72 (11), pp. 1655-1657, Nov. 1984.

[35] A. Yoshizawa and Y. P. Tsividis, "Anti-blocker design techniques for MOSFET-C filters for direct conversion receivers," in *IEEE Journal of Solid-State Circuits*, 37 (3), pp. 357-364, March 2002.

[36] M. H. Koroglu and P. E. Allen, "A 1.9GHz image-reject front-end with automatic tuning in a 0.15 μm CMOS technology," *2003 IEEE International Solid-State Circuits Conference, 2003. Digest of Technical Papers. ISSCC.*, San Francisco, CA, USA, pp. 264-492, 2003.

[37] T. Viswanathan, S. Murtuza, V. Syed, J. Berry, and M. Staszel, "Switched-capacitor frequency control loop," *IEEE J. Solid-State Circuits*, 17 (4), pp. 775–778, Aug. 1982.

[38] Y. Tsividis, M. Banu, and J. Khoury, "Continuous-time MOSFET-C filters in VLSI," *IEEE J. Solid-State Circuits*, 21 (1), pp. 15–29, Feb. 1986.

[39] M. Banu and Y. Tsividis, "Fully integrated active RC filters in MOS technology," *IEEE J. Solid-State Circuits*, 18 (6), pp. 644–651, Dec. 1983.

[40] U. Moon and B. Song, "Design of a low-distortion 22-kHz 5th-order Bessel filter," *IEEE J. Solid-State Circuits*, 28 (12), pp. 1254–1264, Dec. 1993.

[41] H. Khorramabadi and P. R. Gray, "High-frequency CMOS linear continuous-time filters," *IEEE J. Solid-State Circuits*, 19 (6), pp. 939–948, Dec. 1984.

[42] V. Gopinathan, Y. Tsividis, K. Tan, and R. Hester, "Design consideration for high frequency continuous-time filter and implementation of an antialiasing filter for digital video*," IEEE J. Solid-State Circuits,* 25 (12), pp. 1368–1378, Dec. 1990.

[43] J. Shin, S. Min, S. Kim, J. Choi, S. Lee, H. Park, and J. Kim, "3.3-V Baseband Gm-C Filters for Wireless Transceiver Applications," *in IEEE Proc. ISCAS*, 1, pp. 457–460, 2003.

[44] A. I. Karsilayan and R. Schaumann, "Mixed-Mode Automatic Tuning Scheme for High-Q Continuous-Time Filters," in IEE Proc. Circuits, Devices and System, 147 (1), pp. 57–64, 2000.

[45] R. Schaumann and M. A. Tan, "The Problem of On-Chip Automatic Tuning in Continuous-Time Integrated Filters," *in IEEE Proc. ISCAS*, 1, pp. 106–109, 1989.

[46] C. Plett, and M. A. Copeland, “Self-tuned continuous-time notch filters,” *J. VLSI Signal Process. Syst. Signal Image Video Technol*, 8, pp. 227-240, 1994.

[47] G. Vemulapalli, P. Hanumolu, Y. Kook, and U. Moon, " A 0.8V, accurately tuned, linear continuous-time filter," *IEEE J. Solid-State Circuits*, pp. 1972-1977, Sep. 2005.

[48] J. I. Osa, A. Carlosena, and A. J. Lopez-Martin, “MOSFET-C Filter with On Chip Tuning and Wide Programming Range,” *IEEE Trans. on Circuits Syst. II,* 48 (10), pp. 944–951, Oct. 2001.

[49] T. Salo, S. Lindfors, and K. Halonen, “Direct Digital Tuning for Continuous Time Filters,” *in IEEE Proc. MWSCAS*, 1, pp. 216–219, 2000.

[50] Y. Tsividis, “Self-tuned filters,” *Electron. Lett*, 17 (12) pp. 406–407, 1981.

[51] A. I. Karsilayan and R. Schaumann, "Automatic tuning of high-Q filters based on envelope detection," *ISCAS'99. Proceedings of the 1999 IEEE International Symposium on Circuits and Systems VLSI (Cat. No.99CH36349)*, Orlando, FL, pp. 668-671 vol.2, 1999.

[52] F. T. Almutairi and A. I. Karsilayan, "A Tunable Bandstop Filter Based on Source Follower," 2019 IEEE 62nd International Midwest Symposium on Circuits and Systems (MWSCAS), 2019.

[53] J. Kim, J. Shin, S. Kim and H. Shin, "A Wide-Band CMOS LC VCO With Linearized Coarse Tuning Characteristics," in *IEEE Transactions on Circuits and Systems II: Express Briefs*, 55 (5), pp. 399-403, May 2008.

[54] AS. Sedra, KC. Smith, “Microelectronics,” Oxford University Press, 5th edition, 2004.

[55] B. Razavi, "Design of analog CMOS integrated circuits", McGraw-Hill, Boston, 2001.

[56] V. Dhanasekaran, M. Gambhir, J. Silva-Martinez, and E. Sanchez-Sinencio, "A 1.1GHz Fifth Order Active-LC Butterworth Type Equalizer Filter", J. Solid-State Circuits, 42 (11), pp. 2411-2420, 2007.